

Reporting Summary

Nature Portfolio wishes to improve the reproducibility of the work that we publish. This form provides structure for consistency and transparency in reporting. For further information on Nature Portfolio policies, see our [Editorial Policies](#) and the [Editorial Policy Checklist](#).

Statistics

For all statistical analyses, confirm that the following items are present in the figure legend, table legend, main text, or Methods section.

n/a Confirmed

- | | | |
|-------------------------------------|-------------------------------------|--|
| <input type="checkbox"/> | <input checked="" type="checkbox"/> | The exact sample size (n) for each experimental group/condition, given as a discrete number and unit of measurement |
| <input type="checkbox"/> | <input checked="" type="checkbox"/> | A statement on whether measurements were taken from distinct samples or whether the same sample was measured repeatedly |
| <input type="checkbox"/> | <input checked="" type="checkbox"/> | The statistical test(s) used AND whether they are one- or two-sided
<i>Only common tests should be described solely by name; describe more complex techniques in the Methods section.</i> |
| <input checked="" type="checkbox"/> | <input type="checkbox"/> | A description of all covariates tested |
| <input type="checkbox"/> | <input checked="" type="checkbox"/> | A description of any assumptions or corrections, such as tests of normality and adjustment for multiple comparisons |
| <input type="checkbox"/> | <input checked="" type="checkbox"/> | A full description of the statistical parameters including central tendency (e.g. means) or other basic estimates (e.g. regression coefficient) AND variation (e.g. standard deviation) or associated estimates of uncertainty (e.g. confidence intervals) |
| <input type="checkbox"/> | <input checked="" type="checkbox"/> | For null hypothesis testing, the test statistic (e.g. F , t , r) with confidence intervals, effect sizes, degrees of freedom and P value noted
<i>Give P values as exact values whenever suitable.</i> |
| <input checked="" type="checkbox"/> | <input type="checkbox"/> | For Bayesian analysis, information on the choice of priors and Markov chain Monte Carlo settings |
| <input checked="" type="checkbox"/> | <input type="checkbox"/> | For hierarchical and complex designs, identification of the appropriate level for tests and full reporting of outcomes |
| <input checked="" type="checkbox"/> | <input type="checkbox"/> | Estimates of effect sizes (e.g. Cohen's d , Pearson's r), indicating how they were calculated |

Our web collection on [statistics for biologists](#) contains articles on many of the points above.

Software and code

Policy information about [availability of computer code](#)

Data collection	Clampex 9.2, PatchControl v2.1, Yokogawa CQ1 1.0, Powerlab 8/35, Myocyte online Contraction Analysis (MoCA), RHX, Digital Lynx 4S, MATLAB 2012a
Data analysis	python 3.12.2, numpy 1.26.4, pandas 2.2.1, scipy 1.12.0, pingouin 0.5.4, scikit-learn 1.4.1, napari 0.4.19, MATLAB 2021b, Origin 9, Clampfit 10.7, LabChart 8.1.16, PsychoPy, kilosort3, phy, Bonsai, Origin 9, Clampfit 10.7, ImageJ 1.52p, GraphPad Prism 8, ZEN 2.6, custom software is available on Zenodo: https://doi.org/10.5281/zenodo.15210800

For manuscripts utilizing custom algorithms or software that are central to the research but not yet described in published literature, software must be made available to editors and reviewers. We strongly encourage code deposition in a community repository (e.g. GitHub). See the Nature Portfolio [guidelines for submitting code & software](#) for further information.

Data

Policy information about [availability of data](#)

All manuscripts must include a [data availability statement](#). This statement should provide the following information, where applicable:

- Accession codes, unique identifiers, or web links for publicly available datasets
- A description of any restrictions on data availability
- For clinical datasets or third party data, please ensure that the statement adheres to our [policy](#)

The manuscript does include a data availability statement and data is available on Zenodo <https://doi.org/10.5281/zenodo.15210800>

Research involving human participants, their data, or biological material

Policy information about studies with [human participants or human data](#). See also policy information about [sex, gender \(identity/presentation\), and sexual orientation](#) and [race, ethnicity and racism](#).

Reporting on sex and gender N/A

Reporting on race, ethnicity, or other socially relevant groupings N/A

Population characteristics N/A

Recruitment N/A

Ethics oversight N/A

Note that full information on the approval of the study protocol must also be provided in the manuscript.

Field-specific reporting

Please select the one below that is the best fit for your research. If you are not sure, read the appropriate sections before making your selection.

☒ Life sciences ☐ Behavioural & social sciences ☐ Ecological, evolutionary & environmental sciences

For a reference copy of the document with all sections, see [nature.com/documents/nr-reporting-summary-flat.pdf](https://www.nature.com/documents/nr-reporting-summary-flat.pdf)

Life sciences study design

All studies must disclose on these points even when the disclosure is negative.

Sample size For most experiments no particular statistical method was used to predetermine sample sizes. Sample sizes were chosen on the basis of previously published experimental designs whenever disclosed in the manuscript. For some of the animal studies sample size was calculated using power analysis.

Data exclusions No data were excluded from the analyses.

Replication The number of replicated or independently performed experiments is provided in the manuscript. Wherever applicable, the number of unsuccessful attempts is clearly stated in the manuscript.

Randomization Randomization was not performed.

Blinding Experimenters were blinded to the experimental group for the optogenetic stimulation of the auditory pathway in the common marmoset. Experimenters were blinded for histological assessment of cochlea tissue.

Reporting for specific materials, systems and methods

We require information from authors about some types of materials, experimental systems and methods used in many studies. Here, indicate whether each material, system or method listed is relevant to your study. If you are not sure if a list item applies to your research, read the appropriate section before selecting a response.

Materials & experimental systems

n/a Involved in the study

☐ ☒ Antibodies

☐ ☒ Eukaryotic cell lines

☒ ☐ Palaeontology and archaeology

☐ ☒ Animals and other organisms

☒ ☐ Clinical data

☒ ☐ Dual use research of concern

☒ ☐ Plants

Methods

n/a Involved in the study

☒ ☐ ChIP-seq

☒ ☐ Flow cytometry

☒ ☐ MRI-based neuroimaging

Antibodies

Antibodies used For cardiomyocytes: cardiac troponin I (ab47003, Abcam: 1:800); Cy5 (711-175-152, JacksonLab, U.S., 1:400);

Antibodies used

For retinæ: rabbit Proteintech, 50430-2-AP; AlexaFluor 488 (Invitrogen, A32970);
 For rodent cochleæ: chicken anti-GFP (1:500, ab13970 Abcam, USA); guinea pig anti-parvalbumin (1:300, 195004 Synaptic Systems, Germany); goat anti-chicken 488 IgG (1:200, A-11039 Thermo Fisher Scientific, USA); goat anti-guinea pig 568 IgG (1:200, A-1107 Thermo Fisher Scientific, USA);
 for rodent brainstem slides: chicken-anti-GFP (1:500, Abcam, Berlin, Germany), guinea-pig-anti-vGLUT1 (1:1000, Synaptic Systems GmbH, Göttingen, Germany); goat-anti-chicken 488 (1:200, Thermo Fisher Scientific, Waltham, USA) goat-anti-guinea-pig 568 (1:200, Thermo Fisher Scientific, Waltham, USA); for gebril brain histology: antibodies for parvalbumin (1:300, guinea pig, Synaptic Systems, Goettingen, Germany) and GFP (1:500, chicken, Abcam, Cambridge, UK);
 Marmoset histology: chicken anti-GFP (1:500, ab13970 Abcam, USA); guinea pig anti-parvalbumin (1:300, 195004 Synaptic Systems, Germany); mouse anti-NF200 (1:400, Sigma, St. Louis, USA); goat anti-chicken 488 IgG (1:200, Invitrogen Scientific, USA), goat anti-guinea pig 568 IgG (1:200, Invitrogen, USA); anti-mouse 633 (1:200, Invitrogen); guinea pig anti-parvalbumin (1:200; Synaptic systems, Germany), rabbit anti-Otoferlin (1:500; SySy); chicken anti-GFP (1:500; Abcam); anti-chicken 488 (1:1000; Invitrogen), anti-guinea pig 568 (1:1000; Invitrogen); anti-rabbit 633 (1:1000; Thermo Fisher)

Validation

Validation was provided by companies.

Eukaryotic cell lines

Policy information about [cell lines and Sex and Gender in Research](#)

Cell line source(s)

HEK293T cells (DSMZ, Braunschweig, Germany), NG108-15 (ATCC, HB-12377TM, Manassas, USA), Human cardiomyocyte like cells were differentiated from the induced pluripotent stem cell line UMGi014-A clone 2, which was created from peripheral mononuclear blood cells from a healthy male donor using integration-free Sendai virus.

Authentication

The authentication of HEK293T cells and NG108-15 cells were performed by the cell line sources. All cell lines were checked for their morphology and only used in early passage.

Mycoplasma contamination

The HEK293T cells and NG108-15 cells were tested negative for mycoplasma contamination.

Commonly misidentified lines
(See [ICLAC](#) register)

No commonly misidentified cell lines were used.

Animals and other research organisms

Policy information about [studies involving animals](#); [ARRIVE guidelines](#) recommended for reporting animal research, and [Sex and Gender in Research](#)

Laboratory animals

Only laboratory animals were used: Mus musculus (C3HeB/FeJ, JAX 000658; C57B/6J), Mongolian gerbils (Rj:MON), Common marmoset (bred at the German Primate Center)

Wild animals

The study did not involve wild animals.

Reporting on sex

For all animal studies both sex were used as no impact of the sex was expected.

Field-collected samples

No field-collected samples were used for this study.

Ethics oversight

Electrophysiology studies in the visual system were approved by the An"Regierung von Oberbayern". Behavior experiments to test for vision restoration were approved by the Neuro Animal Care Committee (ACC) of the McGill University. Animal studies in the auditory system were approved by "Niedersächsisches Landesamt für Verbraucherschutz und Lebensmittelsicherheit".

Note that full information on the approval of the study protocol must also be provided in the manuscript.

Plants

Seed stocks

Report on the source of all seed stocks or other plant material used. If applicable, state the seed stock centre and catalogue number. If plant specimens were collected from the field, describe the collection location, date and sampling procedures.

Novel plant genotypes

Describe the methods by which all novel plant genotypes were produced. This includes those generated by transgenic approaches, gene editing, chemical/radiation-based mutagenesis and hybridization. For transgenic lines, describe the transformation method, the number of independent lines analyzed and the generation upon which experiments were performed. For gene-edited lines, describe the editor used, the endogenous sequence targeted for editing, the targeting guide RNA sequence (if applicable) and how the editor was applied.

Authentication

Describe any authentication procedures for each seed stock used or novel genotype generated. Describe any experiments used to assess the effect of a mutation and, where applicable, how potential secondary effects (e.g. second site T-DNA insertions, mosaicism, off-target gene editing) were examined.

Efficient and sustained optogenetic control of sensory and cardiac systems

Corresponding Author: Prof Tobias Moser

Version 0:

Decision Letter:

Dear Prof Moser,

Thank you again for submitting to *Nature Biomedical Engineering* your manuscript, "Efficient and sustained optogenetic control of nervous and cardiac systems". The manuscript has been seen by 3 experts, whose reports you will find at the end of this message.

You will see that the reviewers appreciate the work. However, they express concerns about the degree of support for the claims, and provide useful suggestions for improvement. We hope that with substantial further work you can address the criticisms and convince the reviewers of the merits of the study. In particular, we would expect that a revised version of the manuscript provides:

- * Extended discussion on the work's rationale and on the development of ChReef, as highlighted by Reviewer #2 and #3.
- * Assessment of the mechanism at the base of the improved photocurrent.
- * Several additional controls as requested by all the reviewers, with emphasis on the cellular localisation of the opsin.
- * Thorough characterization and methodological reporting.

Editorially, the suggested behavioural studies would be welcomed but not mandatory.

When you are ready to resubmit your manuscript, please [upload](#) the revised files, a point-by-point rebuttal to the comments from all reviewers, the [reporting summary](https://www.nature.com/authors/policies/ReportingSummary.pdf), and a cover letter that explains the main improvements included in the revision and responds to any points highlighted in this decision.

Please follow the following recommendations:

- * Clearly highlight any amendments to the text and figures to help the reviewers and editors find and understand the changes (yet keep in mind that excessive marking can hinder readability).
- * If you and your co-authors disagree with a criticism, provide the arguments to the reviewer (optionally, indicate the relevant points in the cover letter).
- * If a criticism or suggestion is not addressed, please indicate so in the rebuttal to the reviewer comments and explain the reason(s).
- * Consider including responses to any criticisms raised by more than one reviewer at the beginning of the rebuttal, in a section addressed to all reviewers.
- * The rebuttal should include the reviewer comments in point-by-point format (please note that we provide all reviewers will the reports as they appear at the end of this message).
- * Provide the rebuttal to the reviewer comments and the cover letter as separate files.

We hope that you will be able to resubmit the manuscript within 20 weeks from the receipt of this message. If this is the case, you will be protected against potential scooping. Otherwise, we will be happy to consider a revised manuscript as long as

the significance of the work is not compromised by work published elsewhere or accepted for publication at *Nature Biomedical Engineering*.

We hope that you will find the referee reports helpful when revising the work. Please do not hesitate to contact me should you have any questions.

Best wishes,

Valeria

Dr Valeria Caprettini

Associate Editor, *Nature Biomedical Engineering*

Reviewer #1 (Report for the authors (Required)):

This manuscript presents an original work studying the effects of the channelrhodopsin ChReef, a variant of the ChRmine, in cardiomyocytes for inducing a depolarization block in cardiomyocyte clusters generated from neonatal mouse hearts, rd1 mouse model of retinal dystrophy (responses to optogenetic stimulation of the eye to a green LED or an iPad screen and multielectrode array records from the contralateral primary visual cortex) and auditory system in mice and gerbils (spiral ganglion neurons and cochlear nucleus neurons). The results obtained provide evidence about the potential of the assessed optogenetic tools for modeling in experimental conditions or future clinical therapeutic applications.

The improved light sensitivity and the dynamic of responses clearly represent the main advantages of this technology.

Comments and concerns:

The title "Efficient and sustained optogenetic control of nervous and cardiac systems" could be misleading as the observed effects in the visual and auditory systems still do not cover the entire nervous system.

In the abstract: "Towards clinical application we used AAV-based gene transfer to express ChReef in the optic nerve where it restores visual function in blind mice". The retinal ganglion cells (RGC) were targeted and this should be précised in the abstract, moreover, no data about expression in the optic nerve were shown. Such terminology is surprising. The choice of the promoter should be justified, as well as the cell specificity and the ensuing biodistribution in the tissues studied.

The section "Main or Introduction" could provide more general information about the properties of the bacteriorhodopsin-like cation channelrhodopsin ChRmine that make it suitable as optogenetic therapeutic and a rational basis for engineering of ChRmine variants. A detailed comparison of properties to some recently developed alternative proteins should be provided, e.g., ChR variant, *Chloromonas oogamy* (CoChR) mutants, CoChR-L112C and CoChR-H94E/L112C/K264T, with markedly enhanced light sensitivity.

Despite the use of sophisticated electrophysiological methods and nice illustrations, the manuscript could read more fluently with a more structured presentation of the results. Actually, one should rely mainly on the figures to follow the results and this makes difficult their understanding and interpretation during the reading. Some aspects of the experiments could be presented in more details also in the main text and not only in the methods, some points/questions below:

Has the technology been tested in adult cardiac cells, and in cells types other than myocytes?

Did the rd1 mice treated carry also the Gpr179 mutation ?

Have the morphological and functional parameters (eg OCT, ERG) been evaluated before and after treatment (control and transfected animals)?

Has the stage of tissue remodeling after photoreceptor degeneration been considered?

At what time point after intravitreal injection in vivo was assessed the level of expression (3-4 weeks?)

What cells were transduced besides RGCs? Was a dose ranging in terms of titers tested?

For how long did the expression persist in the transfected cells (transgene stability)?

Has the immune response in the transfected retinas been considered/evaluated?

Is it possible to associate the responses in the visual cortex as a result of direct activation of the RGCs expressing AAVPHP.eB carrying either of the EYFP-tagged ChRs under the control of the human synapsin promoter?

To demonstrate functional vision restoration, this work would benefit of including behavioral studies. Methods such as optokinetic stimulation would be relevant.

Reviewer #2 (Report for the authors (Required)):

The authors described an improved version of the very potent and useful channelrhodopsin ChRmine, which was named ChReef. ChReef was shown to have increased unitary conductance and stationary photocurrent due to decreased desensitization. Furthermore, ChReef has faster dark recovery kinetics and off-kinetics compared to its progenitor. Improved

biophysical properties were successfully translated in cultured cells and in vivo, enabling its successful applications for optogenetic stimulation of the mouse auditory nerve and vision restoration and outperforming ChRmine under identical conditions. If ChReef performs as described, it will be a valuable addition to the channelrhodopsin family and described in vivo demos may prompt its further validation in vivo and application for therapies. However, I do have several comments, which I believe the authors should be able to address easily.

It is known that optogenetic stimulation may have many undesired artifacts on cellular state and function. The classic example is neuronal activity rebound after neuronal silencing using activation of chloride light-driven pumps in neurons or acidification of neurons during extended activation of fast ChR2 variants. The exact mechanism of side effects from optogenetic activation depends on the ionic species conducted by rhodopsins and their cellular localization (axon vs soma vs dendrites). It is also known that mutations that increase photocurrent can largely change the selectivity of ionic conductance (ChRH and CatCh are classic examples). However, the authors did not even try to discuss the potential mechanism of improved photocurrent and the potential alternation of ion contribution to the photocurrent compared to the parental protein. This aspect might be crucial for proper validation of ChReef safety in vivo. It would be great if the authors could address this point.

Based on the histological analysis (resolution and magnification of the provided images are not ideal) ChReef demonstrates some internalization in neurons. This aspect can be crucial since it does not matter what unitary conductance a ChR may have if it is not properly localized to the plasma membrane. I could not find any information on the duration of ChReef expression in vivo. Do the authors observe a higher degree of mislocalization upon longer expression duration? Please comment on the localization of ChReef in vivo and provide high-resolution images of single cells.

Overall, the manuscript reads like a technical report, which is very concise and lacks some rationale, specifically in the first two parts of the Results section. The development of ChReef is not described at all. It is hard to follow the logic of the first and second parts of the Results section. The authors refer to Fig. 1a, which presents single and double mutants ChRmine while not mentioning them in the main text when they call this panel for the first time. Even later in the text, the authors did not explain how they arrived at the ChRmine variants that they reported in the manuscript. The statement "Mutations in Helix 6 accelerate open to closed state transition in green algal ChRs18" is not really helpful for understanding introduced mutations, it was never stated that introduced mutations are in helix 6 of ChRmine. I would recommend revising the manuscript to address the following points: what was the rationale behind introduced mutations? What is the potential mechanism of the increased photocurrent?

The authors presented lots of data on ChReef. However, it is not properly discussed in the manuscript. Please discuss ChReef development, its advantages and limitations compared to its progenitor and other established ChRs, and discuss its performance in vivo and how well it correlates with expected performance based on the measured biophysical parameters in vitro. Provide brief perspectives and outlook for future improvements of ChReef or further characterization/validation.

Minor comments:

The authors presented great results on photocurrent profiles for ChRmine and its mutants in Fig S2; why not further characterize rate of desensitization? It seems to be different among the mutants. It would be great to have the traces in the main text figure with absolute amplitude rather than normalized, as shown in Fig. S2.

Fig S2b,d,f – Y-axis label is missing. If these are normalized values, what was the normalization coefficient, and why should it be normalized?

Do the authors have any comments on the correlation of the results shown in Supp Fig 11f and Fig. 4o-r?

ChReef is not properly introduced in the main text and further inconsistent naming of the ChReef protein in the manuscript makes it difficult to read the manuscript. For example, in Fig. 1 it is referred to as ChReef (even before it was named later in the text) while in the first and second sections of Results it is referred to as ChRmine/T218L/S220A. Why not simply introduce in the last paragraph of introduction and use it throughout since then (all Figures have it as ChReef anyway). Also, in Fig S2, S4, and S5 there is ChREEF (is it the same with ChReef?).

I did not find a reference to Fig S1 in the main text.

"a major driver of progress in the life sciences" – quite an overstatement.

Reviewer #3 (Report for the authors (Required)):

Review nBME-24-0098

In this manuscript the authors present ChReef, an improved variant of the light-gated cation channel ChRmine. The advantage of ChReef over ChRmine is the low desensitization at largely preserved single-channel conductance and overall kinetics. The stationary photocurrent density is increased approx. by a factor of 4 compared to ChRmine and 2.6 compared to CatCh – an opsin that was previously used by the group for optogenetic manipulation of the cochlea. The authors compare the performance of ChReef and ChRmine in several model systems reaching from cultures of cardiomyocytes to the mouse retina in vivo to the cochlea and auditory brain stem in mice and gerbils. Overall, ChReef shows superior performance compared to ChRmine. Due to the red-shifted action spectrum compared to CatCh, it can still be activated with orange-red light, which presents an additional advantage given that long-wavelength light is less scattered and absorbed in biological tissue. Thus, ChReef is potentially useful for a number of in vivo applications, which are demonstrated in this study. However, a number of concerns remain.

Major

1. The choice of the mutation sites to generate ChReef is not well explained and does not become apparent. It is not clear why these particular two amino acid exchanges were chosen to generate ChReef. The two mutations do not seem to be related to any of the helix F mutations in the paper cited for the acceleration of closing kinetics (doi: 10.1038/s41467-018-

04146-3). The sentence “Next, we aimed to overcome ChRmine desensitization by introducing helix 6 mutations to unleash its potential for life science and medical applications.” does not make sense / is not followed by a reasonable motivation. According to how this paragraph is written, it appears as if the authors aimed for a faster version of ChRmine (again, why exactly those 2 point mutations?), but rather discovered a variant with lower desensitization. The strategy and the rationale need to be better explained. Were only these two mutations made? Were other residues targeted? If not, why did the authors stick to exactly those two mutations?

In addition, ChRmine mutants with similarly improved desensitization properties were previously reported (doi: 10.1016/j.cell.2022.01.007). One mutant (Y260F, helix 7 or G) showed similarly low desensitization with preserved photocurrent amplitudes. A comparison of ChReef to this mutant and an explanation of the authors’ strategy is required to assess the advance of the current tool.

2. The authors need to show wavelength-dependency of the desensitization. ChRmine does almost not desensitize under red light (doi: 10.1126/science.aaw5202 and 10.1016/j.cell.2022.01.007). Given this low desensitization and the same spectral response of ChRmine and ChReef (suppl. Fig. 1) it is surprising that ChReef performs so much better than ChRmine under red light in Fig. 2e and f. Without a proper spectral characterization of photocurrents, this effect is difficult to explain.

3. The manuscript contains exaggerated claims in many places. For example:

- The abstract states “...we used AAV-based gene transfer to express ChReef in the optic nerve where it restores visual function in blind mice”. From what I can see, no experiments were done that assess vision. Only responses in V1 were reported.
 - Keywords include “hearing, vision, cardiac defibrillation”. However, none of these aspects is shown in the paper. These are clearly not keywords of the present study and mislead the reader.
 - The same goes for the running title and the last sentence of the intro. No control of “the heart” is shown.
- Such statements are strongly overselling the content of the paper and are not backed up by the data. In this form the manuscript should not be published.

4. No raw traces/example recordings are shown in figure 1, 3, 5. Furthermore, the entire figure 1 is not very well composed and makes a very provisional impression. The plots are hard to read due to the legends being positioned inside the data area. Particularly bad examples are panel c and e. Additionally, the order of the symbols in the legends is inconsistent (compare c and d). In panels 1c-d the values for ChReef and perhaps other opsins are highly skewed and a comparison of the mean values appears inappropriate. Statistics and plots should take into account the non-normality of the data distribution. In particular in the case of ChReef, a few extreme outliers seem to dominate the mean value. The authors need to perform normality tests on all their data and apply correct statistics accordingly.

5. Fig. 2: Why was there an irregular electrical stimulation interval used in panel e? The stimulation rhythm changes within the recording and the stimulation frequency is different between the ChRmine and ChReef conditions. Thus, comparison between the two opsins is limited.

6. No negative controls are shown anywhere in the paper. Especially the “vision restoration” experiments need a control with no opsin expression. Moreover given the use of PHP.eB viruses in these experiments, expression in other brain regions than the retina needs to be excluded. In general, histology is very limited. The example in panel a suggests that expression density was higher for ChReef. Expression needs to be quantified (see also next point).

7. Fig. 4: According to the methods, it seems that the data shown in panels h-r were obtained from two mice – one of them deafened. What is the purpose and why is this not indicated in the figure or the text? It also seems like deafening was not validated anywhere. I find it quite concerning that at those numbers of animals (n = 2) mixed treatments are used – especially in the case where two opsins are compared. Which mouse was ChReef and which one ChRmine injected? These experiments need to be repeated under proper conditions. In addition, histological characterization is not very conclusive. From Suppl. Fig. 9 it looks like ChReef expression was stronger than ChRmine expression, at least in the left cochlea. Can this explain the difference in performance? What is the number of animals compared? It is not indicated in the legend. This aspect needs to be properly evaluated and quantified. If better expression explains the better performance of ChReef, this is fine, but at this stage, cannot be judged properly.

8. I am very skeptical about figure 5. It does not add any additional value to the manuscript (the relevant information is already in figure 4). It shows neither comparison to ChRmine, to any other opsin, or any auditory stimulation. Panels g-h are not even referred to in the main text. Why are they plotted? It is not explained why different animal numbers were used (5c n = 7, ABR recordings in suppl. fig. 14 n = 5). More importantly, the authors used a PHP.S capsid for viral transduction in neonatal animals. Thus, it is highly likely that the virus spread further into the brain and did not remain local in the cochlea. In fact, this is directly seen in suppl. fig. 11. Here, large photocurrents are observed in cells of the ventral cochlear nucleus. Thus direct light effects in the inferior colliculus from non-cochlear sources cannot be disentangled from those responses originating in the cochlea itself. Also the synaptic recordings in suppl. fig. 11 are problematic, because residual photocurrents and local network effects cannot be excluded. According to suppl. fig. 12 it seems that the virus even spread to the contralateral cochlea. These gerbil experiments weaken the manuscript and should be removed.

Minor

9. It is not clear why closing kinetics of 30 ms are reported in the abstract and discussion. The fastest off kinetics reported for ChReef are between 50 and 60 ms (Suppl. Fig. 4 and suppl. tables 1 and 2).

10. Fig. 2: The legend states that 625 nm was used for photostimulation. However, given the optical filters used in this experiment, the light emitted from a 625 nm LED that reached the cells was between 626 and 644 nm. This is relevant with regard to the low desensitization of ChRmine in this wavelength range and therefore requires proper spectral characterization of the photocurrents as stated under main point 2.

11. Fig. 4.: The caption mentions radiant flux in mW, but the legend is given in uJ

12. Suppl. Fig. 4.: why are data points missing? Is this due to absence of currents at the reversal wavelength? If so, why is this not an issue with ChRmine photocurrents?

13. Suppl. fig. 8: why are the red lines in drawn over the data?

14. Suppl. Fig. 11.: "AVCN" nowhere defined

Version 1:

Decision Letter:

Dear Tobias,

Thank you for your revised manuscript, "Efficient and sustained optogenetic control of nervous and cardiac systems", which has been seen by the original reviewers. In their reports, which you will find at the end of this message, you will see that they acknowledge the improvements to the work and raise a few additional technical criticisms that we hope you will be able to address.

As before, when you are ready to resubmit your manuscript, please [upload](#) the revised files, a point-by-point rebuttal to the comments from all reviewers, the [reporting summary](https://www.nature.com/authors/policies/ReportingSummary.pdf), and a cover letter that explains the main improvements included in the revision and responds to any points highlighted in this decision.

As a reminder, please follow the following recommendations:

- * Clearly highlight any amendments to the text and figures to help the reviewers and editors find and understand the changes (yet keep in mind that excessive marking can hinder readability).
- * If you and your co-authors disagree with a criticism, provide the arguments to the reviewer (optionally, indicate the relevant points in the cover letter).
- * If a criticism or suggestion is not addressed, please indicate so in the rebuttal to the reviewer comments and explain the reason(s).
- * Consider including responses to any criticisms raised by more than one reviewer at the beginning of the rebuttal, in a section addressed to all reviewers.
- * The rebuttal should include the reviewer comments in point-by-point format (please note that we provide all reviewers will the reports as they appear at the end of this message).
- * Provide the rebuttal to the reviewer comments and the cover letter as separate files.

We expect that you will be able to resubmit the manuscript within 15 weeks of receiving this message. If this is the case, you will be protected against potential scooping. Otherwise, we will be happy to consider a revised manuscript as long as the significance of the work is not compromised by work published elsewhere or accepted for publication at *Nature Biomedical Engineering*.

We look forward to receive a further revised version of the work. Please do not hesitate to contact me should you have any questions.

Best wishes,

Valeria

Reviewer #1 (Report for the authors (Required)):

The Authors performed an extensive revision of the manuscript, properly addressing almost all of the points raised by the reviewers. A substantial amount of new data and analyses has been added and this improved significantly the quality of study results and conclusions. The newly introduced descriptive and experimental material (including the demonstration of functional vision restoration upon the studied optogenetic approach), supplementary figures and references further supported the working hypothesis and scientific importance of the obtained results.

They don't address some of the comments as they state that existing knowledge of the animal models makes it unnecessary to analyze potential changes induced by the therapy on retinal morphology. Inflammatory responses should also be investigated. This will certainly be part of their future work.

José-Alain Sahel

Reviewer #2 (Report for the authors (Required)):

The authors addressed all my concerns and comments in full by providing new experimental results and revising the text. The revised manuscript was substantially improved. The quality and data representation in Figures were also improved. In addition, the authors demonstrated the possibility of optogenetic hearing in common marmosets, which is crucial for the clinical value of ChReef applicability. Unfortunately, the manuscript contains a major issue. In the checklist, the authors checked two main items:

"The exact sample size (n) for each experimental group/condition, given as a discrete number and unit of measurement"

"A statement on whether measurements were taken from distinct samples or whether the same sample was measured repeatedly"

However, the figure legends for Figure 1, Figure 4, Supplementary Figures 1,2,4,6 contain neither a unit of measurement nor a statement on whether measurements were taken from distinct samples or whether the same sample was measured repeatedly". However, Supplementary Figure 5 contains proper description of both units and repeated measurements.

Furthermore, I have two concerns regarding data and code availability statements:

Data availability statement: The data that support the findings of this study is available from the corresponding authors upon reasonable request.

Code availability statement: The code used for analysis is available from the corresponding authors upon reasonable request.

Why not upload the source data files for Supplementary Figures and the most critical raw dataset to a public repository such as FigShare or Zenodo? This is a great work, but the lack of immediate transparency may complicate the independent reproducibility of the results by other researchers. Do the authors have any concerns regarding sharing the most critical files on public file repositories and providing DOI in the manuscript?

Moreover, I did not see source data files for the figures. I thought providing source files during the review process was mandatory for all Nature journals.

Reviewer #3 (Report for the authors (Required)):

The authors have addressed a number of concerns and added a lot of new analyses to the manuscript. While the manuscript has improved considerably, there are still some remaining questions. It is essential to address these points, given the prominent claims it makes about the breakthrough applications attributed to the new ChReef.

Now that the authors included raw traces in figure 1, it looks like ChReef has overall larger photocurrents, both stationary, but also peak (1e). This notion is also supported by the fact that photocurrent density is almost 5x higher compared to ChRmine, whereas the ratio between stationary and peak photocurrent is improved only 3x (see suppl. Table 1). It is important to address this point and explain this overall improved photocurrent density. Is it due to better membrane trafficking / expression of the opsin? Single channel conductance is ruled out as a candidate mechanism, as it is identical between ChRmine and ChReef (1j). Since this is a biomedical engineering journal, there must be a rigorous explanation and experimental confirmation of the observed effects. As it is now, the community will not get sufficient insight into the actual improvements of the tool itself.

Even though figure 1 has improved, there are still some problems with it. Labels and legends are still inside the plotting area. Especially in panels c and d this is problematic as the horizontal significance lines are inside the range of plotted data points. Another problem is the re-use of the same data in panels b and c (ChRmine and ChReef). Even though the authors indicate that the data are re-plotted, they cannot use them twice for different statistical tests. Either all variants shown in b and c need to be compared against each other in one test, or ChReef and ChRmine data have to be compared to those measurements that were done in the same experimental cohort. The same applies to supplementary tables 1 and 2. It is also

not clear why statistical differences are shown by asterisks in some panels and not in others (e.g. a, d,).

Figure 3: The new behavioral analyses should be shown in the main manuscript (and the typos in the figure caption should be fixed). This would add relevance to the vision restoration aspect of the paper.

The authors now show new experiment with a multichannel optical cochlear LED implant emitting green light used for the first time, which is a major improvement compared to blue light emitting ones. This aspect is important, especially since these LEDs match the action spectrum of ChReef and thus, require less light energy (enabling deeper tissue penetrance). This aspect is highly relevant and should be presented more prominently in the main paper. Related to this, Supplementary fig. 24d is not readable due to low quality.

Figure 4d now shows a comparison of opsin-expressing cells in the cochlea. The density of ChRmine expressing cells appears to be higher on average (approx. 25 vs. 15 GFP+SGNs/1000um²). In the text, it is stated that "Expression of both ChR variants under the control of the human synapsin promotor was found in approximately 75% of the SGNs". This contradicts the plot in panel d – at least if we assume that the total density of SGNs was the same between animals. Or were more cells lost with ChRmine over time, despite initial similar transduction rate?

Figure 5j: it is not obvious in which of the traces there is an objectively measurable response. It looks like we see one single experiment with single trials at different light intensities. The authors state that "auditory responses were observed from 4.7 mW" (is this the 4th line from the bottom?). According to the methods section, "one of the (...) 2 waves (oABR) was reliably visible." What is meant by "reliable", given that I see only one trial? Where is this wave in the 4.7 mW trial and where is it in the ones with higher irradiance?

Except for one t-test in figure 4 g, I could not see any statistical analyses of all the auditory data presented in the entire manuscript (figures 4 and 5 and supplementary figures 18-26). There are many quantitative plots comparing ChRmine and ChReef and various manipulations or expression levels where it remains unclear what the data mean. For example, suppl. fig 18, 19, 21, fig. 4 c, d, h, i, 5 c all need quantitative statistics. If no significant differences are found, p values need to be shown and the reader needs to know why superiority of ChReef over ChRmine may be less pronounced in the auditory system. Along these lines, it looks like there is only a clear difference between ChRmine and ChReef at oABRs evoked with 594 nm.

All the experiments that follow are showing some convincing improvements towards optogenetic hearing restauration in general. However, it remains unclear to what extent this is due to ChReef being superior to ChRmine. All gerbil and marmoset experiments are done exclusively done with ChReef. This needs to be more clearly pointed out by mentioning that they opted for the best opsin/virus combination to realize applications in the auditory system that failed with other constructs previously and that similar results may be achieved with ChRmine using the improved parameters (PHP.S capsid, early virus transduction, green LEDs, etc.).

It is nowhere mention whether ChReef will be made publicly available. Ideally, the authors should deposit the DNA on a public repository, so that the community can benefit from the new tool in an unrestricted way.

Color schemes are not consistent throughout the manuscript. Sometimes, magenta/green, sometimes red/green lookup tables are used. The latter is not recommended due to discrimination of people with impaired color vision.

Version 2:

Decision Letter:

Dear Prof Moser,

Thank you for your revised manuscript, "Efficient and sustained optogenetic control of sensory and cardiac systems", which has been seen by Reviewers #3. In their reports, which you will find at the end of this message, you will see that the reviewer acknowledge the improvements to the work and raise a few additional technical criticisms that we hope you will be able to address. In particular, we would expect that the next version of the manuscript adress in detail factors that helped improve optogenetic control of the auditory system,, and a thorough rewrite of the discussion to highlight the meaning of the results without overselling the proposed tool.

As before, when you are ready to resubmit your manuscript, please [upload](#) the revised files, a point-by-point rebuttal to the comments from all reviewers, the [reporting summary](https://www.nature.com/authors/policies/ReportingSummary.pdf), and a cover letter that explains the main improvements included in the revision and responds to any points highlighted in this decision.

As a reminder, please follow the following recommendations:

* Clearly highlight any amendments to the text and figures to help the reviewers and editors find and understand the changes (yet keep in mind that excessive marking can hinder readability).

* If you and your co-authors disagree with a criticism, provide the arguments to the reviewer (optionally, indicate the relevant points in the cover letter).

* If a criticism or suggestion is not addressed, please indicate so in the rebuttal to the reviewer comments and explain the reason(s).

* Consider including responses to any criticisms raised by more than one reviewer at the beginning of the rebuttal, in a section addressed to all reviewers.

* The rebuttal should include the reviewer comments in point-by-point format (please note that we provide all reviewers will the reports as they appear at the end of this message).

* Provide the rebuttal to the reviewer comments and the cover letter as separate files.

We expect that you will be able to resubmit the manuscript within 12 weeks of receiving this message. If this is the case, you will be protected against potential scooping. Otherwise, we will be happy to consider a revised manuscript as long as the significance of the work is not compromised by work published elsewhere or accepted for publication at *Nature Biomedical Engineering*.

We look forward to receive a further revised version of the work. Please do not hesitate to contact me should you have any questions.

Best wishes,

Valeria

Dr Valeria Caprettini

Senior Editor, *Nature Biomedical Engineering*

Reviewer #3 (Report for the authors (Required)):

After this new round of revisions, some issues remain unaddressed. Contrary to what is stated in the response to my points regarding Figure 5j, no changes were made to the figure panel or the legend. Actually, the legend is misleading. "oABR recordings in a common marmoset resulting in successful activation of the auditory pathway." is not correct. Rather, oABR recordings in a common marmoset resulting FROM successful activation of the auditory pathway is correct. It is still not apparent where the visually detected ABR waves occur in the 4.7 mW trial (or which one the 4.7 mW trial even is). Every trial needs to be labeled with the corresponding radiant flux. The color code is useless. The authors should rather color the non-response trials in one color and the trials showing a response in another color. The response itself needs to be labeled by some kind of indicator (arrow head, etc.), so that it becomes evident to a non-expert reader. The first response, which is clearly visible to me only occurs at around 15.1 mW. For plausibility, the response latencies should also be compared to electrically evoked ones (can be literature values).

The authors also did not seriously address my concern regarding other factors that helped improve optogenetic control of the auditory system. In this study, several factors were optimized compared to their previous work (virus capsids, expression/transduction protocols/light sources) and this needs to be made clear to the reader. The authors mention in their response that they now "communicate the purposeful focus on ChReef for the more demanding studies with gerbils and marmosets". First, I cannot see what has changed in the manuscript from the previous version. Second, the marmoset ABR responses required supra-uJ light energies and are therefore not yet compatible with the microscale green LED emitters. As mentioned above, these aspects need to be critically discussed. The discussion section is currently not worth its title and still reads like an advertisement section with some trivial suggestions on how to improve ChReef. As mentioned in the previous two rounds, the manuscript clearly shows a greatly improved optogenetic approach for stimulating multiple systems. However, the discussion also needs to clearly point out the overall improvements achieved with ChRmine itself, new light sources, new virus serotypes, etc. It also needs to take into account the limitations and discrepancies of the study (just one example: much larger difference in steady-state photocurrent densities between ChRmine and ChReef in NG cells (about 5x) compared to HEK cells (about 2x) and only small differences in the auditory system).

Version 3:

Decision Letter:

Dear Prof Moser,

Thank you for your revised manuscript, "Efficient and sustained optogenetic control of sensory and cardiac systems", which has been seen by Reviewer #3. In their reports, which you will find at the end of this message, you will see that the reviewers acknowledge the improvements to the work and raise a few additional technical criticisms that we hope you will be able to address. In particular, we would expect that the next version of the manuscript could comment in particular on the 4.7mW wave, and to fix the range of stimulation.

As before, when you are ready to resubmit your manuscript, please [upload](#) the revised files, a point-by-point rebuttal to the comments from all reviewers, the [reporting summary](https://www.nature.com/authors/policies/ReportingSummary.pdf), and a cover letter that explains the main improvements included in the revision and responds to any points highlighted in this decision.

As a reminder, please follow the following recommendations:

- * Clearly highlight any amendments to the text and figures to help the reviewers and editors find and understand the changes (yet keep in mind that excessive marking can hinder readability).
- * If you and your co-authors disagree with a criticism, provide the arguments to the reviewer (optionally, indicate the relevant points in the cover letter).
- * If a criticism or suggestion is not addressed, please indicate so in the rebuttal to the reviewer comments and explain the reason(s).
- * Consider including responses to any criticisms raised by more than one reviewer at the beginning of the rebuttal, in a section addressed to all reviewers.
- * The rebuttal should include the reviewer comments in point-by-point format (please note that we provide all reviewers will the reports as they appear at the end of this message).
- * Provide the rebuttal to the reviewer comments and the cover letter as separate files.

We expect that you will be able to resubmit the manuscript within 6 weeks of receiving this message. If this is the case, you will be protected against potential scooping. Otherwise, we will be happy to consider a revised manuscript as long as the significance of the work is not compromised by work published elsewhere or accepted for publication at *Nature Biomedical Engineering*.

We look forward to receive a further revised version of the work. Please do not hesitate to contact me should you have any questions.

Best wishes,

Valeria

Dr Valeria Caprettini

Senior Editor, <http://www.nature.com/nbme> *Nature Biomedical Engineering*

Reviewer #3 (Report for the authors (Required)):

The authors have now labeled the trials in Figure 5j and indicated the ABR waves. They also compare these waves to aABRs from the literature. Thank you.

However, since there is apparently no objective/quantitative way to detect ABR waves, I refuse to believe that the wave in the 4.7 mW trial represents a real signal. I leave it to the editors to decide how to handle this.

Regardless, the statement (line 489-490) "Together, these data prove the principle of nano-Joule and sustained optogenetic stimulation of the rodent and primate auditory pathway,..." is still not correct. $4.7 \text{ mW} \times 1 \text{ ms} = 4.7 \text{ micro joules}$. This is not in the nano-joule range, as stated in the manuscript.

I have criticized these inaccuracies in all rounds of review. But they are still not completely removed from the paper.

There is also an incorrect figure reference in line 481 (Fig. SX) of the newly added text.

Although still quite compact, the discussion has improved considerably.

As a last remark, my criticism was not about underestimating ChRmine. It was about not considering many other factors that have contributed to the general improvement of optogenetics in the auditory system. It is clear that ChReef is a great tool. However, because other factors also improved (more potent viruses, improved light delivery), some of the performance improvement would have been seen with other opsins, as well. There is no harm in discussing this openly.

Version 4:

Decision Letter:

Dear Tobias,

Thank you for your revised manuscript, "Efficient and sustained optogenetic control of sensory and cardiac systems". Having checked your responses to the remaining criticisms, I am pleased to write that we shall be happy to publish the manuscript in *Nature Biomedical Engineering*.

We will be performing detailed checks on your manuscript, and in due course will send you a checklist detailing our editorial and formatting requirements. You will need to follow these instructions before you upload the final manuscript files.

Please do not hesitate to contact me if you have any questions.

Best wishes,

Valeria

Dr Valeria Caprettini

Senior Editor, *Nature Biomedical Engineering*

Version 5:

Decision Letter:

Dear Prof Moser,

I am happy to inform you that your manuscript, "Efficient and sustained optogenetic control of sensory and cardiac systems", has now been accepted for publication in *Nature Biomedical Engineering*.

Over the next few weeks, the figures will be checked for production quality, the text edited to ensure that it conforms to house style, and the manuscript typeset.

Our Articles are published about 40 days after the acceptance date (we recommend that you inform your institutional press office of this timeframe), and you will be notified of the actual publication date a few days in advance. Articles can be published any working day of the week, and are pushed live shortly after 10 am London time.

Publishing agreement. You will be asked to digitally sign a publishing agreement (grant of rights). After the signed publishing agreement has been received, the proofs of the article will be sent to you for review. If you have any queries during the production process, or you cannot meet the requested deadline for returning the proofs, please contact rjsproduction@springernature.com.

Nature Biomedical Engineering is a Transformative Journal. Authors may publish their research with us through the traditional subscription access route, or make their paper immediately open access through payment of an article-processing charge. More information about publication options is available.

You may need to take specific actions to comply with funder and institutional open-access mandates. If the

work described in the accepted manuscript is supported by a funder that requires immediate open access (as outlined, for example, by [Plan S](https://www.springernature.com/gp/open-research/plan-s-compliance)) and your manuscript was originally submitted on or after January 1st 2021, then you should select the gold OA route. Authors selecting subscription publication will need to accept our standard licensing terms (including our [self-archiving policies](https://www.springernature.com/gp/open-research/policies/journal-policies)), and these will supersede any other terms that the author or any third party may assert apply to any version of the manuscript.

Acceptance of your manuscript is conditional on agreement, by all authors, with both our [media embargo](http://www.nature.com/authors/policies/embargo.html) and [confidentiality and pre-publicity](http://www.nature.com/authors/policies/confidentiality.html) policies. In particular, you may arrange your own publicity of the Article (for instance, through your institutional press office), as long as you ensure that journalists strictly adhere to the media embargo.

To assist you in disseminating the work, as soon as the Article is published you will be able to take advantage of the Springer Nature [SharedIt](https://www.springernature.com/gp/researchers/sharedit) initiative to [generate a unique shareable link to the Article](http://authors.springernature.com/share) that will allow anyone (with or without a subscription) to read it. Recipients of the link who are subscribers will also be able to download and print the PDF.

Thank you for having submitted this work to *Nature Biomedical Engineering*.

Best wishes,

Barbara Cheifet
Editor
Nature Biomedical Engineering

Open Access This Peer Review File is licensed under a Creative Commons Attribution 4.0 International License, which permits use, sharing, adaptation, distribution and reproduction in any medium or format, as long as you give appropriate credit to the original author(s) and the source, provide a link to the Creative Commons license, and indicate if changes were made.

In cases where reviewers are anonymous, credit should be given to 'Anonymous Referee' and the source.

The images or other third party material in this Peer Review File are included in the article's Creative Commons license, unless indicated otherwise in a credit line to the material. If material is not included in the article's Creative Commons license and your intended use is not permitted by statutory regulation or exceeds the permitted use, you will need to obtain permission directly from the copyright holder.

To view a copy of this license, visit <https://creativecommons.org/licenses/by/4.0/>

Reviewer #1:

This manuscript presents an original work studying the effects of the channelrhodopsin ChReef, a variant of the ChRmine, in cardiomyocytes for inducing a depolarization block in cardiomyocyte clusters generated from neonatal mouse hearts, rd1 mouse model of retinal dystrophy (responses to optogenetic stimulation of the eye to a green LED or an iPad screen and multielectrode array records from the contralateral primary visual cortex) and auditory system in mice and gerbils (spiral ganglion neurons and cochlear nucleus neurons). The results obtained provide evidence about the potential of the assessed optogenetic tools for modeling in experimental conditions or future clinical therapeutic applications. The improved light sensitivity and the dynamic of responses clearly represent the main advantages of this technology.

We would like to thank the reviewer for the appreciation of our work and the comments that helped us to further improve our manuscript. We have addressed all points, performed additional experiments and added a substantial amount of new data and analysis. We detail our responses to the comments below.

Comments and concerns:

The title “Efficient and sustained optogenetic control of nervous and cardiac systems” could be misleading as the observed effects in the visual and auditory systems still do not cover the entire nervous system.

Thanks for the comment, changed to “Efficient and sustained optogenetic control of sensory and cardiac systems”

In the abstract: “Towards clinical application we used AAV-based gene transfer to express ChReef in the optic nerve where it restores visual function in blind mice”. The retinal ganglion cells (RGC) were targeted and this should be précised in the abstract, moreover, no data about expression in the optic nerve were shown. Such terminology is surprising. The choice of the promoter should be justified, as well as the cell specificity and the ensuing biodistribution in the tissues studied.

We changed abstract as requested to “Towards clinical application we used AAV-based gene transfer to express ChReef in retinal ganglion cells where it restores visual function in blind mice with light sources as weak as an iPad screen.”

Moreover, we performed behavioral experiments that show restoration of vision in blind mice by ChReef expression in the retina.

In response to the comment on the promotor choice, we added a section in the results as well as two supplementary figures proving looking on ChReef expression among other cells in the retina as well as in the whole brain (Fig. S14 and S15). Moreover, we also mention the need for further studies including those aiming at more target cell specificity in the discussion section.

The section “Main or Introduction” could provide more general information about the properties of the bacteriorhodopsin-like cation channelrhodopsin ChRmine that make it suitable as optogenetic therapeutic and a rational basis for engineering of ChRmine variants. A detailed comparison of properties to some recently developed alternative proteins should be provided, e.g., ChR variant, Chloromonas oogamy (CoChR) mutants, CoChR-L112C and CoChR-H94E/L112C/K264T, with markedly enhanced light sensitivity.

We are grateful for this comment and now provide more information about the beneficial properties of the ChRmine variants. The low single-channel conductance of depolarizing ChRs limits their utility, as the required high levels of expression and high light doses bear the risk of proteostatic stress and

phototoxicity in the target tissue. Therefore, a key property, which qualifies ChRmine variants, in particular ChReef, for future optogenetic therapies, namely the comparatively high unitary conductance, is now explicitly mentioned in the introduction. In addition, we provide a detailed comparison to CoChR wt and CoChR-H94E/L112C/K264T (CoChR-3M), which generates bigger photocurrents than other CoChR variants (Ganjawala *et al.*, 2019), in the results section. The photocurrent densities of ChReef and CoChR-3M are comparable (Fig S5), which is in accordance with the enhanced light sensitivity of both. Due to the more red-shifted action spectrum and much faster channel closing kinetics, which reduces the risk of phototoxic effects and enables higher frequency photostimulation, we deem ChReef better suited for future optogenetic treatments than CoChR-3M (Fig S5, Fig S7, Ganjawala *et al.*, 2019).

Discussion:

Despite the use of sophisticated electrophysiological methods and nice illustrations, the manuscript could read more fluently with a more structured presentation of the results. Actually, one should rely mainly on the figures to follow the results and this makes difficult their understanding and interpretation during the reading.

We completely overhauled the manuscript and further improved the reading flow.

Some aspects of the experiments could be presented in more details also in the main text and not only in the methods, some points/questions below:

Has the technology been tested in adult cardiac cells, and in cells types other than myocytes?

The technology of optogenetic stimulation has been tested and demonstrated by us and others many times in adult cardiomyocytes and intact hearts (first: Bruegmann *et al.*, Nature methods 2010, first defibrillation: Bruegmann, Boyle *et al.*, J Clin Invest 2016 and many others). Expression and function of ChReef have so far not been tested in adult cardiac cells. In response to the reviewer's comment we have performed additional experiments with cardiomyocytes derived from human induced pluripotent stem cell (hiPSC) and confirmed the data obtained with neonatal mouse cardiomyocytes (Fig. S13). While those cells do not necessarily offer the phenotype of adult cardiomyocytes, they are a relevant model given their human origin. To test ChReef in adult cardiomyocytes, experiments with transgenic animals would be required or an in vivo gene transfer both of which we deem to be beyond the scope of the current study. We more clearly conveyed the potential impact of the choice of the cellular models in the MS.

Did the rd1 mice treated carry also the Gpr179 mutation ?

No, this strain was tested negative for the Gpr179 mutation (Change *et al.* 2015, PMC4575902).

Have the morphological and functional parameters (eg OCT, ERG) been evaluated before and after treatment (control and transfected animals)?

No – this is a well described mouse line, frequently used in optogenetic vision restoration experiments¹⁻³.

Has the stage of tissue remodeling after photoreceptor degeneration been considered?

Not in detail: we relied on previous characterization⁴⁻⁶ and consider rd1 mice a standard animal model in the field for vision restoration¹⁻³ and use them in a comparable time window.

At what time point after intravitreal injection in vivo was assessed the level of expression (3-4 weeks?)

4-5 weeks

What cells were transduced besides RGCs?

We performed immunohistochemical analysis of the retinas used for the vision restoration experiments. We observe strong expression in the RGCs and inner plexiform layers and sparse expression in cells of the inner and outer nuclear layers (Supplementary Figure 14).

Was a dose ranging in terms of titers tested?

For the presented electrophysiology data for vision restoration only one titer was tested per opsin:

PHP.eB-hsyn-ChRmine-TS-EYFP-ES (1,89E+13 GC/ml, dPCR)

PHP.eB-hsyn-ChReef-TS-EYFP-ES (8,59E+13 GC/ml, dPCR)

A newly added supplementary figure (Supplementary Figure 14a, b) shows that there was no difference between the transduction rate and the two constructs.

For how long did the expression persist in the transfected cells (transgene stability)?

Intravitreal injections were performed 3-4 weeks before the electrophysiological measurements. We added further histological analysis of retina cells as well as brain tissue of animals used for vision restoration experiments (Fig. S15).

Has the immune response in the transfected retinas been considered/evaluated?

No not at this point. We and the field are under the general impression that the immunoprivilege of the retina^{e.g. 7,8} prevents major immune responses to capsid and transgene, yet careful analysis is warranted in follow up studies.

Is it possible to associate the responses in the visual cortex as a result of direct activation of the RGCs expressing AAVPHP.eB carrying either of the EYFP-tagged ChRs under the control of the human synapsin promoter?

To ensure that recorded responses originate from RGCs stimulation we performed additional tissue analysis. Histology of retina cells as well as brain tissue of animals used for vision restoration experiments (Fig. S14 and S15) proof main expression in RGC cells which is why we believe that recorded signal originate from RGCs.

To demonstrate functional vision restoration, this work would benefit of including behavioral studies. Methods such as optokinetic stimulation would be relevant.

Thanks for the advice. We are happy to provide the requested proof on behavioral level. (Supplementary Figure 16)

Reviewer #2 (Report for the authors (Required)):

The authors described an improved version of the very potent and useful channelrhodopsin ChRmine, which was named ChReef. ChReef was shown to have increased unitary conductance and stationary photocurrent due to decreased desensitization. Furthermore, ChReef has faster dark recovery kinetics and off-kinetics compared to its progenitor. Improved biophysical properties were successfully translated in cultured cells and in vivo, enabling its successful applications for optogenetic stimulation of the mouse auditory nerve and vision restoration and outperforming ChRmine under identical conditions. If ChReef performs as described, it will be a valuable addition to the channelrhodopsin family and described in vivo demos may prompt its further validation in vivo and application for therapies. However, I do have several comments, which I believe the authors should be able to address easily.

We would like to thank the reviewer for the appreciation of our work and the comments that helped us to improve our manuscript. We have addressed all points, performed additional experiments and added an substantial amount of new data and analysis. We detail our responses to the comments below.

It is known that optogenetic stimulation may have many undesired artifacts on cellular state and function. The classic example is neuronal activity rebound after neuronal silencing using activation of chloride light-driven pumps in neurons or acidification of neurons during extended activation of fast ChR2 variants. The exact mechanism of side effects from optogenetic activation depends on the ionic species conducted by rhodopsins and their cellular localization (axon vs soma vs dendrites). It is also known that mutations that increase photocurrent can largely change the selectivity of ionic conductance (ChRH and CatCh are classic examples). However, the authors did not even try to discuss the potential mechanism of improved photocurrent and the potential alternation of ion contribution to the photocurrent compared to the parental protein. This aspect might be crucial for proper validation of ChReef safety in vivo. It would be great if the authors could address this point.

We agree to the reviewer that information regarding the conducted ions is of importance and therefore determined ion permeability ratios from the shift of the reversal potential upon ion replacement using the Goldman–Hodgkin–Katz equation (Results, Fig. S8). The ion permeability ratios were not significantly different in ChReef and ChRmine wt (Fig. S8). ChReef is an unselective cation channel ($P_K/P_{Na} \sim 1$) that exhibits a considerable proton conductance ($P_H/P_{Na} \sim 10^5$) and virtually no Ca^{2+} conductance. In regard to ChReef safety validation, we reason that the compared to ChR2 much lower proton and calcium permeability (ChR2: $P_H/P_{Na} \sim 10^6$, $P_{Ca}/P_{Na} \sim 0.15$)⁹ of ChReef reduces a possible risk for adverse effects that may result from Ca^{2+} influx or lowered intracellular pH values, which could occur upon long-term stimulation of the cells.

Based on the histological analysis (resolution and magnification of the provided images are not ideal) ChReef demonstrates some internalization in neurons. This aspect can be crucial since it does not matter what unitary conductance a ChR may have if it is not properly localized to the plasma membrane. I could not find any information on the duration of ChReef expression in vivo. Do the authors observe a higher degree of mislocalization upon longer expression duration? Please comment on the localization of ChReef in vivo and provide high-resolution images of single cells.

We have discussed the points raised by the reviewer.

We added example images of retina ganglion cells clearly showing membrane expression of ChReef (Supplementary Figure: 14d).

Furthermore, we performed line profile analysis in spiral ganglion neurons of mice used for hearing restoration experiments. They clearly prove that ChReef and ChRmine are mainly localized at the cell membrane (Fig. 4c-d).

Overall, the manuscript reads like a technical report, which is very concise and lacks some rationale, specifically in the first two parts of the Results section. The development of ChReef is not described at all. It is hard to follow the logic of the first and second parts of the Results section. The authors refer to Fig. 1a, which presents single and double mutants ChRmine while not mentioning them in the main text when they call this panel for the first time. Even later in the text, the authors did not explain how they arrived at the ChRmine variants that they reported in the manuscript. The statement “Mutations in Helix 6 accelerate open to closed state transition in green algal ChRs¹⁸” is not really helpful for understanding introduced mutations, it was never stated that introduced mutations are in helix 6 of ChRmine. I would recommend revising the manuscript to address the following points: what was the rationale behind introduced mutations? What is the potential mechanism of the increased photocurrent?

We thank the reviewer for the constructive criticism and accordingly provide a more detailed description of the development of ChReef and the potential mechanism in the results part. In our own prior work it was shown that the F219Y mutation in helix 6 and mutations at homologous positions significantly accelerated channel closing in green algal ChRs¹⁰. We investigated the effect of mutations at the homologous position (F219Y) and the adjacent positions (T218L and S220A) to the ChR2 F219Y mutation in the cryptophyte ChR ChRmine. The electrophysiological characterization of the ChRmine mutants showed that the channel closing kinetics of ChRmine F219Y, ChRmine T218L and ChRmine T218L/S220A (ChReef) were similar to the channel closing kinetics of ChRmine wt, whereas ChRmine S220A had slower channel closing kinetics. ChRmine F219Y showed strongly reduced photocurrents. In contrast, the photocurrents of ChRmine T218L, ChRmine S220A and ChReef were considerably bigger than the photocurrent of ChRmine wt. In those mutants, the light dependent inactivation mechanism resembling a substrate inhibition of the partial type was abrogated, desensitization was reduced and, as shown for ChReef, the high-frequency power spectral density component was absent. We therefore hypothesize that the T218L mutation and the S220A mutation accelerate the transition from a low conducting parallel photocycle into the main photocycle, thereby increasing the stationary photocurrent.

The authors presented lots of data on ChReef. However, it is not properly discussed in the manuscript. Please discuss ChReef development, its advantages and limitations compared to its progenitor and other established ChRs, and discuss its performance in vivo and how well it correlates with expected performance based on the measured biophysical parameters in vitro. Provide brief perspectives and outlook for future improvements of ChReef or further characterization/validation.

Done: In response, we have completely overhauled the MS to provide more rationale, guidance and information on the experiments and also expanded the discussion section. The brevity of MS is reinforced by the journal's requirements and we request the editorial team to accommodate the changes implemented on request of the reviewers.

Minor comments:

The authors presented great results on photocurrent profiles for ChRmine and its mutants in Fig S2; why not further characterize rate of desensitization? It seems to be different among the mutants.

We thank the reviewer for the helpful suggestion to further characterize the rate of desensitization, which gave valuable insights that we added to the results part. The photocurrent desensitization kinetics of the ChRmine variants at saturating light intensities could be approximated by a bi-exponential function ($\tau_{DES1} \sim \tau_{off}$, $\tau_{DES2} > 1$ s, Fig. S9). The values of the fast time constants were similar to channel closing kinetics. The relative amplitude factor of the slow time constant, which shows the contribution of a slow process that might reflect the substrate inhibition of the partial type to photocurrent desensitization, was much smaller in ChReef than in ChRmine wt (Fig. S9).

It would be great to have the traces in the main text figure with absolute amplitude rather than normalized, as shown in Fig. S2. Fig S2b,d,f – Y-axis label is missing. If these are normalized values, what was the normalization coefficient, and why should it be normalized?

As suggested by the reviewer, we now show the photocurrent traces in the main text figure (Fig. 1) with absolute amplitude rather than normalized. Fig. S2 b, d, f shows peak normalized values. The figure caption is corrected accordingly. Normalization enables a better visual assessment of the extent of desensitization, the desensitization kinetics and the channel closing kinetics.

Do the authors have any comments on the correlation of the results shown in Supp Fig 11f and Fig. 4o-r?

We increased the number of measurements as well as the analysis for the juxtacellular recordings which now lines up nicely with the measurements in the brain slice physiology.

ChReef is not properly introduced in the main text and further inconsistent naming of the ChReef protein in the manuscript makes it difficult to read the manuscript. For example, in Fig. 1 it is referred to as ChReef (even before it was named later in the text) while in the first and second sections of Results it is referred to as ChRmine/T218L/S220A. Why not simply introduce in the last paragraph of introduction and use it throughout since then (all Figures have it as ChReef anyway).

We thank the reviewer. In the revised manuscript ChReef is as suggested, introduced in the last paragraph of the introduction.

Also, in Fig S2, S4, and S5 there is ChREEF (is it the same with ChReef?).

We corrected the figures accordingly.

I did not find a reference to Fig S1 in the main text.

We now give a reference to Fig S1 (now Fig. S7) in the main text.

“a major driver of progress in the life sciences” – quite an overstatement.

We toned down the statement: “With an ever-growing toolkit of light-sensitive proteins (opsins) and optical devices, optogenetics has driven progress in the life sciences¹¹.”

Reviewer #3 (Report for the authors (Required)):

Review nBME-24-0098

In this manuscript the authors present ChReef, an improved variant of the light-gated cation channel ChRmine. The advantage of ChReef over ChRmine is the low desensitization at largely preserved single-channel conductance and overall kinetics. The stationary photocurrent density is increased approx. by a factor of 4 compared to ChRmine and 2.6 compared to CatCh – an opsin that was previously used by the group for optogenetic manipulation of the cochlea. The authors compare the performance of ChReef and ChRmine in several model systems reaching from cultures of cardiomyocytes to the mouse retina in vivo to the cochlea and auditory brain stem in mice and gerbils. Overall, ChReef shows superior performance compared to ChRmine. Due to the red-shifted action spectrum compared to CatCh, it can still be activated with orange-red light, which presents an additional advantage given that long-wavelength light is less scattered and absorbed in biological tissue. Thus, ChReef is potentially useful for a number of in vivo applications, which are demonstrated in this study. However, a number of concerns remain.

We would like to thank the reviewer for the appreciation of our work and the comments that helped us to improve our manuscript. We have addressed all points, performed additional experiments, and added an substantial amount of new data and analysis. We detail our responses to the comments below.

Major

1. The choice of the mutation sites to generate ChReef is not well explained and does not become apparent. It is not clear why these particular two amino acid exchanges were chosen to generate ChReef. The two mutations do not seem to be related to any of the helix F mutations in the paper cited for the acceleration of closing kinetics (doi: 10.1038/s41467-018-04146-3). The sentence “Next, we aimed to overcome ChRmine desensitization by introducing helix 6 mutations to unleash its potential for life science and medical applications.” does not make sense / is not followed by a reasonable motivation. According to how this paragraph is written, it appears as if the authors aimed for a faster version of ChRmine (again, why exactly those 2 point mutations?), but rather discovered a variant with lower desensitization. The strategy and the rationale need to be better explained. Were only these two mutations made? Were other residues targeted? If not, why did the authors stick to exactly those two mutations?

We thank the reviewer for the constructive criticism and accordingly provide a more detailed description of the development of ChReef in the results part. In our own prior work it was shown that the F219Y mutation in helix 6 and mutations at homologous positions significantly accelerated channel closing in green algal ChRs¹⁰. We investigated the effect of mutations at the homologous position (F219Y) and the adjacent positions (T218L and S220A) to the ChR2 F219Y mutation in the cryptophyte ChR ChRmine. The electrophysiological characterization of the ChRmine mutants showed that the channel closing kinetics of ChRmine F219Y, ChRmine T218L and ChRmine T218L/S220A (ChReef) were similar to the channel closing kinetics of ChRmine wt, whereas ChRmine S220A had slower channel closing kinetics. ChRmine F219Y showed strongly reduced photocurrents. In contrast, the photocurrents of ChRmine T218L, ChRmine S220A and ChReef were considerably bigger than the photocurrent of ChRmine wt. In those mutants, the light dependent inactivation mechanism resembling a substrate inhibition of the partial type was abrogated, desensitization was reduced and, as shown for ChReef, the high-frequency power spectral density component was absent. We therefore hypothesize that the T218L mutation and the S220A mutation accelerate the transition from a low

conducting parallel photocycle into the main photocycle, thereby increasing the stationary photocurrent.

2. In addition, ChRmine mutants with similarly improved desensitization properties were previously reported (doi: 10.1016/j.cell.2022.01.007). One mutant (Y260F, helix 7 or G) showed similarly low desensitization with preserved photocurrent amplitudes. A comparison of ChReef to this mutant and an explanation of the authors' strategy is required to assess the advance of the current tool.

We performed additional experiments with ChRmine Y260F for the comparative assessment of its properties. ChRmine Y260F exhibits considerably smaller photocurrents and slower channel closing kinetics than ChReef (Fig S5).

3. The authors need to show wavelength-dependency of the desensitization. ChRmine does almost not desensitize under red light (doi: 10.1126/science.aaw5202 and 10.1016/j.cell.2022.01.007). Given this low desensitization and the same spectral response of ChRmine and ChReef (suppl. Fig. 1) it is surprising that ChReef performs so much better than ChRmine under red light in Fig. 2e and f. Without a proper spectral characterization of photocurrents, this effect is difficult to explain.

We understand the reviewers' concern. In order to address it, we investigated photocurrent desensitization at different light intensities upon stimulation with green ($\lambda \sim 530$ nm), orange ($\lambda \sim 590$ nm) and red light ($\lambda \sim 632$ nm) (Fig. S10). The photocurrent desensitization kinetics of the ChRmine variants at saturating light intensities could be approximated by a bi-exponential function ($\tau_{DES1} \sim \tau_{off}$, $\tau_{DES2} > 1$ s, Fig. S9). The relative amplitude factor of the slow time constant (τ_{DES2}), which shows the contribution of a slow process that might reflect the substrate inhibition of the partial type to photocurrent desensitization, was much smaller in ChReef than in ChRmine wt (Fig. S9). Photocurrent desensitization generally results from the difference in the distribution of open and closed states in the pre-steady-state (peak current at high intensities) and the steady-state (stationary current). Experiments at suboptimal wavelength ($\lambda \sim 632$ nm) and subsaturating intensities (~ 1 mW/mm²) showed that even at conditions at which, due to asynchronous activation, no peak current could be measured, the stationary photocurrent of ChReef remained elevated (Fig. S11), which indicates a favorable open to closed state distribution in the steady-state that may, as proposed, result from the accelerated transition of the low conducting parallel photocycle into the main photocycle.

About data in figure 2, we would like to point out that we have a different interpretation when looking at the traces in the mentioned paper analyzing the currents of ChRmine also with red light stimulation. We rather see no peak current anymore and only steady state currents similar to low light intensities with blue and green light. Independent of the interpretation and explanation of this observation, the steady state current will play the important role and we carefully checked other potential causes such as different expression rate. The reason that the effect of the higher required light intensity is visible only for red light and not blue/green light is the huge current of both variants making pacing possible with very low light intensities which are rarely above detection threshold (in most cases ~ 10 μ W/mm²). Thus, we lose the sensitivity to detect the differences at such low light intensities. This is enabled for red light since currents are <20% of the currents induced by 510 nm. To clarify this, we changed the wording in the text.

4. The manuscript contains exaggerated claims in many places. For example: - The abstract states "...we used AAV-based gene transfer to express ChReef in the optic nerve where it restores visual function in blind mice". From what I can see, no experiments were done that assess vision. Only responses in V1 were reported. - Keywords include "hearing, vision, cardiac defibrillation".

However, none of these aspects is shown in the paper. These are clearly not keywords of the present study and mislead the reader.

We have toned down the statement in abstract and changed keywords. In addition, we have performed behavioral experiments on vision and now also include immunohistochemical data demonstrating ChReef expression in retinal ganglion cells. Since auditory brainstem responses are a clinically established method to assess hearing, we have refrained from changing the key word “hearing”. Furthermore, we now included two different mouse models of deafness (Fig. 4f) and performed the newly added measurement in gerbils and non-human primates in deafened individuals.

- The same goes for the running title and the last sentence of the intro. No control of “the heart” is shown. Such statements are strongly overselling the content of the paper and are not backed up by the data. In this form the manuscript should not be published.

Thanks for the comment, we have changed the title to “Efficient optogenetic control of sensory pathways and cardiomyocytes” as well as some other sentences.

5. No raw traces/example recordings are shown in figure 1, 3, 5. Furthermore, the entire figure 1 is not very well composed and makes a very provisional impression. The plots are hard to read due to the legends being positioned inside the data area. Particularly bad examples are panel c and e. Additionally, the order of the symbols in the legends is inconsistent (compare c and d). In panels 1c-d the values for ChReef and perhaps other opsins are highly skewed and a comparison of the mean values appears inappropriate. Statistics and plots should take into account the non-normality of the data distribution. In particular in the case of ChReef, a few extreme outliers seem to dominate the mean value. The authors need to perform normality tests on all their data and apply correct statistics accordingly.

We thank the reviewer for the helpful comment. The revised figure 1 now includes raw traces. We revised Figure 1 according to the reviewers suggestions. In order to take into account the non-normality of the data distribution we employed Kruskal-Wallis with a Dunn’s Bonferroni post hoc test for statistical comparisons.

6. Fig. 2: Why was there an irregular electrical stimulation interval used in panel e? The stimulation rhythm changes within the recording and the stimulation frequency is different between the ChRmine and ChReef conditions. Thus, comparison between the two opsins is limited.

a) We thank the reviewer for pointing out the different pacing rates in the example. We stated in the methods that pacing rate was set to be 0.5 Hz above the spontaneous beating rate but did not further mention this in the legends. To clarify this now, we show you the actual pacing rates of all examples below including the information how many of them have been successful:

(first number = successful depolarization block; second number = total number of tested cardiac clusters):

	0.5 Hz	1 Hz	1.5 Hz	2 Hz	2.5 Hz
ChRmine		3/6	4/6	0/2	0/3
ChReef	1/1	9/10	5/5		
ChRmine hIPS		6/19			
ChReef hIPS		18/18			

As you can see, unsuccessful attempts can be found in the case of ChRmine at any pacing rate. We still thought that an example with the same pacing rate would be more representative and less misleading and thus exchanged the example accordingly. Furthermore, we have done experiments in hPSC-derived cardiomyocytes expressing ChRmine and ChReef. Since these have a much lower spontaneous beating rate, all attempts could be performed at the same pacing rate (1 Hz) and we observed the same difference.

b) In regard to the new start of the electrical pacing simultaneous with the start of the continuous light pulse, we chose this way of stimulation since the light will induce an extrabeat when illumination starts after the refractory period of the previous beat. Starting both together, guaranteed that within the time window of 5 s illumination duration, we always tested the same amount of electrical pulses to be able to excite the cardiomyocytes or not.

7. No negative controls are shown anywhere in the paper. Especially the “vision restoration” experiments need a control with no opsin expression. Moreover given the use of PHP.eB viruses in these experiments, expression in other brain regions than the retina needs to be excluded. In general, histology is very limited. The example in panel a suggests that expression density was higher for ChReef. Expression needs to be quantified (see also next point).

We added examples for optical pacing of WT controls in the case of hPSC derived cardiomyocytes as well as representative examples of negative wildtype cells for the conduction block with 510 nm (n=4) and 630 nm (n=1).

We added histological analysis of transduced cells in the retina of ChRmine and ChReef injected mice (Supplementary figure: 14). We do not observe a difference between number of cells transduced between the two groups. Furthermore, we provided an example image of a coronal brain slice of an ChReef injected mouse used for the vision restoration experiments. Despite using PHP.eB we do not observe expression of ChReef in the brain except for RGC axons in the lateral geniculate nucleus and superior colliculus (Supplementary figure: 15).

In addition, we also checked in brains of the Mongolian gerbils used for IC recordings. Here we also do not find GFP expression (Supplementary Figure 22d).

Furthermore, we now included two additional mouse models of deafness to proof ChReef’s potential for optogenetic hearing restoration (Fig. 4f; S18)

8. Fig. 4: According to the methods, it seems that the data shown in panels h-r were obtained from two mice – one of them deafened. What is the purpose and why is this not indicated in the figure or the text? It also seems like deafening was not validated anywhere. I find it quite concerning that at those numbers of animals (n = 2) mixed treatments are used – especially in the case where two opsins are compared. Which mouse was ChReef and which one ChRmine injected? These experiments need to be repeated under proper conditions. In addition, histological characterization is not very conclusive. From Suppl. Fig. 9 it looks like ChReef expression was stronger than ChRmine expression, at least in the left cochlea. Can this explain the difference in performance? What is the number of animals compared? It is not indicated in the legend. This aspect needs to be properly evaluated and quantified. If better expression explains the better performance of ChReef, this is fine, but at this stage, cannot be judged properly.

We thank the reviewer for this comment. We performed additional experiments. Now the figure shows data only from mice expressing ChReef (n=3) and undergoing acute kanamycin treatment inducing

hair cell death. This was done to be sure that the measured response was originating for optical stimulation of SGNs not hair cells.

In addition, we improved our histological analysis for the ChReef and ChRmine comparison and provide a line profile analysis showing no difference in the expression between the two (Fig. 4c).

9. I am very skeptical about figure 5. It does not add any additional value to the manuscript (the relevant information is already in figure 4). It shows neither comparison to ChRmine, to any other opsin, or any auditory stimulation. Panels g-h are not even referred to in the main text. Why are they plotted? It is not explained why different animal numbers were used (5c n = 7, ABR recordings in suppl. fig. 14 n = 5). More importantly, the authors used a PHP.S capsid for viral transduction in neonatal animals. Thus, it is highly likely that the virus spread further into the brain and did not remain local in the cochlea. In fact, this is directly seen in suppl. fig. 11. Here, large photocurrents are observed in cells of the ventral cochlear nucleus. Thus direct light effects in the inferior colliculus from non-cochlear sources cannot be disentangled from those responses originating in the cochlea itself. Also the synaptic recordings in suppl. fig. 11 are problematic, because residual photocurrents and local network effects cannot be excluded. According to suppl. fig. 12 it seems that the virus even spread to the contralateral cochlea. These gerbil experiments weaken the manuscript and should be removed.

Thank you for your feedback. We have carefully reworked this section of results as well as figure 4. This includes data of additional experiments into the revised MS obtained from gerbils and marmosets. We consider this data and extended presentation a very important part of the study: gerbils and marmosets are key species of translational hearing research and the proof of concept achieved in both species is important for preparing clinical trials. We very much hope that the revised MS will convince the reviewer.

For the inferior colliculus recordings in the gerbil, we now moved to stimulations with an LED based multichannel optical cochlear implant first time operating green LEDs. In contrast to prior shown data in mice, recordings in the mid brain allow analysis of the spectral spread of excitation, which is the key advantage of the optical cochlea implant¹². The data shows that stimulation with an optical fiber as well as with the LED implant, spectral spread is comparable to acoustic pure tone stimulation. Furthermore, we now also included data of acutely deafened gerbils, mimicking the future cochlea implant patient.

In reference to this, we would like to apologize that it was not clear that the data from S11 was generated in mice injected with AAV2/9, while the inferior colliculus recordings were performed in Mongolian gerbils injected with PHP.S. To show that the ChR is limited to the spiral ganglion neurons, we provided an additional supplementary figure 22.

Finally, we now also provide proof of principle that our newly developed optogenetic tool is working in a non-human primate model (Fig. 5h-j; S25,26).

Minor

10. It is not clear why closing kinetics of 30 ms are reported in the abstract and discussion. The fastest off kinetics reported for ChReef are between 50 and 60 ms (Suppl. Fig. 4 and suppl. tables 1 and 2).

We thank the reviewer for making us aware of the missing description of our measurements at 36 °C, from which the closing kinetics of ~30 ms (35 ± 3 ms, n=6) was derived. We added the missing information to the results part.

11. Fig. 2: The legend states that 625 nm was used for photostimulation. However, given the optical filters used in this experiment, the light emitted from a 625 nm LED that reached the cells was between 626 and 644 nm. This is relevant with regard to the low desensitization of ChRmine in this wavelength range and therefore requires proper spectral characterization of the photocurrents as stated under main point 2.

We agree with the reviewer's remark and have changed the wavelength accordingly.

12. Fig. 4.: The caption mentions radiant flux in mW, but the legend is given in uJ

Thanks for spotting: changed to radiant energy in caption.

13. Suppl. Fig. 4.: why are data points missing? Is this due to absence of currents at the reversal wavelength? If so, why is this not an issue with ChRmine photocurrents?

The missing τ_{off} values are close to the reversal potential. As the photocurrent close to the reversal potential is small, the quality of the mono-exponential fits was compromised by suboptimal signal-to-noise ratios. In revised Figure S4 (now Fig. S6), we accordingly removed the τ_{off} value of ChRmine wt at 0 mV.

14. Suppl. fig. 8: why are the red lines in drawn over the data?

Thanks for spotting this. We reworked the figure.

Suppl. Fig. 11.: "AVCN" nowhere defined

Thanks for spotting this. The figure caption now includes a definition of the anteroventral cochlear nucleus.

References

1. Cehajic-Kapetanovic, J. *et al.* Restoration of Vision with Ectopic Expression of Human Rod Opsin. *Current biology : CB* **25**, 2111–22 (2015).
2. Berry, M. H. *et al.* Restoration of high-sensitivity and adapting vision with a cone opsin. *Nature Communications* **10**, 1221 (2019).
3. Lagali, P. S. *et al.* Light-activated channels targeted to ON bipolar cells restore visual function in retinal degeneration. *Nat Neurosci* **11**, 667–675 (2008).
4. Strettoi, E. & Pignatelli, V. Modifications of retinal neurons in a mouse model of retinitis pigmentosa. *Proc. Natl. Acad. Sci. U.S.A.* **97**, 11020–11025 (2000).

5. Strettoi, E., Porciatti, V., Falsini, B., Pignatelli, V. & Rossi, C. Morphological and functional abnormalities in the inner retina of the rd/rd mouse. *J. Neurosci.* **22**, 5492–5504 (2002).
6. Strettoi, E., Pignatelli, V., Rossi, C., Porciatti, V. & Falsini, B. Remodeling of second-order neurons in the retina of rd/rd mutant mice. *Vision Res.* **43**, 867–877 (2003).
7. Maguire, A. M. *et al.* Safety and efficacy of gene transfer for Leber’s congenital amaurosis. *New England Journal of Medicine* **358**, 2240–2248 (2008).
8. Bennett, J. *et al.* AAV2 gene therapy readministration in three adults with congenital blindness. *Sci Transl Med* **4**, 120ra15 (2012).
9. Kleinlogel, S. *et al.* Ultra light-sensitive and fast neuronal activation with the Ca²⁺-permeable channelrhodopsin CatCh. *Nat Neurosci* **14**, 513–518 (2011).
10. Mager, T. *et al.* High frequency neural spiking and auditory signaling by ultrafast red-shifted optogenetics. *Nat Commun* **9**, 1750 (2018).
11. Emiliani, V. *et al.* Optogenetics for light control of biological systems. *Nat Rev Methods Primers* **2**, 1–25 (2022).
12. Dieter, A., Duque-Afonso, C. J., Rankovic, V., Jeschke, M. & Moser, T. Near physiological spectral selectivity of cochlear optogenetics. *Nature Communications* **10**, 1962 (2019).

Reviewer #1 (Report for the authors (Required)):

The Authors performed an extensive revision of the manuscript, properly addressing almost all of the points raised by the reviewers. A substantial amount of new data and analyses has been added and this improved significantly the quality of study results and conclusions. The newly introduced descriptive and experimental material (including the demonstration of functional vision restoration upon the studied optogenetic approach), supplementary figures and references further supported the working hypothesis and scientific importance of the obtained results.

They don't address some of the comments as they state that existing knowledge of the animal models makes it unnecessary to analyze potential changes induced by the therapy on retinal morphology. Inflammatory responses should also be investigated. This will certainly be part of their future work.

José-Alain Sahel

We would like to thank Professor Sahel for appreciating the work and the revisions and his advice that helped us to improve the manuscript. We understand the need for further studies in the future and take strong motivation from his encouragement.

Reviewer #2 (Report for the authors (Required)):

The authors addressed all my concerns and comments in full by providing new experimental results and revising the text. The revised manuscript was substantially improved. The quality and data representation in Figures were also improved. In addition, the authors demonstrated the possibility of optogenetic hearing in common marmosets, which is crucial for the clinical value of ChReef applicability.

We would like to thank the reviewer for appreciating the work and the revisions and his advice that helped us to improve the manuscript. We have carefully addressed the additional points raised during re-review: please see our point-per-point response below and the revised MS.

Unfortunately, the manuscript contains a major issue. In the checklist, the authors checked two main items: "The exact sample size (n) for each experimental group/condition, given as a discrete number and unit of measurement", "A statement on whether measurements were taken from distinct samples or whether the same sample was measured repeatedly". However, the figure legends for Figure 1, Figure 4, Supplementary Figures 1,2,4,6 contain neither a unit of measurement nor a statement on whether measurements were taken from distinct samples or whether the same sample was measured repeatedly". However, Supplementary Figure 5 contains proper description of both units and repeated measurements.

We now reworked the indicated sections and added information on the unit of measurement and statements on whether measurements were taken from distinct samples or whether they were measured repeatedly.

Furthermore, I have two concerns regarding data and code availability statements: Data availability statement: The data that support the findings of this study is available from the corresponding authors upon reasonable request. Code availability statement: The code used for analysis is available from the corresponding authors upon reasonable request. Why not upload the source data files for Supplementary Figures and the most critical raw dataset to a public repository such as FigShare or Zenodo? This is a great work, but the lack of immediate transparency may complicate the independent reproducibility of the results by other researchers. Do the authors have any concerns regarding sharing the most critical files on public file repositories and providing DOI in the manuscript? Moreover, I did

not see source data files for the figures. I thought providing source files during the review process was mandatory for all Nature journals.

We agree with the concerns of the reviewer and now uploaded data and code on Zenodo to follow the idea of open science. The information can be found under the following doi: [10.5281/zenodo.13963753](https://doi.org/10.5281/zenodo.13963753)

Reviewer #3 (Report for the authors (Required)):

The authors have addressed a number of concerns and added a lot of new analyses to the manuscript. While the manuscript has improved considerably, there are still some remaining questions. It is essential to address these points, given the prominent claims it makes about the breakthrough applications attributed to the new ChReef.

We would like to thank the reviewer for appreciating the work and the revisions and the advice that helped us to improve the manuscript. We have carefully addressed the additional points raised during re-review: please see our point-per-point response below and the revised MS.

Now that the authors included raw traces in figure 1, it looks like ChReef has overall larger photocurrents, both stationary, but also peak (1e). This notion is also supported by the fact that photocurrent density is almost 5x higher compared to ChRmine, whereas the ratio between stationary and peak photocurrent is improved only 3x (see suppl. Table 1). It is important to address this point and explain this overall improved photocurrent density. Is it due to better membrane trafficking / expression of the opsin? Single channel conductance is ruled out as a candidate mechanism, as it is identical between ChRmine and ChReef (1j). Since this is a biomedical engineering journal, there must be a rigorous explanation and experimental confirmation of the observed effects. As it is now, the community will not get sufficient insight into the actual improvements of the tool itself.

We thank the reviewer for raising this point. Given the variability of the data shown in Fig. 1a and Fig. 1b, we deemed the observation that the photocurrent density of ChReef-TS-EYFP-ES in NG cells is 4.5x higher compared to ChRmine-TS-EYFP-ES, whereas the stationary-to-peak-ratio is improved only 2.8x of minor relevance. In order to address the reviewer's comment, we have performed additional experiments in which we compared the plasma membrane targeted expression of ChRmine-TS-EYFP-ES and ChReef-TS-EYFP-ES in NG cells (Fig S7). From the fluorescence line profile analysis and the quantification of the average fluorescence within the cells by the determination of CPCF/area values as described in the materials and methods section, it becomes apparent that there is no considerable difference in plasma membrane targeted expression of ChReef and ChRmine in NG cells (Fig S7). We now provide this important finding in the main text.

Even though figure 1 has improved, there are still some problems with it. Labels and legends are still inside the plotting area. Especially in panels c and d this is problematic as the horizontal significance lines are inside the range of plotted data points. Another problem is the re-use of the same data in panels b and c (ChRmine and ChReef). Even though the authors indicate that the data are re-plotted, they cannot use them twice for different statistical tests. Either all variants shown in b and c need to be compared against each other in one test, or ChReef and ChRmine data have to be compared to those measurements that were done in the same experimental cohort. The same applies to supplementary tables 1 and 2. It is also not clear why statistical differences are shown by asterisks in some panels and not in others (e.g. a, d,).

We thank the reviewer for the helpful comments and accordingly provide a revised version of Figure 1. In panel b of the revised Fig. 1, we now provide a statistical comparison of all ChR variants, which were previously shown in panels 1b and 1c. Supplementary Table 1 shows the comparison (Stationary-

Peak-Ratio, EC₅₀ values, stationary current densities and τ_{off} values in NG cells) of the optimized ChRmine variants to ChRmine wt. Supplementary Table 2 shows the comparison (stationary current densities and τ_{off} values in NG cells) of the best ChRmine variant (ChReef) to other state-of-the-art ChRs.

Figure 3: The new behavioral analyses should be shown in the main manuscript (and the typos in the figure caption should be fixed). This would add relevance to the vision restoration aspect of the paper.

We appreciate that the reviewer acknowledges the value of this new data. As advised, we have added behavioral data to the vision restoration figure.

The authors now show new experiment with a multichannel optical cochlear LED implant emitting green light used for the first time, which is a major improvement compared to blue light emitting ones. This aspect is important, especially since these LEDs match the action spectrum of ChReef and thus, require less light energy (enabling deeper tissue penetrance). This aspect is highly relevant and should be presented more prominently in the main paper. Related to this, Supplementary fig. 24d is not readable due to low quality.

Done, we appreciate that the reviewer acknowledges the value of this new data. We also updated figure 24d allowing better readability.

Figure 4d now shows a comparison of opsin-expressing cells in the cochlea. The density of ChRmine expressing cells appears to be higher on average (approx. 25 vs. 15 GFP+SGNs/1000 μm^2). In the text, it is stated that “Expression of both ChR variants under the control of the human synapsin promotor was found in approximately 75% of the SGNs”. This contradicts the plot in panel d – at least if we assume that the total density of SGNs was the same between animals. Or were more cells lost with ChRmine over time, despite initial similar transduction rate?

We were able to analyze some additional cochleae to check for the reviewer’s concerns. We observe a difference when comparing transduction rate per SGNs of ChRmine and ChReef, but only in the mid turn of the cochlea. We indicate this in the main figure and changed the text accordingly.

Figure 5j: it is not obvious in which of the traces there is an objectively measurable response. It looks like we see one single experiment with single trials at different light intensities. The authors state that “auditory responses were observed from 4.7 mW” (is this the 4th line from the bottom?). According to the methods section, “one of the (...) 2 waves (oABR) was reliably visible.” What is meant by “reliable”, given that I see only one trial? Where is this wave in the 4.7 mW trial and where is it in the ones with higher irradiance?

We have now also mentioned in the legend that each trace is the average of 1000 trials (was in the methods and is standard in the field). Moreover, we have connected the numbers to respective traces for ease of orientation. Visual detection of ABR waves is still the standard of the field and reliable refers to the fact that the same wave can be found across suprathreshold traces where its latency typically gets shorter as the intensity increases.

Except for one t-test in figure 4 g, I could not see any statistical analyses of all the auditory data presented in the entire manuscript (figures 4 and 5 and supplementary figures 18-26). There are many quantitative plots comparing ChRmine and ChReef and various manipulations or expression levels where it remains unclear what the data mean. For example, suppl. fig 18, 19, 21, fig. 4 c, d, h, i, 5 c all need quantitative statistics. If no significant differences are found, p values need to be shown and the reader needs to know why superiority of ChReef over ChRmine may be less pronounced in the auditory system. Along these lines, it looks like there is only a clear difference between ChRmine and ChReef at oABRs evoked with 594 nm.

The reviewer has correctly concluded from our presentation of the data at 594 nm: this is exactly what we aimed to convey. We now added p values for all indicated figures.

All the experiments that follow are showing some convincing improvements towards optogenetic hearing restoration in general. However, it remains unclear to what extent this is due to ChReef being superior to ChRmine. All gerbil and marmoset experiments are done exclusively done with ChReef. This needs to be more clearly pointed out by mentioning that they opted for the best opsin/virus combination to realize applications in the auditory system that failed with other constructs previously and that similar results may be achieved with ChRmine using the improved parameters (PHP.S capsid, early virus transduction, green LEDs, etc.).

As the reviewer correctly pointed out, we consider the demonstration of sub- μ J thresholds for ChReef and ChRmine an important finding that better matches the radiant flux levels available from microscale emitters such as the green LEDs in this study. ChReef tended to allow still lower thresholds which was significant for 594 nm. We have followed the advice of the reviewer to communicate the purposeful focus on ChReef for the more demanding studies with gerbils and marmoset.

It is nowhere mention whether ChReef will be made publicly available. Ideally, the authors should deposit the DNA on a public repository, so that the community can benefit from the new tool in an unrestricted way.

Absolutely, we will reposit it at Addgene.

Color schemes are not consistent throughout the manuscript. Sometimes, magenta/green, sometimes red/green lookup tables are used. The latter is not recommended due to discrimination of people with impaired color vision.

We thank the reviewer for this comment. We now changed the look up table to magenta/ green for all provided histology.

Reviewer #3:

After this new round of revisions, some issues remain unaddressed. Contrary to what is stated in the response to my points regarding Figure 5j, no changes were made to the figure panel or the legend. Actually, the legend is misleading. "oABR recordings in a common marmoset resulting in successful activation of the auditory pathway." is not correct. Rather, oABR recordings in a common marmoset resulting FROM successful activation of the auditory pathway is correct. It is still not apparent where the visually detected ABR waves occur in the 4.7 mW trial (or which one the 4.7 mW trial even is). Every trial needs to be labeled with the corresponding radiant flux. The color code is useless. The authors should rather color the non-response trials in one color and the trials showing a response in another color. The response itself needs to be labeled by some kind of indicator (arrow head, etc.), so that it becomes evident to a non-expert reader. The first response, which is clearly visible to me only occurs at around 15.1 mW. For plausibility, the response latencies should also be compared to electrically evoked ones (can be literature values).

We would like to apologize. We by now realized that the uploaded file did not include the final version of the figure which we prepared for revision round 2. We have now labelled each individual trace in the colors, as requested by the reviewer, with its correspondent radiant flux. We have added graphical aids to highlight ABR waves. As we are not aware of any published work describing electrically evoked ABRs we have chosen to present the latencies of the waves as a function of radiant flux, compared to acoustically evoked ABRs from the literature (Harada & Tokuriki, 1997; doi: 10.1292/jvms.59.561) in supplementary figure 25.

The authors also did not seriously address my concern regarding other factors that helped improve optogenetic control of the auditory system. In this study, several factors were optimized compared to their previous work (virus capsids, expression/transduction protocols/light sources) and this needs to be made clear to the reader. The authors mention in their response that they now "communicate the purposeful focus on ChReef for the more demanding studies with gerbils and marmosets". First, I cannot see what has changed in the manuscript from the previous version. Second, the marmoset ABR responses required supra-ul light energies and are therefore not yet compatible with the microscale green LED emitters. As mentioned above, these aspects need to be critically discussed. The discussion section is currently not worth its title and still reads like an advertisement section with some trivial suggestions on how to improve ChReef. As mentioned in the previous two rounds, the manuscript clearly shows a greatly improved optogenetic approach for stimulating multiple systems. However, the discussion also needs to clearly point out the overall improvements achieved with ChRmine itself, new light sources, new virus serotypes, etc. It also needs to take into account the limitations and discrepancies of the study (just one example: much larger difference in steady-state photocurrent densities between ChRmine and ChReef in NG cells (about 5x) compared to HEK cells (about 2x) and only small differences in the auditory system).

We have revised and extended the discussion following the advice of the reviewer and are thankful for the help with improving the manuscript.

However, we respectfully disagree with the statements of the reviewer that suggest we did not carefully compare ChReef to ChRmine, underestimate ChRmine and overemphasize ChReef's utility. First of all, as shown in Figure 1 and stated throughout the MS, we recognize the relatively large single channel conductance of ChRmine and the ChRmine mutant ChReef described here, as beneficial for the various applications including the ones in the present MS. We have introduced the landmark study of Marshell et al., 2019 discovering, characterizing and applying ChRmine very prominently as the starting point for our work. Second, we have carefully compared the two ChRs by using the same experimental approach in parallel experiments (e.g. cells, same virus, promoter, experimental set-up

etc.). This way, we scrutinized differences in photocurrents and in the applications of ChRmine and ChReef to cardiomyocytes, retina and cochlea, which we largely attribute to the reduced desensitization of ChReef.

In regard to the statement that the marmoset experiments are not a proper comparison between ChReef and ChRmine, we would like to further clarify on this point: First, we consider the marmoset experiment as preliminary, as stated in the manuscript, and has yet to be further optimized. Second, given the ethical considerations of working with non-human primates we focused on the improved ChR variant, and reported the successful case along with the challenges of moving from rodents to primates.

Reviewer 3

The authors have now labeled the trials in Figure 5j and indicated the ABR waves. They also compare these waves to aABRs from the literature. Thank you.

We thank the reviewer for the appreciation of the work and continued effort.

However, since there is apparently no objective/quantitative way to detect ABR waves, I refuse to believe that the wave in the 4.7 mW trial represents a real signal. I leave it to the editors to decide how to handle this.

As mentioned before, this is a subjective analysis and done here by several observers. To please the reviewer we have removed the asterisk from the 4.7 mW trace and now state the threshold to be ≤ 6.2 mW (≤ 6 μ J).

Regardless, the statement (line 489-490) "Together, these data prove the principle of nano-Joule and sustained optogenetic stimulation of the rodent and primate auditory pathway,..." is still not correct. $4.7 \text{ mW} \times 1 \text{ ms} = 4.7$ micro joules. This is not in the nano-joule range, as stated in the manuscript. This has now been specified accordingly.

"Together, these data prove the principle of nano-Joule and sustained optogenetic stimulation of the **rodent auditory pathway (micro-Joule for the preliminary primate report)**, capitalizing on the comparatively high single-channel conductance and sustained photocurrents of ChReef."

I have criticized these inaccuracies in all rounds of review. But they are still not completely removed from the paper.

There is also an incorrect figure reference in line 481 (Fig. SX) of the newly added text.

done

Although still quite compact, the discussion has improved considerably.

As a last remark, my criticism was not about underestimating ChRmine. It was about not considering many other factors that have contributed to the general improvement of optogenetics in the auditory system. It is clear that ChReef is a great tool. However, because other factors also improved (more potent viruses, improved light delivery), some of the performance improvement would have been seen with other opsins, as well. There is no harm in discussing this openly.

We have no problem discussing things openly as the reviewer might have realized but needed to deal with the word limit imposed by the journal. So, we thank the reviewer for letting us elaborate further. In response to the reviewer's comment, we have added the following section:

"We note that optical SGN thresholds also depend on the level of plasma membrane expression of the ChR achieved. This is co-determined by the time point, route and dose of viral vector administration as well as the choice of vector and promoter and last not least, the membrane targeting of the ChR. This study found lower (nano-Joule) thresholds in three rodent models of deafness (mouse: ototoxic and genetic, gerbil: ototoxic) with two different AAVs (mouse: AAV2/9, gerbil: AAV.PHP.S) applied early postnatally with a doses of $\sim 3\text{-}7 \times 10^{13}$ viral genomes achieving expression rates similar to previous studies employing similar titers of other powerful vectors AAV2/6, AAV-PHP.B and AAV-PHP.eB and the same human synapsin promoter^{14,18,40,42}. Like in previous studies^{14,40,42} we employed Kir2.1 sequences to improve the membrane targeting. Together, we conclude that the lower thresholds are primarily caused by the favorable properties of ChReef rather than by differences in the AAV-mediated gene transfer."

Efficient and sustained optogenetic control of sensory and cardiac systems

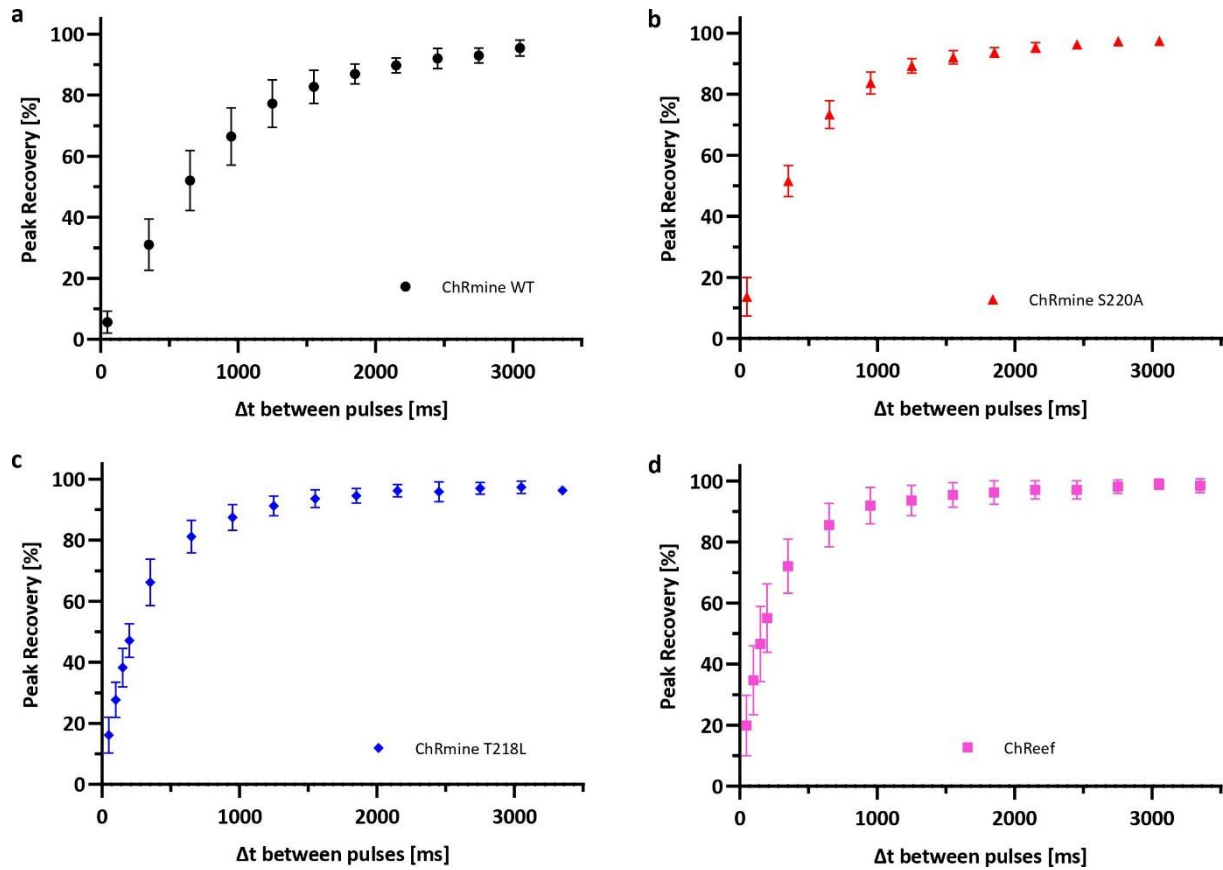
In the format provided by the
authors and unedited

Supplementary Material

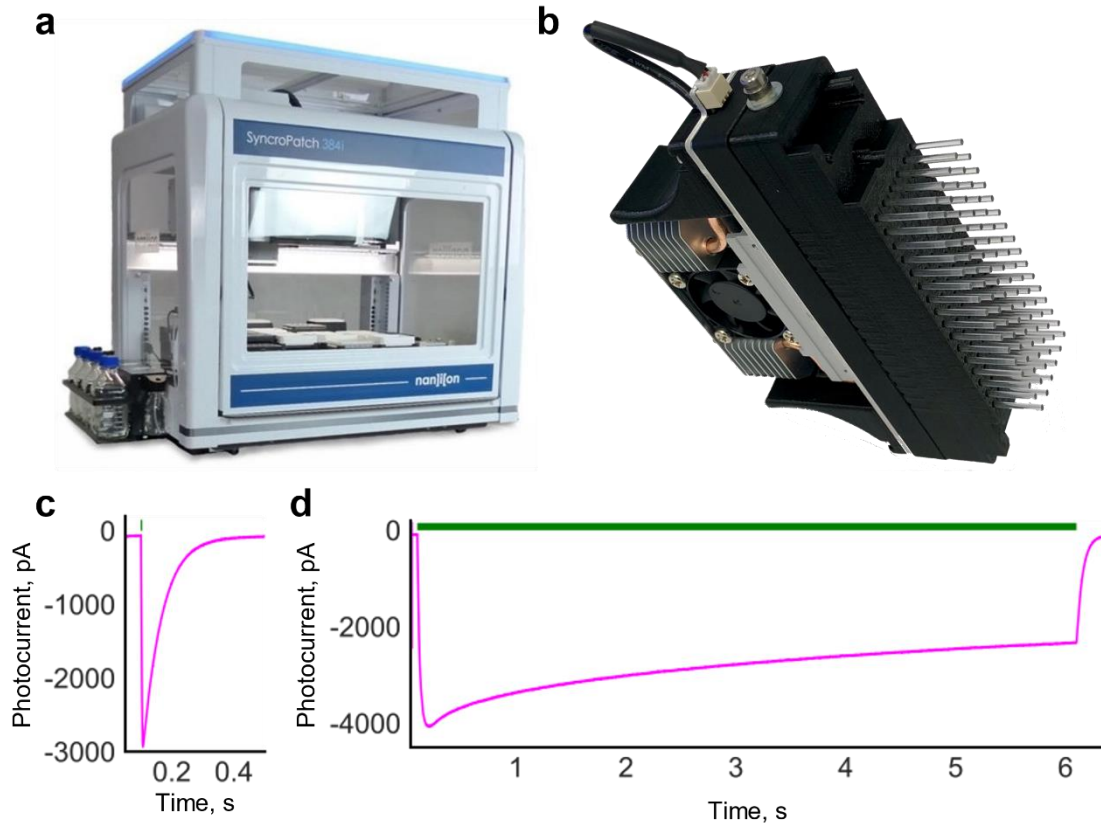
List of supplementary material:

1. Supplementary Figure 1: Peak recovery of ChRmine variants.
2. Supplementary Figure 2. Automated photocurrent measurements.
3. Supplementary Figure 3: Noise analysis of ChReef and ChRmine photocurrents.
4. Supplementary Figure 4: Voltage dependence of closing kinetics of ChRmine variants.
5. Supplementary Figure 5: Subcellular localization of ChRmine and ChReef in NG cells
6. Supplementary Figure 6: Action spectra of ChRmine wt and ChReef.
7. Supplementary Figure 7: Assessment of relative permeabilities of ChRmine and ChReef.
8. Supplementary Figure 8: Dependence of photocurrents of NG cells expressing ChRmine and ChReef on the intensity of light of different colors.
9. Supplementary Figure 9: Comparison of photocurrent densities of HEK293T cells expressing ChReef and ChRmine in response to red light of different intensities.
10. Supplementary Figure 10 Optical pacing and depolarization block of hIPS-derived CM clusters.
11. Supplementary Figure 11: ChReef expression in other brain regions in animals for vision restoration experiments
12. Supplementary Figure 12: Characterization of oABR P1-N1 amplitudes among stimulation with 594nm.
13. Supplementary Figure 13: Immunohistochemical analysis of ChReef expression in the AAV-injected gerbil cochlea.
14. Supplementary Figure 14: Inferior colliculus recordings in ChReef-injected Mongolian gerbils.
15. Supplementary Figure 15: Temporal resolution of optogenetic activation of the auditory pathway by means of inferior colliculus recordings in Mongolian gerbils.
16. Supplementary Figure 16: Comparison of oABR from Figure 5 and published aABR data.
17. Supplementary Figure 17: Quantification of hair cell loss following deafening of the injected left side in the common marmoset.
18. Supplementary Table 1. Stationary-Peak-Ratio, EC_{50} values, stationary current densities and τ_{off} values of ChRmine variants.
19. Supplementary Table 2. Stationary current densities and τ_{off} values of ChR variants.
20. Supplementary Table 3. Exact (Mann-Whitney U-test) and adjusted (Bonferroni) p-values from the Figure 1a.
21. Supplementary Table 4. Exact (Mann-Whitney U-test) and adjusted (Bonferroni) p-values from the Figure 1b.
22. Supplementary Table 5. Exact (Student's t-test) and adjusted (Bonferroni) p-values from the Figure 1c.
23. Supplementary Table 6. Exact p-values (Tukey's HSD test) from the Figure 1i.
24. Supplementary Table 7. List of primers used for ChRmine mutant generation.
25. Supplementary Table 8. Solutions used for acute slice in vitro electrophysiology.
26. Supplementary Table 9. Exact (Mann-Whitney U-test) and adjusted (Bonferroni) p-values from the Figure 5b.
27. Supplementary Table 10. Exact (Mann-Whitney U-test) and adjusted (Bonferroni) p-values from the Figure 5c.

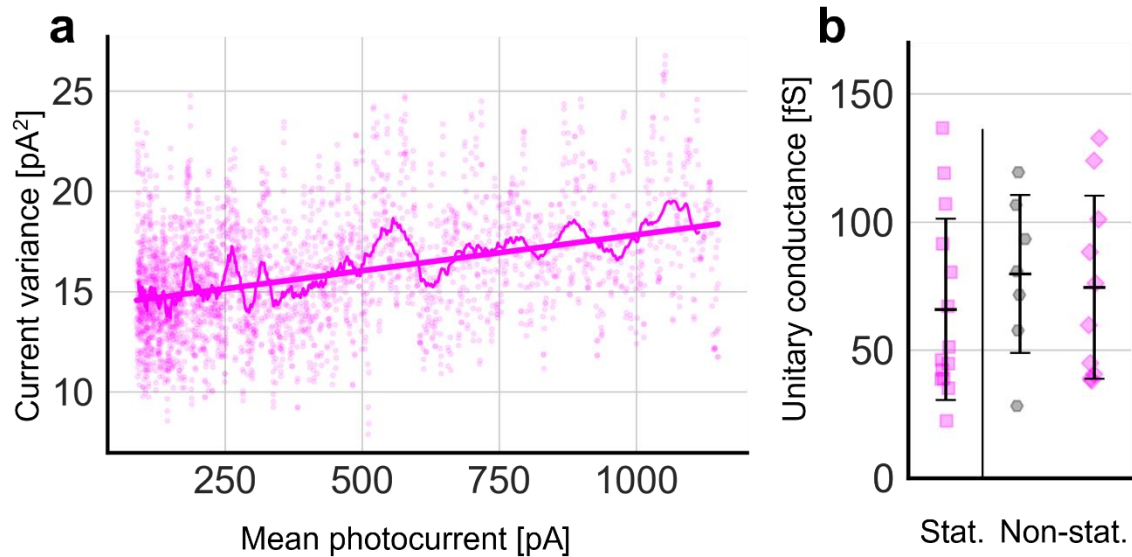
28. Supplementary Table 11. Exact p-values (Tukey's HSD test) from the Supplementary Figure 5d.



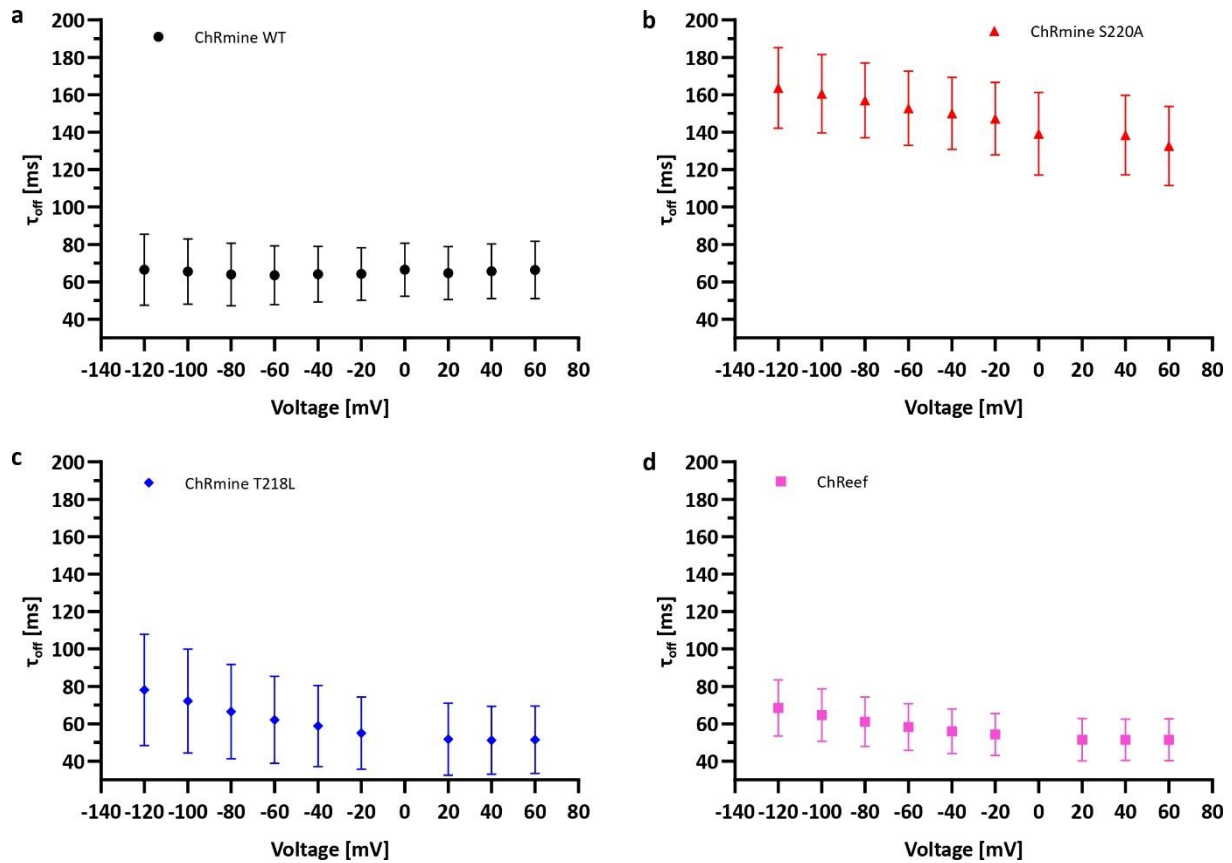
Supplementary Figure 1: Peak recovery of ChRmine variants. NG cells transiently transfected with **(a)** ChRmine WT (black circle, $n=4$), **(b)** ChRmine S220A (red triangle, $n=4$), **(c)** ChRmine T218L (blue rhombus, $n=5$) and **(d)** ChReef (magenta square, $n=5$) were investigated by whole-cell patch-clamp recordings at a membrane potential of -60 mV. Photocurrents were measured upon illumination with two subsequent 3 s light pulses of a wavelength of $\lambda=532$ nm at a light intensity of 23 mW/mm² with a varying time between the light pulses (Δt between pulses, ms). Peak recovery was calculated as the quotient of the difference between the peak and stationary current of pulse two ($I_{p2}-I_{s2}$) and peak and stationary current of pulse one ($I_{p1}-I_{s1}$) in %. The symbols indicate the mean, error bars show SD, n indicates the number of measured cells.



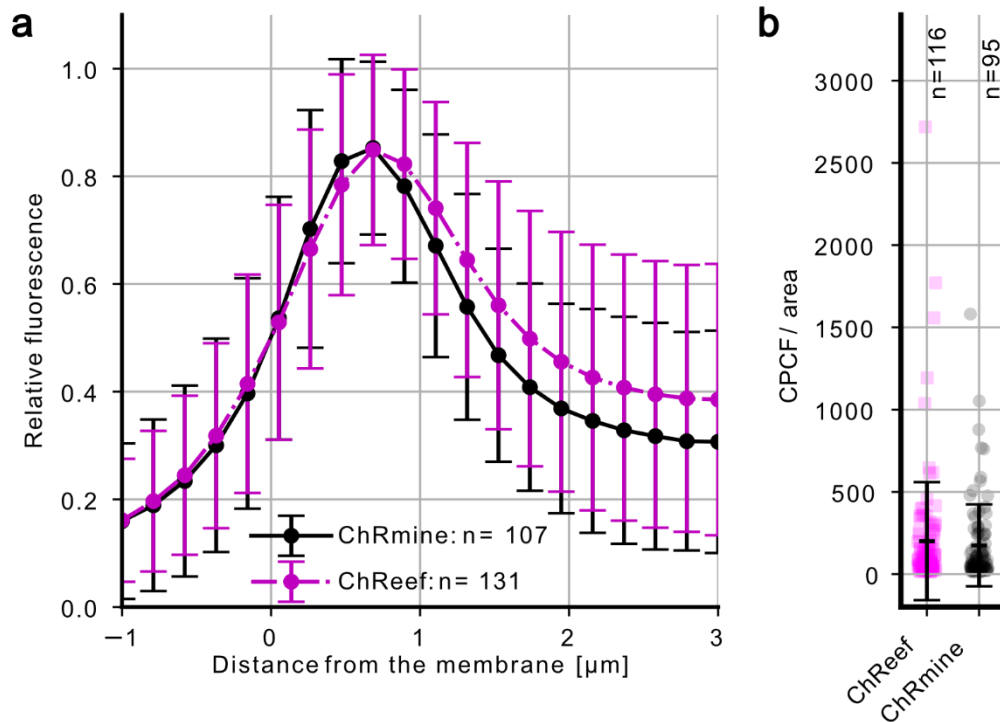
Supplementary Figure 2. Automated photocurrent measurements. **a**, Picture showing the high-performance automated patch-clamp system SyncroPatch384 (Nanion) **b**, Picture showing the illumination unit (Nanion), which comprises 96 LEDs coupled to 96 individual light fibers and a cooling system with a fan. **c**, Exemplary ChReef photocurrent at a membrane potential of -100 mV evoked by a 5-ms green light pulse, which was used for non-stationary noise analysis. **d**, Exemplary ChReef photocurrent at a membrane potential of -100 mV evoked by a 6-s green light pulse, which was used for stationary noise analysis.



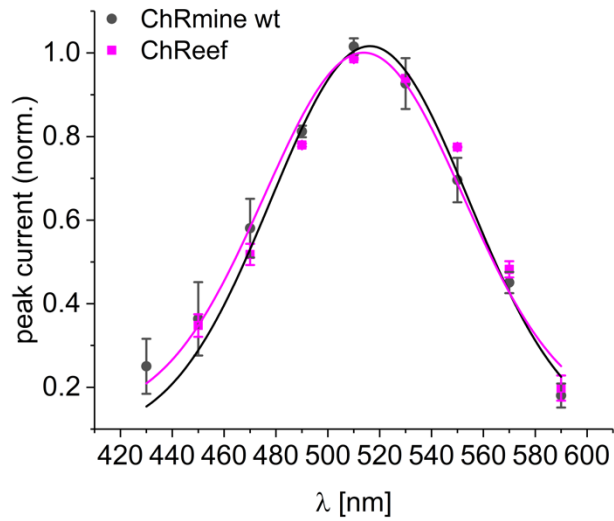
Supplementary Figure 3. Noise analysis of ChReef and ChRmine photocurrents **a**, Non-stationary noise analysis of ChReef. Exemplary plot showing the relation between the variance of the photocurrent and its average value. The photocurrents were measured in automated whole-cell patch-clamp experiments at a membrane potential of -60 mV. The thin line shows the moving average of the variance. The bold line indicates a linear fit. **b**, Statistical comparison of single channel conductance values at a membrane potential of -60 mV. The single channel conductance values of ChReef (magenta diamonds, $n=10$) and ChRmine (grey hexagons, $n=7$) derived from non-stationary noise analysis are shown on the right. On the left side the single channel conductance value of ChReef (magenta squares, $n=14$) derived from stationary noise analysis is shown. n indicates the number of measured cells.



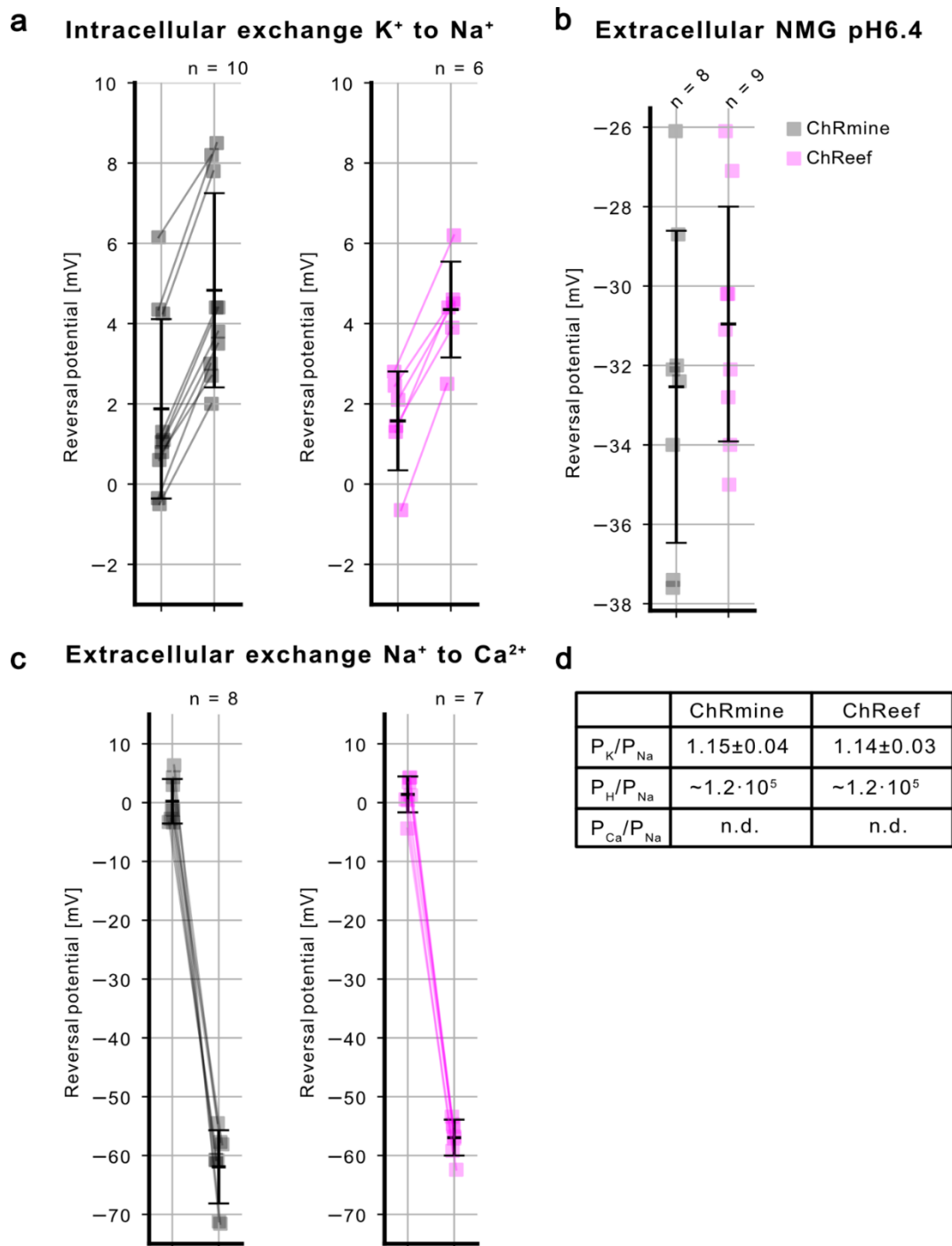
Supplementary Figure 4: Voltage dependence of closing kinetics of ChRmine variants. NG cells transiently transfected with ChRmine (black circle, WT), ChRmine S220A (red triangle), ChRmine T218L (blue rhombus) and ChReef (magenta square) were investigated by whole-cell patch-clamp recordings at different membrane potentials ranging from -120 mV to 60 mV. Photocurrents were measured upon illumination with a 3 ms light pulse of a wavelength of $\lambda=532$ nm at a light intensity of 23 mW/mm². The closing kinetics (τ_{off} value) were determined by a fit of the decaying photocurrent elicited in response to the light pulse to a monoexponential function. Shown are the time constants of the closing kinetics τ_{off} for **(a)** ChRmine WT (n=7), **(b)** ChRmine S220A (n=6), **(c)** ChRmine T218L (n=7) and **(d)** ChReef (n=7). The symbols indicate the mean, error bars show SD, n indicates the number of measured cells.



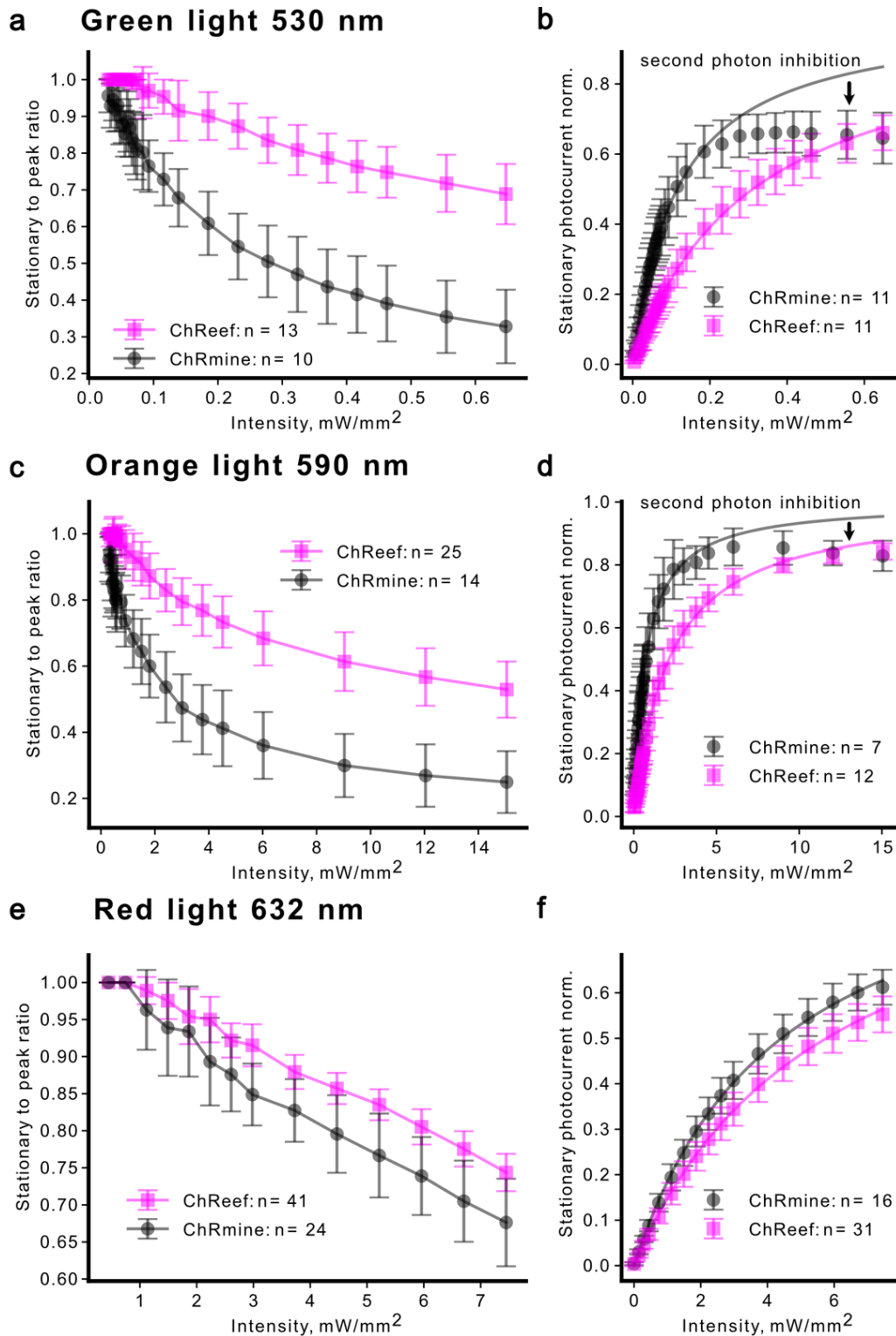
Supplementary Figure 5: Subcellular localization of ChRmine and ChReef in NG cells. NG cells transiently transfected with ChRmine-TS-EYFP-ES (black circle, WT) and ChReef-TS-EYFP-ES (magenta square) were imaged by automated spinning-disc confocal microscopy (Yokogawa CQ1). **(a)** Fluorescence line profile analysis of ChRmine-TS-EYFP-ES and ChReef-TS-EYFP-ES in NG cells. Shown is the average relative EYFP fluorescence intensity as a function of the estimated distance from the plasma membrane. Markers represent mean values, and vertical bars indicate standard deviation (SD). **(b)** Quantification of total protein abundance, represented by corrected partial cell fluorescence per area (CPCF/area), for NG cells expressing ChReef-TS-EYFP-ES and ChRmine-TS-EYFP-ES. Horizontal and vertical bars indicate mean values and standard deviation (SD), n indicates the number of measured cells.



Supplementary Figure 6: Action spectra of ChRmine wt (black circles, n=3) and ChReef (magenta squares, n=3). Shown are normed peak currents in response to ns light-pulses of the indicated wavelengths measured in whole-cell patch-clamp experiments at a membrane potential of -60 mV. The pulse energies at the different wavelengths were set to equal photon counts. The symbols indicate average values, the error bars show SD, n indicates the number of measured cells.

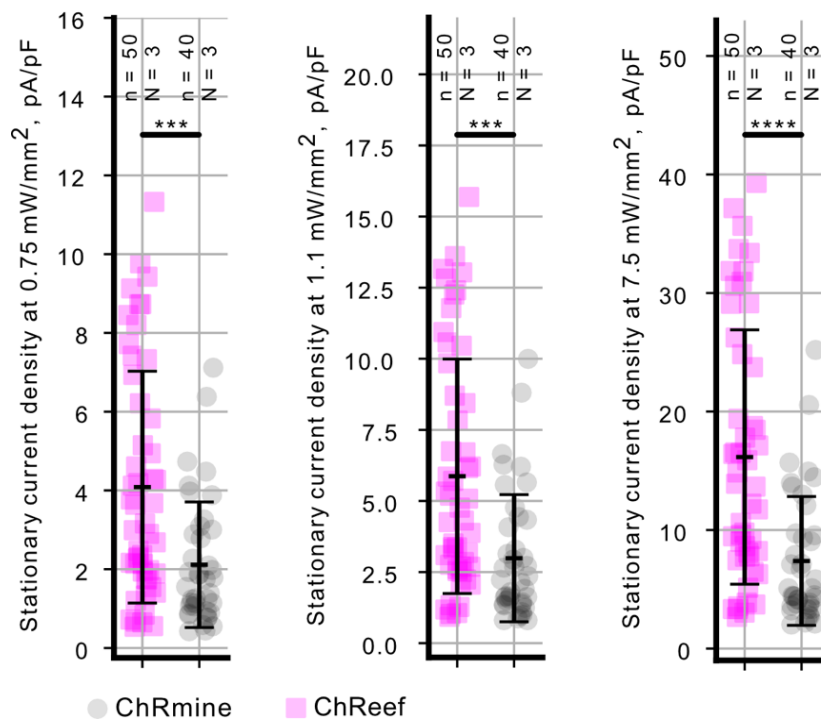


Supplementary Figure 7: Assessment of relative permeabilities of ChRmine and ChReef. (a) Reversal potential shifts as a result of intracellular solution exchange from high K^+ concentration to high Na^+ for estimation of relative K^+ permeability. (b) Reversal potentials of photocurrents of NG cells measured in standard high K^+ intracellular solution (pH 7.2) and NMG-based extracellular solution with increased proton concentration (pH 6.4) (c) Reversal potential shifts due to extracellular solution exchange from high Na^+ concentration to high Ca^{2+} for estimation of relative Ca^{2+} permeability. (d) Summary table with permeabilities of different cations relative to Na^+ permeability. n indicates the number of measured cells.

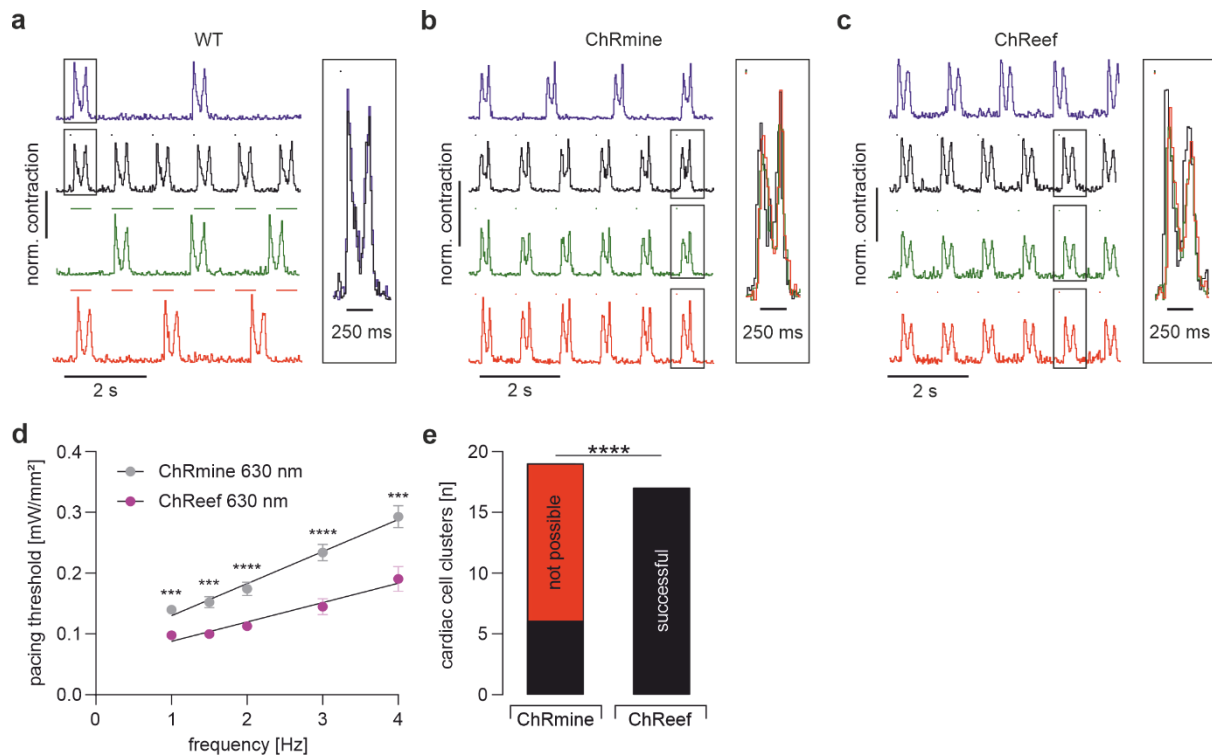


Supplementary Figure 8: Dependence of photocurrents of NG cells expressing ChRmine and ChReef on the intensity of light of different colors. (a, b) Green light (LED 530 nm) intensity dependence of the photocurrent peak-to-stationary ratios (a) and stationary photocurrent sizes (b). (c, d) Orange light (LED 590 nm) intensity dependence of the photocurrent peak-to-stationary ratios (c) and stationary photocurrent sizes (d). (e, f) Red light (LED 632 nm) intensity dependence of the photocurrent peak-to-stationary ratios (e) and stationary photocurrent sizes (f). Markers represent mean values and error bars represent SD in all panels. n indicates the number of measured cells.

NG108-15: red light activation (632 nm)

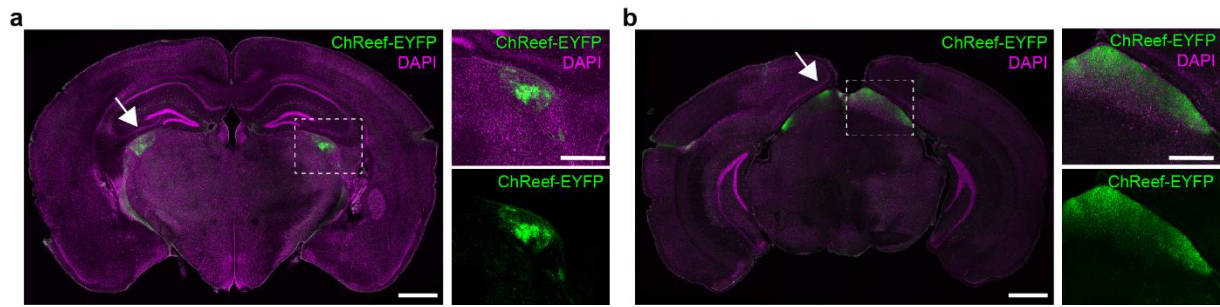


Supplementary Figure 9. Comparison of photocurrent densities of HEK293T cells expressing ChReef and ChRmine in response to red light of different intensities. Numbers at the top represent number of individual cells (small n) and number of transfections on different days (big N). The statistical comparisons were done with Mann-Whitney U-test (p-value < 0.05 (*), 0.005 (**), 0.001 (***), 0.0001(****)).



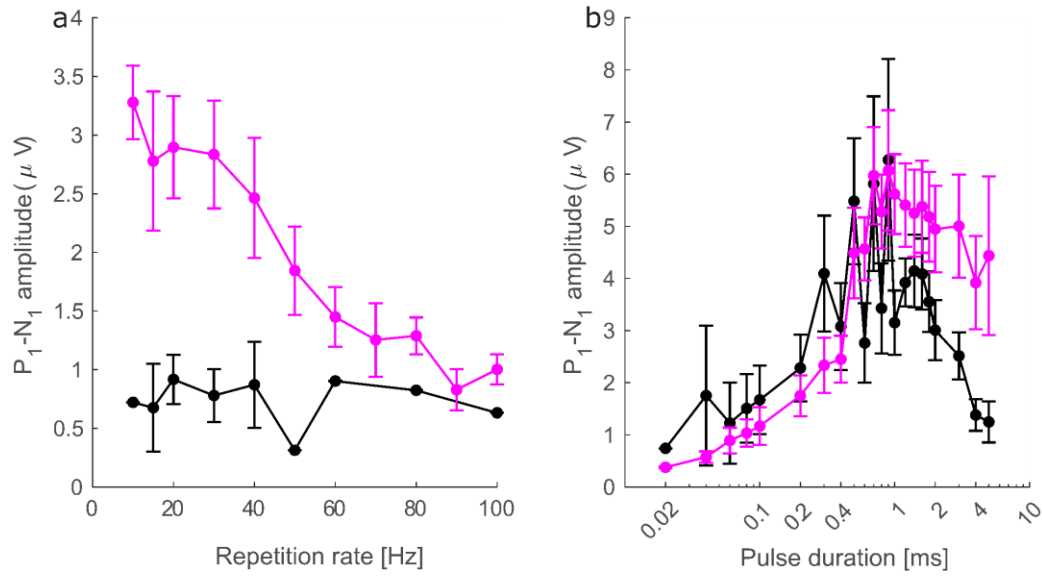
Supplementary Figure 10. Optical pacing and depolarization block of hIPSC-derived CM clusters

a-c, Representative contractions of wild type (a, for 36 CM clusters), ChRmine (b) and ChReef (c) expressing CM cluster (representative for n numbers indicated in d and e) during spontaneous beating (blue), upon electrical stimulation (black; dots: 0.2 ms biphasic, 25 V), green light illumination (green; dots: 510 nm, 1 ms, 1.9 mW/mm² (a); 8.5 μW/mm² (b, c)) and red light illumination (red; dots: 630 nm, 1 ms, 5.2 mW/mm² (a); , 0.5 mW/mm² (b); 0.4 mW/mm² (c)). **d**, Relationship between optical pacing threshold (630 nm) and pacing frequency for ChRmine (black, n = 19) and ChReef (pink, n = 17)). Statistical comparison between ChRmine and ChReef with an unpaired t-test and significances displayed for the individual frequencies (all p values < 0.001). Analysis of the slope factor reveals a significantly steeper relationship for ChRmine (two-sided student's t-test p = 0.04). **e**, Aggregated data of the efficiency in preventing contractions with red light (maximal light intensity: 5.2 mW/mm²) for ChRmine and ChReef expressing CM clusters. Statistical analysis performed with Fisher's exact contingency test (p < 0.0001; N = 3 MyoAAV transductions; n = 19 (ChRmine expressing CM clusters) n = 17 (ChReef expressing CM clusters)). *** indicate p-value < 0.001 and **** indicate p-value < 0.0001;



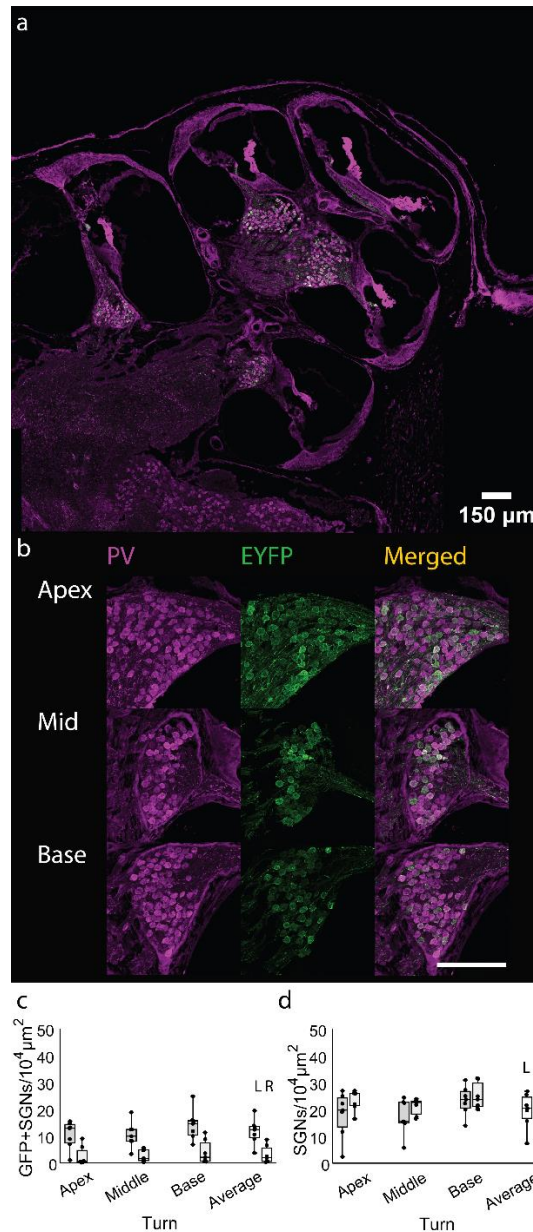
Supplementary Figure 11. ChReef expression in other brain regions in animals for vision restoration experiments

a-b Example coronal brain slices from an animal with ChReef injection in the retina. We find no expression of ChReef in the brain except for RGC axons in the lateral geniculate nucleus (rectangle and arrow in **a**) and superior colliculus (rectangle and arrow in **b**). Scale bars represent 1mm (whole slice) and 0.5mm (zoom in).



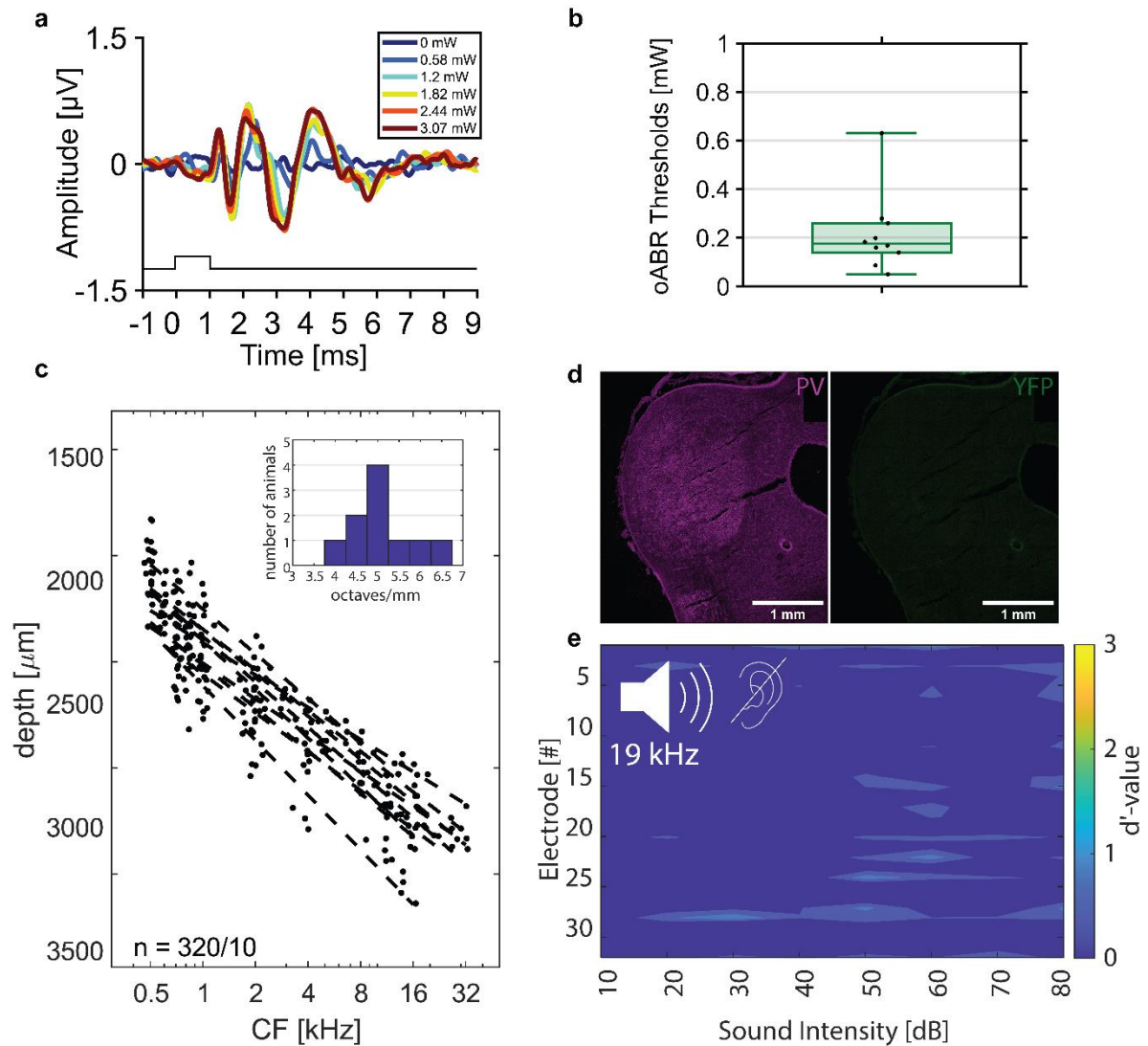
Supplementary Figure 12. oABR P1-N1 amplitudes for different rates of stimulation with 594 nm laser light

a, P1-N1 amplitudes with increasing repetition rates (for 1 ms pulses at ~10 mW radiant flux) in mice expressing ChRmine (black, N=12) or ChReef (magenta, N=15) in SGNs. **b**, P1-N1 amplitudes for varying pulse durations (at 10 Hz and ~10 mW radiant flux) in mice expressing ChRmine (black, N=12) or ChReef (magenta, N=15) in SGNs.

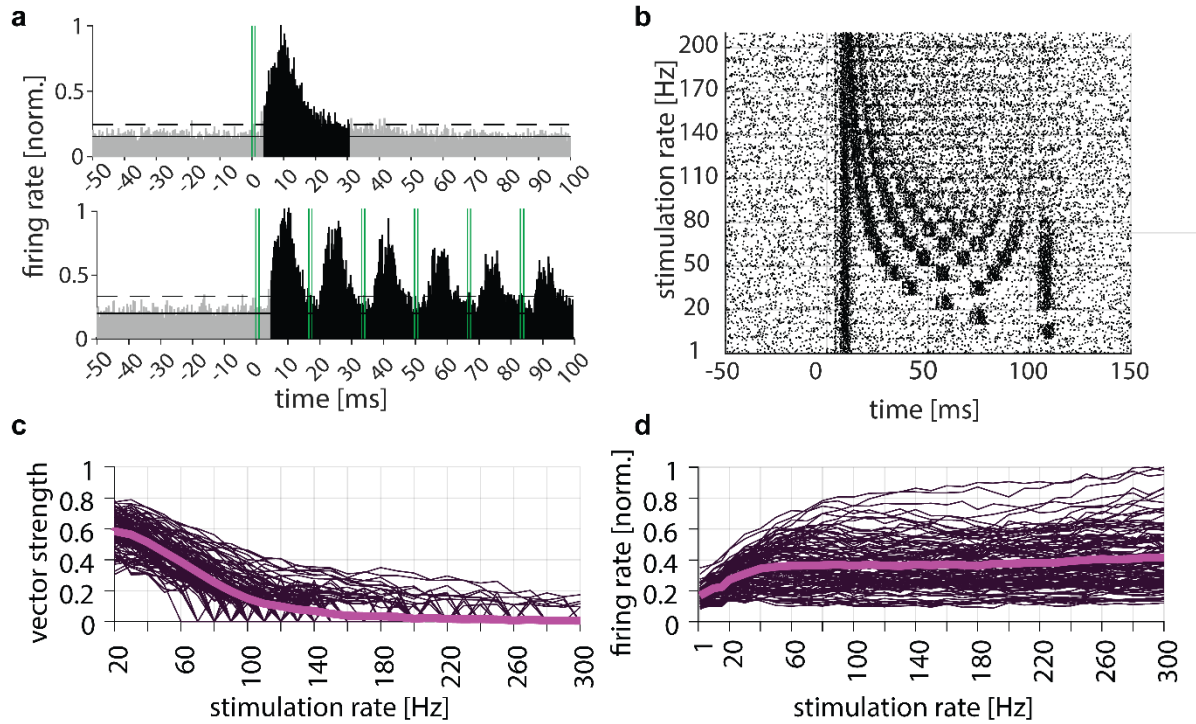


Supplementary Figure 13. Immunohistochemical analysis of ChReef expression in the AAV-injected gerbil cochlea.

a, Overview of exemplary cryosection of an AAV-injected left cochlea imaged at 20x displays expression in spiral ganglion neurons (SGNs) across all turns (representative of N=7 ChReef-injected cochleae) **b**, Exemplary cryosection of an AAV-injected left cochlea imaged at 40x shows ChR expression in SGNs across all cochlear turns (representative of N=7 ChReef-injected cochleae, staining: anti-parvalbumin (PV) as context marker, anti-GFP detecting ChR-EYFP and merged shown from left to right resp.) **c**, Boxplot computing the density of ChR-expressing SGN cells (GFP+) to the area of Rosenthal's canal observed on slice (left and right cochleae as indicated, L: injected left cochleae, N=7 gerbils, R: right non-injected cochleae, N=7 gerbils). Cell counting was performed using a custom MATLAB tool that performs assisted automatic selection of SGN. SGNs are delineated and ChR expressing GFP+ SGNs contrasted to non-expressing SGNs through principal component analysis. **d**, Boxplot computing total SGN density (left and right cochleae as indicated, L: injected left cochleae, N=7 gerbils, R: right non-injected cochleae, N=7 gerbils).

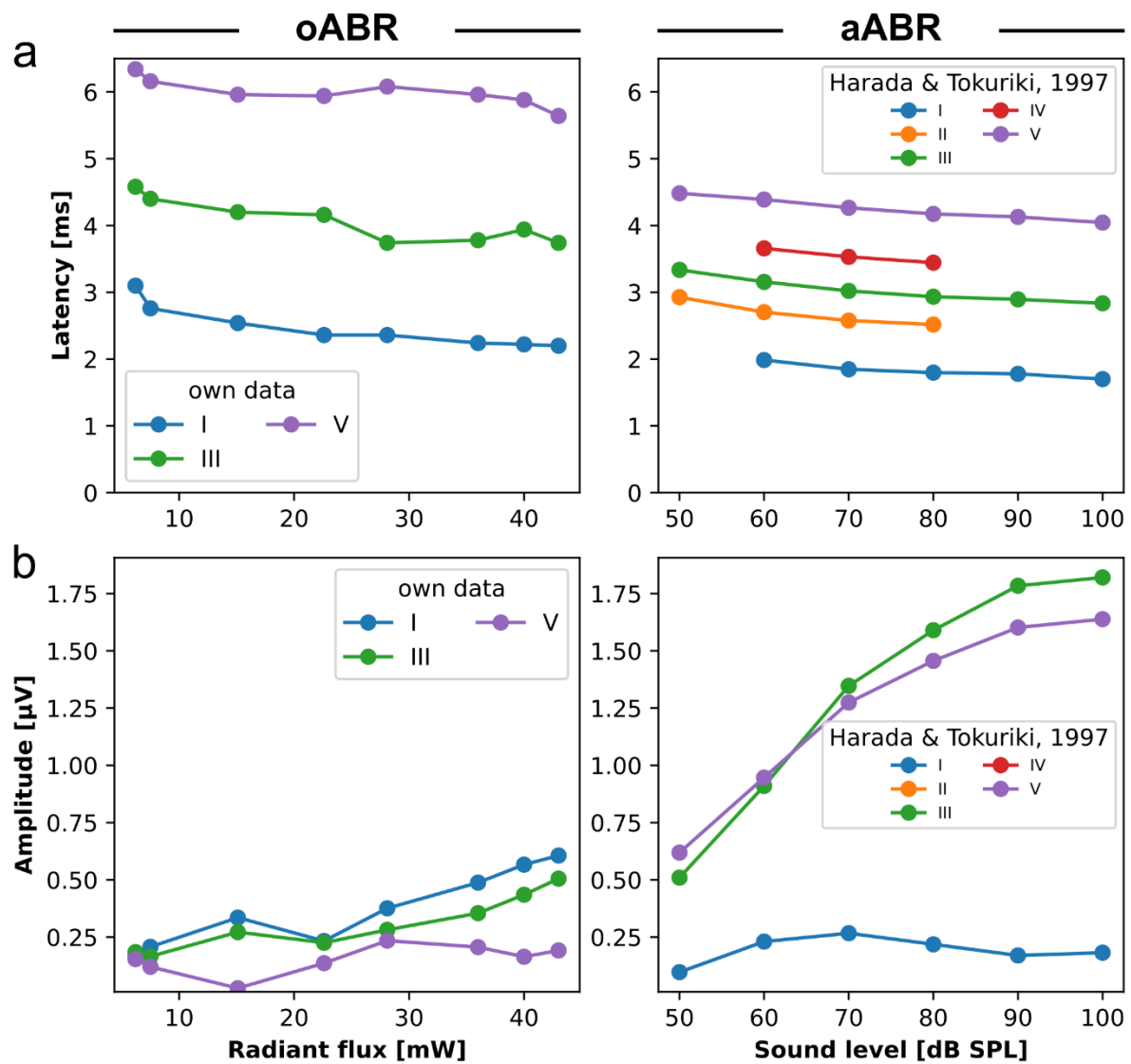


Supplementary Figure 14. Inferior colliculus recordings in ChReef-injected Mongolian gerbils. **a**, Exemplary oABR trace (representative of N=10 ChReef-injected animals). **b**, oABR thresholds computed across animals with a clear oABR responses, points represent individual gerbils (N=10). **c**, Characteristic frequencies (CF) as a function of recording depth. Dashed line: linear fit of all CFs for each animal, according to Pearson's correlation coefficient. Inset displays distribution of tonotopic slopes computed from linear fits across all animals. **d**, Example coronal brain slice of the inferior colliculus of a gerbil injected with ChReef-YFP (representative of N=2 brains) stained for Parvalbumin (PV, red) and GFP (green). **e**, Heatmap computed like in Fig. 5 for acoustic stimulation after kanamycin injection (no activity indicating deafening, representative of N=8 ChReef-injected and deafened animals).



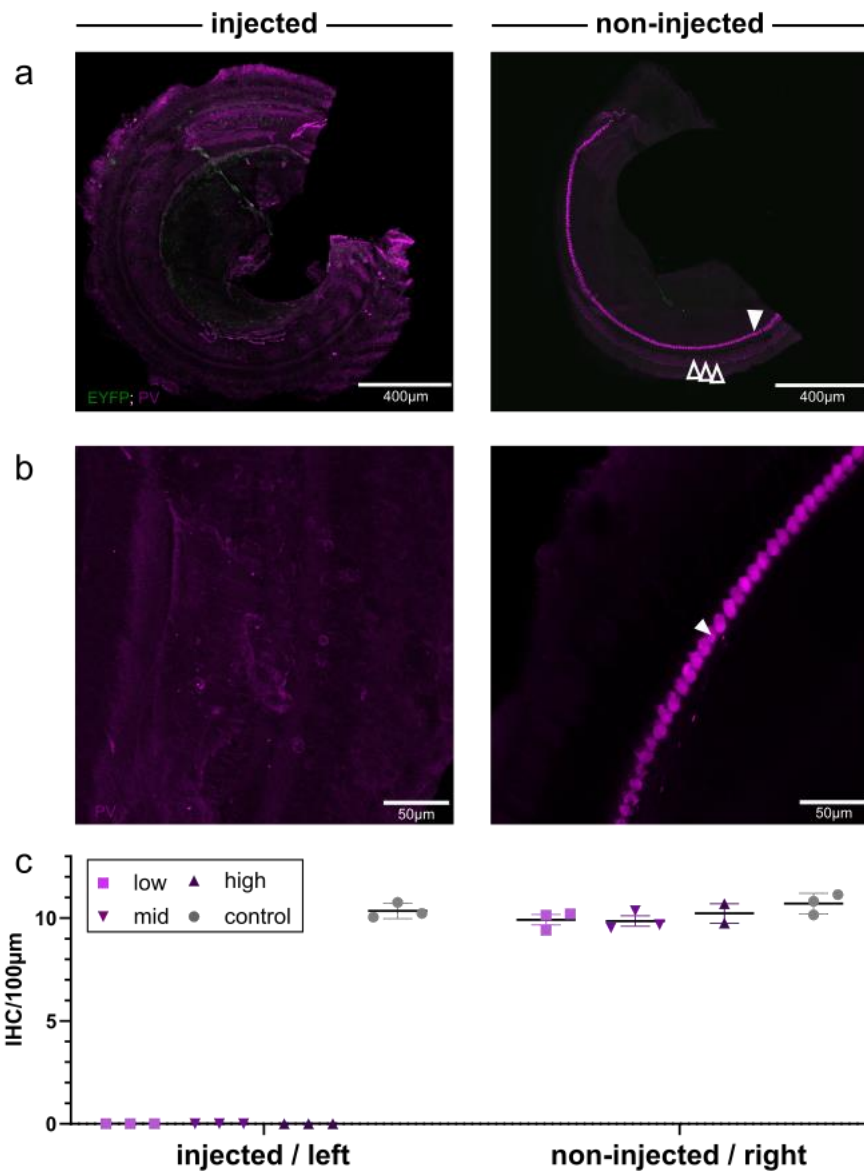
Supplementary Figure 15. Temporal resolution of optogenetic activation of the auditory pathway by means of inferior colliculus recordings in Mongolian gerbils.

a, Peri-Stimulus Time Histogram (PSTH) computing spike rates in bins of 0.2 ms recorded from stimulation at ~1 mW with an optical fiber emitting green light (522 nm) for single pulses (N = 10, top) and pulsing at 60Hz (N = 10 gerbils, bottom) normalized to the highest spike rate across animals. Green lines indicate stimulus timing. Dashed horizontal lines indicate 3x mean absolute deviation (MAD) used for thresholding and bins reaching threshold condition are highlighted in black. b, Exemplary spike raster computed from stimulating at 1 mW across different stimulation rates used for each of the 30 repetitions. Stimulus used were 100 ms pulse trains of 1 ms light pulses delivered at various stimulation rates. c-d, Individual traces computed across all animals and all responsive channels demonstrating vector strength (c) and firing rates (d) recorded and normalized to highest firing rate computed respectively. Average shown in bold magenta lines.



Supplementary Figure 16. Comparison of oABR from Figure 5j and published aABR data.

oABR (left panels) and aABR (right panels) peaks were labelled according to their latency of occurrence and their latency (**a**) as well as their amplitude (**b**) plotted as a function of stimulus intensity for the oABR positive animal ($n = 1/9$). Published aABR data (replotted from Harada & Tokuriki, 1997; their Fig. 3 and 5)² were gathered after stimulation with broadband clicks of varying sound level and presented at a similar repetition rate as oABR (10 Hz for aABR vs. 9 Hz for oABR).



Supplementary Figure 17. Quantification of inner hair cell loss following deafening of the injected left side in the common marmoset.

a, Confocal images of cochlear whole mounts of an injected and fully deafened inner ear (left panel: 0 inner hair cells (IHC) observed) vs. the contralateral, non-injected side of the same animal (right panel: 9.678 cells/100μm). IHCs are indicated by a closed arrow head, outer hair cells by open arrow heads. **b**, Confocal images of zoomed-in ROI of the IHC (if present), same preparation as in a. **c**, IHC cell density across the across the different titer (n = 9) and control groups (n = 3). Note, that the IHC density on the non-injected, right side was comparable to IHC density in control animals (left: mean = 10.3 cells/100μm, right: mean = 10.7 cells/100μm).

Supplementary Table 1. Stationary-Peak-Ratio, EC₅₀ values, stationary current densities and τ_{off} values of ChRmine variants.

ChR variant	Stationary-Peak-Ratio	EC ₅₀ [$\mu\text{W}/\text{mm}^2$]	J _{-60 mV} [pA/pF]	τ_{off} [ms]
ChReef	0.62 \pm 0.15	20 \pm 8	97.6 \pm 65.0	58.3 \pm 12.5
ChRmine	0.22 \pm 0.12	14 \pm 5	21.6 \pm 15.8	63.5 \pm 15.7
ChRmine T218L	0.44 \pm 0.13	29 \pm 15	64.8 \pm 38.8	59.1 \pm 21.3
ChRmine S220A	0.62 \pm 0.14	31 \pm 17	54.3 \pm 27.2	152.7 \pm 9.8

NG cells, transiently transfected with the shown ChRmine variants were investigated by whole-cell patch-clamp recordings at a membrane potential of -60 mV. Photocurrents were measured upon illumination with green light pulses (saturating intensity of 23 mW/mm², $\lambda=532$ nm) of 2 s for stationary current density determination and of 3 ms for τ_{off} determination. The stationary current densities (J_{-60mV}) were calculated as the quotient of the mean stationary current and the capacitance of the cell. The τ_{off} values were determined by a fit of the decaying photocurrent, immediately after cessation of the light pulse, to a monoexponential function. The half maximal activation (EC₅₀) was determined by hyperbolic fitting. For ChRmine wt the fitting range was restricted to the range, which could be approximated by a hyperbolic function. The stationary-peak-ratio was calculated as the quotient of the mean stationary current of the last 100 ms of the 2s light pulse and the peak current. Shown are mean and standard deviation (SD).

Supplementary Table 2. Stationary current densities and τ_{off} values of ChR variants.

ChR variant	$J_{-60 \text{ mV}}$ [pA/pF]	τ_{off} [ms]
ChReef (a)	97.6 ± 65.0	58.3 ± 12.5
Catch (b)	37.0 ± 12.5	34.4 ± 7.3
ChR2 T159C (c)	30.6 ± 18.4	28.3 ± 7.4
Chronos (d)	24.0 ± 7.5	3.5 ± 0.6
Chrimson (e)	24.0 ± 6.8	23.6 ± 1.5
f-Chrimson (f)	34.2 ± 12.7	5.7 ± 0.4

NG cells transfected with the shown ChR variants were investigated by whole-cell patch-clamp recordings at a membrane potential of -60 mV. Photocurrents were measured upon illumination with saturating light pulses of 0.5 s or 2 s for stationary current density determination and of 3 ms for τ_{off} determination. The stationary current densities ($J_{-60\text{mV}}$) were calculated as the quotient of the mean stationary current and the capacitance of the cell. The τ_{off} values were determined by a fit of the decaying photocurrent, immediately after cessation of the light pulse, to a monoexponential function. Shown are mean and standard deviation (SD).

Supplementary Table 3. Exact (Mann-Whitney U-test) and adjusted (Bonferroni) p-values from the Figure 1a.

	protein1	protein2	p-value	adjusted p-value	significance
0	ChRmine	ChRmine S220A	1,28E-14	7,65E-14	****
1	ChRmine	ChRmine T218L	6,33E-07	3,8E-06	****
2	ChRmine	ChReef	5,84E-09	3,51E-08	****
3	ChRmine S220A	ChRmine T218L	7,09E-05	0,000426	***
4	ChRmine S220A	ChReef	0,955443	1	NS
5	ChRmine T218L	ChReef	0,006471	0,038826	*

Supplementary Table 4. Exact (Mann-Whitney U-test) and adjusted (Bonferroni) p-values from the Figure 1b.

	protein1	protein2	p-value	adjusted p-value	significance
0	Chronos	Chrimson	0,365031116	1	NS
1	Chronos	fChrimson	0,010907843	0,392682347	NS
2	Chronos	CatCh	0,001362043	0,049033555	*
3	Chronos	ChR2 T159C	0,468800617	1	NS
4	Chronos	ChRmine	0,120278866	1	NS
5	Chronos	ChReef	6,47041E-06	0,000232935	***
6	Chronos	ChRmine S220A	5,89845E-05	0,002123442	**
7	Chronos	ChRmine T218L	0,000774258	0,027873292	*
8	Chrimson	fChrimson	0,012066365	0,43438914	NS
9	Chrimson	CatCh	0,012066365	0,43438914	NS
10	Chrimson	ChR2 T159C	0,480707528	1	NS
11	Chrimson	ChRmine	0,264624907	1	NS
12	Chrimson	ChReef	2,71935E-06	9,78965E-05	****
13	Chrimson	ChRmine S220A	0,000147026	0,005292931	**
14	Chrimson	ChRmine T218L	0,003350242	0,120608728	NS
15	fChrimson	CatCh	0,843831425	1	NS
16	fChrimson	ChR2 T159C	0,594853424	1	NS
17	fChrimson	ChRmine	0,00356568	0,128364494	NS
18	fChrimson	ChReef	0,000131121	0,004720342	**
19	fChrimson	ChRmine S220A	0,005860854	0,210990738	NS
20	fChrimson	ChRmine T218L	0,012612069	0,454034489	NS
21	CatCh	ChR2 T159C	0,403317565	1	NS
22	CatCh	ChRmine	0,001150439	0,041415819	*
23	CatCh	ChReef	0,000286779	0,010324048	*
24	CatCh	ChRmine S220A	0,016623175	0,598434306	NS
25	CatCh	ChRmine T218L	0,023219344	0,835896385	NS
26	ChR2 T159C	ChRmine	0,13872372	1	NS
27	ChR2 T159C	ChReef	0,000614487	0,022121537	*
28	ChR2 T159C	ChRmine S220A	0,012341309	0,444287123	NS
29	ChR2 T159C	ChRmine T218L	0,016770456	0,603736421	NS
30	ChRmine	ChReef	4,38554E-08	1,5788E-06	****
31	ChRmine	ChRmine S220A	1,90348E-08	6,85252E-07	****
32	ChRmine	ChRmine T218L	3,95657E-06	0,000142436	***
33	ChReef	ChRmine S220A	0,004073119	0,146632286	NS
34	ChReef	ChRmine T218L	0,108625377	1	NS
35	ChRmine S220A	ChRmine T218L	0,324126588	1	NS

Supplementary Table 5. Exact (Student's t-test) and adjusted (Bonferroni) p-values from the Figure 1c.

	protein1	protein2	p-value	adjusted p-value	significance
0	Chronos	Chrimson	1,63E-12	3,43286E-11	****
1	Chronos	fChrimson	1,15E-05	0,000241192	***
2	Chronos	CatCh	1,75E-09	3,66694E-08	****
3	Chronos	ChR2 T159C	1,81E-07	3,8001E-06	****
4	Chronos	ChRmine	7,15E-08	1,50064E-06	****
5	Chronos	ChReef	1,28E-08	2,69656E-07	****
6	Chrimson	fChrimson	7,1E-09	1,49005E-07	****
7	Chrimson	CatCh	0,007169	0,150557442	NS
8	Chrimson	ChR2 T159C	0,189567	1	NS
9	Chrimson	ChRmine	0,000239	0,005013337	**
10	Chrimson	ChReef	0,000113	0,002380895	**
11	fChrimson	CatCh	8,63E-07	1,81211E-05	****
12	fChrimson	ChR2 T159C	3,26E-05	0,000684998	***
13	fChrimson	ChRmine	1,07E-05	0,000225602	***
14	fChrimson	ChReef	3,07E-06	6,4388E-05	****
15	CatCh	ChR2 T159C	0,20822	1	NS
16	CatCh	ChRmine	0,000198	0,004150877	**
17	CatCh	ChReef	0,000183	0,003835063	**
18	ChR2 T159C	ChRmine	7,83E-05	0,00164414	**
19	ChR2 T159C	ChReef	6,58E-05	0,001380869	**
20	ChRmine	ChReef	0,511891	1	NS

Supplementary Table 6. Exact p-values (Tukey's HSD test) from the Figure 1i.

	protein1	protein2	p-value	significance
0	CatCh_stat	ChReef_ns	2,51E-05	****
1	CatCh_stat	ChReef_stat	0,00596	**
2	CatCh_stat	ChRmine_ns	4,52E-07	****
3	CatCh_stat	ChRmine_stat	0,001495	**
4	ChReef_ns	ChReef_stat	0,61518	NS
5	ChReef_ns	ChRmine_ns	0,898008	NS
6	ChReef_ns	ChRmine_stat	0,904588	NS
7	ChReef_stat	ChRmine_ns	0,150454	NS
8	ChReef_stat	ChRmine_stat	0,987161	NS
9	ChRmine_ns	ChRmine_stat	0,41686	NS

Supplementary Table 7. List of primers used for ChR mutant generation.

construct	template	sequence of forward primer	sequence of reverse primer
ChRmine F219Y	humanized ChRmine	5'-GCCGTGTT TACCTACTCCA TGCTGTGG-3'	5'-CCACAGCA TGGAGTAGGTAA ACACGGC-3'
ChRmine T218L	humanized ChRmine	5'-GTTCGCCGTG TTTCTGTTCTCCA TGCTGTG-3'	5'-CACAGCATGG AGAACAGAAACAC GGCGAAC-3'
ChRmine S220A	humanized ChRmine	5'-GTGTTTACCTT CGCCATGCTG TGGATTC-3'	5'- GAATCCACAG CATGGCGAAG GTAAACAC -3'
ChRmine T218L/S220A	humanized ChRmine T218L	5'-CGTGTCTTCTG TTCGCCATGCT GTGGATTCTG -3'	5'- CAGAATCCAC AGCATGGCGAA CAGAAACACG -3'
ChR2 T159C	humanized ChR2	5'-TCCGACAT CGGCTGTATCGTAT GGGG-3'	5'- CCCCAT ACGATACAGCCG ATGTCGGA-3'
ChRmine Y260F	humanized ChRmine	5'-TGGCCA AGTCCTGTTTTG GCTTTGCCCTG-3'	5'-CAGGG CAAAGCCAAAACA GGACTTGGCCA-3'
CoChR L112C	humanized CoChR	5'-ACTTGTC CCGTCATCTGTATCC ACCTGAGCAAC-3'	5'-GTTGCTCA GGTGGATACAGA TGACGGGACAAGT-3'
CoChR H94E/L112C	humanized CoChR L112C	5'-TGGCTA ACGGAGAGCGAG TCCAGTGGC-3'	5'-GCCACTGG ACTCGCTCTCCGT TAGCCA-3'
CoChR H94E/L112C/ K264T	humanized CoChR H94E/L112C	5'- CGACATC CGGAAGACCACCA AGATCAACGTG-3'	5'-CACGTTG ATCTTGGTGGTC TTCCGGATGTCG-3'

Supplementary Table 8. Solutions used for acute slice in vitro electrophysiology

All compounds used are listed with their concentrations. QX314 stands for N-(2,6-dimethylphenylcarbamoylmethyl) triethylammonium chloride, an intracellular sodium channel blocker.

<i>aCSF 2mM Ca²⁺</i>		<i>Intracellular solution</i>	
Compound Name (Source)	Concentration (mM)	Compound name (Source)	Concentration (mM)
Glucose (Merck)	13	K-gluconate (Merck)	108
NaCl (Merck)	125	HEPES (Merck)	9
CaCl ₂ (Merck)	2	EGTA (Merck)	9
MgCl ₂ (Merck)	1	Na ₂ Phosphocreatine (Merck)	14
NaHCO ₃ (Merck)	26	ATP-Mg (Merck)	4
NaH ₂ PO ₄ * H ₂ O (Merck)	1.25	GTP-Na (Merck)	0.3
KCl (Merck)	2.5	MgCl ₂ (Merck)	4.5
Na-Pyruvate (Merck)	2	QX-314 (Merck)	1
Na L-ascorbate (Merck)	0.7		

<i>Cutting Solution</i>	
Compound Name (Source)	Concentration (mM)
Glucose (Merck)	20
Sucrose (Merck)	120
NaCl (Merck)	50
CaCl ₂ (Merck)	0.2
MgCl ₂ (Merck)	6
NaHCO ₃ (Merck)	26
NaH ₂ PO ₄ * H ₂ O (Merck)	1.25
KCl (Merck)	2.5
Na-Pyruvate (Merck)	2
Na L-ascorbate (Merck)	0.7
Na L-Lactate (Merck)	3

1. Dieter, A., Duque-Afonso, C. J., Rankovic, V., Jeschke, M. & Moser, T. Near physiological spectral selectivity of cochlear optogenetics. *Nature Communications* **10**, 1962 (2019).
2. Harada, T. & Tokuriki, M. Effects of click intensity and frequency on the brain-stem auditory evoked potentials in the common marmoset (*Callithrix jacchus*). *Journal of Veterinary Medical Science* **59**, 561–567 (1997).

Supplementary Table 9. Exact (Mann-Whitney U-test) and adjusted (Bonferroni) p-values from the Extended Data Figure 2b.

	protein1	protein2	p-value	adjusted p-value	significance
0	ChRmine	ChReef	1,22E-08	1,22E-07	****
1	ChRmine	ChRmine T218L	8,66E-05	0,000866	***
2	ChRmine	ChRmine S220A	0,040016	0,400158	NS
3	ChRmine	ChRmine F219Y	6,52E-11	6,52E-10	****
4	ChReef	ChRmine T218L	0,038726	0,38726	NS
5	ChReef	ChRmine S220A	0,00321	0,032098	*
6	ChReef	ChRmine F219Y	2,72E-11	2,72E-10	****
7	ChRmine T218L	ChRmine S220A	0,271432	1	NS
8	ChRmine T218L	ChRmine F219Y	5,36E-10	5,36E-09	****
9	ChRmine S220A	ChRmine F219Y	4,96E-09	4,96E-08	****

Supplementary Table 10. Exact (Mann-Whitney U-test) and adjusted (Bonferroni) p-values from the Extended Data Figure 2c.

	protein1	protein2	p-value	adjusted p-value	significance
0	GtCCR4	ChRmine	3,34E-10	9,35E-09	****
1	GtCCR4	GtCCR2	0,338786	1	NS
2	GtCCR4	CoChR-3M	1,31E-09	3,66E-08	****
3	GtCCR4	CatCh	1,44E-07	4,02E-06	****
4	GtCCR4	ChReef	1,57E-10	4,4E-09	****
5	GtCCR4	ChRmine Y260F	1,52E-09	4,26E-08	****
6	GtCCR4	CoChR	1,59E-10	4,46E-09	****
7	ChRmine	GtCCR2	2,16E-13	6,05E-12	****
8	ChRmine	CoChR-3M	5,88E-06	0,000165	***
9	ChRmine	CatCh	1,58E-06	4,43E-05	****
10	ChRmine	ChReef	1,22E-08	3,41E-07	****
11	ChRmine	ChRmine Y260F	0,743772	1	NS
12	ChRmine	CoChR	0,071397	1	NS
13	GtCCR2	CoChR-3M	2,41E-12	6,76E-11	****
14	GtCCR2	CatCh	4,15E-11	1,16E-09	****
15	GtCCR2	ChReef	5,45E-14	1,52E-12	****
16	GtCCR2	ChRmine Y260F	3,12E-12	8,75E-11	****
17	GtCCR2	CoChR	7,75E-15	2,17E-13	****
18	CoChR-3M	CatCh	1,08E-10	3,03E-09	****
19	CoChR-3M	ChReef	0,363146	1	NS
20	CoChR-3M	ChRmine Y260F	2,49E-06	6,97E-05	****
21	CoChR-3M	CoChR	1,22E-08	3,42E-07	****
22	CatCh	ChReef	2,91E-13	8,15E-12	****
23	CatCh	ChRmine Y260F	5,09E-06	0,000143	***
24	CatCh	CoChR	0,000283	0,007921	**
25	ChReef	ChRmine Y260F	4,51E-09	1,26E-07	****
26	ChReef	CoChR	1,03E-12	2,9E-11	****
27	ChRmine Y260F	CoChR	0,175989	1	NS

Supplementary Table 11. Exact p-values (Tukey's HSD test) from the Extended Data Figure 2d.

	protein1	protein2	p-value	significance
0	CatCh	ChReef	0,346598051	NS
1	CatCh	ChRmine	0,000225641	***
2	CatCh	ChRmine Y260F	<1E-13	****
3	CatCh	CoChR	0,998691665	NS
4	CatCh	CoChR-3M	<1E-13	****
5	CatCh	GtCCR2	0,022199136	*
6	CatCh	GtCCR4	0,703629469	NS
7	ChReef	ChRmine	0,27132902	NS
8	ChReef	ChRmine Y260F	7,63148E-09	****
9	ChReef	CoChR	0,159017706	NS
10	ChReef	CoChR-3M	<1E-13	****
11	ChReef	GtCCR2	2,73628E-06	****
12	ChReef	GtCCR4	0,018664277	*
13	ChRmine	ChRmine Y260F	0,000402241	***
14	ChRmine	CoChR	0,000127347	***
15	ChRmine	CoChR-3M	<1E-13	****
16	ChRmine	GtCCR2	6,73428E-12	****
17	ChRmine	GtCCR4	1,55577E-05	****
18	ChRmine Y260F	CoChR	2,2593E-13	****
19	ChRmine Y260F	CoChR-3M	<1E-13	****
20	ChRmine Y260F	GtCCR2	<1E-13	****
21	ChRmine Y260F	GtCCR4	4,16334E-13	****
22	CoChR	CoChR-3M	<1E-13	****
23	CoChR	GtCCR2	0,22726708	NS
24	CoChR	GtCCR4	0,960896094	NS
25	CoChR-3M	GtCCR2	<1E-13	****
26	CoChR-3M	GtCCR4	<1E-13	****
27	GtCCR2	GtCCR4	0,974017951	NS

Supplementary Notes

Supplementary Note 1: Cell culture and transfection

The manual patch-clamp recordings of ChR variants were conducted in the neuroma glioblastoma cell line NG108-15 (ATCC, HB-12377TM, Manassas, USA) cultured in Dulbecco's Modified Eagle Medium (DMEM, Sigma, St. Louis, USA) supplemented with 10 % fetal calf serum (Sigma, St. Louis, USA) and 1 % penicillin/streptomycin (Sigma, St. Louis, USA) (supplemented DMEM: DMEM⁺) at 37 °C and 5 % CO₂. Cells were seeded on 24-well plates one day prior to transfection by Lipofectamine with pcDNA3.1(-) derivatives carrying the aforementioned ChR variants at a NG108-15 cell confluency of 50-70 %. For each well, a transfection mix of 100 µl DMEM, 3 µl Lipofectamine LTX (Invitrogen, Carlsbad, USA) and 500 ng of the pcDNA3.1(-) derivatives was prepared and added to a well with 400 µl of DMEM⁺. Twenty-four hours after transfection the medium was exchanged against 500 µl DMEM⁺ supplemented with 1 µM all-trans retinal.

For automated patch-clamp recordings and automated spinning-disc confocal microscopy, HEK293T cells (DSMZ, Braunschweig, Germany) or NG108-15 (ATCC, HB-12377TM, Manassas, USA) cells were seeded in a T75 culture flasks or 6-well plates and allowed to grow for one day before transfection. The cells were seeded at a density of 16 thousands cells/cm² in DMEM⁺ (initial concentration before adhesion 80 thousands cells/ml). For noise analysis experiments transfection of HEK293T cells was done in T75 flasks. Immediately prior to transfection, the media was replaced with 12 mL of OptiMEM (ThermoFisher, Waltham, Massachusetts, U.S.) with 1.25 µM all-trans-retinal (Sigma, St. Louis, MO, U.S.). Then, 19.5 µg of plasmid DNA and 78.1 µg of polyethyleneimine (PEI, Polysciences, Warrington, PA, U.S.) were separately dissolved in 1.5 ml of OptiMEM (ThermoFisher, Waltham, Massachusetts, U.S.) each. The DNA and PEI solutions were then combined and incubated for 15 minutes at room temperature. The resulting DNA/PEI mix was

added to the cells and incubated at 37°C and 5% CO₂ for 4 hours. After transfection, the media in the flask was changed back to DMEM⁺ supplemented with 1 µM all-trans-retinal. The cells were then incubated at 37°C and 5% CO₂ for 40 hours prior to the automated patch-clamp experiment. For all other experiments with automated patch-clamp transfections of HEK293T or NG108-15 cells were done in 6-well plates without prior media exchange. For each well 2.5 µg of plasmid DNA and 7.5 µg of PEI were separately dissolved in 0.2 ml of OptiMEM. The DNA and PEI solutions were then combined and incubated for 15 minutes at room temperature. The resulting DNA/PEI mix was added to the wells of 6-well plate and incubated at 37°C and 5% CO₂ for 16 hours. After transfection, the media in the flask was exchanged to new DMEM⁺ supplemented with 1 µM all-trans-retinal. The cells were then incubated at 37°C and 5% CO₂ for 28 hours prior to the automated patch-clamp experiment. For automated spinning-disc confocal microscopy NG108-15 cell transfections were done in 96-well glass bottom microscopy grade plates (Greiner, Sensoplate microplate 96 well, 655892). For each well 83 ng of plasmid DNA and 0.25 µg of PEI were separately dissolved in 7 µl of OptiMEM. The DNA and PEI solutions were then combined and incubated for 15 minutes at room temperature. The resulting DNA/PEI mix was added to the wells of the 96-well plate and incubated at 37°C and 5% CO₂ for 16 hours. After transfection, the media in the flask was exchanged to new DMEM⁺ supplemented with 1 µM all-trans-retinal. The cells were then incubated at 37°C and 5% CO₂ for 28 hours prior to the automated spinning-disc confocal microscopy experiment.

Supplementary Note 2: Protocols for manual patch-clamp recordings and data analysis

Patch pipettes with a resistance of 2-6 MΩ were fabricated from thin-walled borosilicate glass on a horizontal puller (Model P-1000, Sutter Instruments, Novato, USA). The series resistance was <15 MΩ. Light pulses were applied by a fast computer-controlled shutter (Uniblitz LS6ZM2, Vincent Associates, Rochester, USA) using diode-pumped solid-state lasers focused into an optic fiber (d=400 µm). The open-source statistic software “R” as well as Origin 9.0

(OriginLab, Inc., Northampton, MA, USA) and GraphPad Prism (GraphPad Software, La Jolla, CA, USA) were employed for data analysis.

The photocurrents of the ChRmine variants were measured in response to green light pulses ($\lambda=532$ nm) of varying duration with a saturating intensity of 23 mW/mm². The photocurrents of Chronos, Catch and ChR2 T159C were measured upon the application of blue light pulses ($\lambda=473$ nm) of varying duration with a saturating intensity of 31 mW/mm². The stationary current densities ($J_{-60\text{ mV}}$) of the ChRmine variants were calculated as the quotient of the mean stationary current upon stimulation with a 2 s light pulse and the capacitance of the cell. The stationary current densities ($J_{-60\text{ mV}}$) of Chronos, Catch and ChR2 T159C were calculated as the quotient of the mean stationary current upon stimulation with a 0.5 s light pulse and the capacitance of the cell. To avoid an experimental bias, cells were chosen for the recordings independent of the brightness of their fluorescent signal.

The stationary-peak-ratio of the photocurrents of the ChRmine variants was calculated as the quotient of the mean stationary current upon stimulation with a 2 s light pulse and the peak current. The peak recovery of the ChRmine variants was assessed by photocurrent recordings upon illumination with two subsequent 3 s light pulses with a varying time between the light pulses (Δt between pulses, ms, ranging from 50 to 3350 ms). Peak recovery was calculated as the quotient of the difference between the peak and stationary current of pulse two ($I_{p2}-I_{s2}$) and peak and stationary current of pulse one ($I_{p1}-I_{s1}$) in %. The time constant of the peak recovery ($\tau_{\text{peak-recovery}}$) was determined by a fit of the quotient of the difference between the peak and stationary currents of two subsequent 3s light pulses at saturating intensity to a monoexponential function.

The τ_{off} values of all shown ChR variants were determined by a fit of the decaying photocurrent elicited in response to a 3 ms light pulse to a monoexponential function. In order to investigate the dependence of the off-kinetics on the membrane potential τ_{off} values were determined at membrane potentials ranging from -120 mV to +60 mV.

The action spectra of the ChRmine variants were determined by peak current recordings in response to ns-light-pulses of wavelengths ranging from 430 to 590 nm with pulse energies at the different wavelengths set to equal photon counts of 5×10^{18} photons/m² using the Opolette 355 tunable laser system (Opotek Inc, Carlsbad, USA).

Supplementary Note 3: Automated patch clamping procedure

To begin, the S-type chip (Nanion, Munich, Germany) was filled with 80 µl per well of Divalent-Free solution, and the chamber's bottom was subsequently filled with Internal solution. The Divalent Free solution contained 140 mM NaCl, 4 mM KCl, and 10 mM HEPES, with pH adjusted to 7.4 using NaOH. The osmolarity of the solution was set to 289 mOsm by adjusting the concentration of glucose. The Internal solution was composed of 10 mM NaCl, 10 mM KCl, 110 mM KF, 10 mM HEPES, and 10 mM EGTA, with pH adjusted to 7.2 using KOH. The osmolarity of the solution was set to 285 mOsm by adjusting the concentration of glucose. Next, 20 µl per well of solution was removed, and 20 µl per well of detached cells were introduced to the chip. The cells were then captured by a suction pulse of -200 mbar for 5 s, followed by consecutive suction pulses of -50 mbar for 1 min. Subsequently, the voltage was decreased incrementally from 0 mV to -100 mV in steps of 25 mV while maintaining the cells under a pressure of -50 mbar (HEK293T) or -80 mbar (NG108-15). After this, 20 µl per well of solution was removed from the chip, and 40 µl per well of seal enhancer solution was added. The seal enhancer solution contained 130 mM NaCl, 4 mM KCl, 10 mM CaCl₂, 1 mM MgCl₂, and 10 mM HEPES, with pH adjusted to 7.4 using NaOH. The osmolarity of the solution was set to 302 mOsm by adjusting the concentration of glucose. The chip then underwent three wash steps, during which 40 µl of solution was removed from each well and replaced with 40 µl per well of standard external solution (unless another extracellular solution composition is specified). After the second wash step, two suction pulses of -220 mbar were applied for 2 s each to

establish a whole-cell configuration for HEK293T cells or three suction pulses of -350 mbar were applied for 5 s each to establish a whole-cell configuration for NG108-15 cells. After completing all of the procedures described, the remaining volume of solution in the wells was 100 μ l.

Supplementary Note 4: Cell treatment prior automated patch-clamp experiments

The cells that were transfected were washed twice with DPBS (ThermoFisher, Waltham, Massachusetts, U.S.) and then treated with 3 ml of TrypLE (ThermoFisher, Waltham, Massachusetts, U.S.) at 37°C for 7 minutes (HEK293T) or 15 minutes (NG108-15). After the TrypLE treatment, 3 ml of standard external solution was added to the cells and incubated at 4°C for 5 minutes. The standard external solution was composed of 140 mM NaCl, 4 mM KCl, 2 mM CaCl_2 , 1 mM MgCl_2 , and 10 mM HEPES, with pH adjusted to 7.4 using NaOH. The osmolarity of the solution was set to 298 mOsm by adjusting the concentration of glucose. The cells were then resuspended by pipetting and centrifuged at 200 g for 10 minutes, and the supernatant was discarded. Finally, the cells were resuspended in 10 mL of Standard External Solution.

Supplementary Note 5: Illumination in automated patch clamp experiment

To illuminate the cells during the planar patch clamp experiment, a specialized illumination unit was used. The unit consists of 96 LEDs (Lumileds Luxeon Z, Schiphol, Haarlemmermeer, The Netherlands) that are coupled to light fibers. During the experiment, the end of the fiber is submerged under the solution and positioned 7 mm from the cell being measured. The illumination units with LEDs of different colors were used in the planar patch-clamp experiments: green LEDs ($\lambda_{\text{max}} = 530$ nm, LXZ1-PM01), blue LEDs ($\lambda_{\text{max}} = 470$ nm, LXZ1-

PB01), orange LEDs ($\lambda_{\text{max}} = 590 \text{ nm}$, LXZ1-PL02) and red LEDs ($\lambda_{\text{max}} = 632 \text{ nm}$, LXZ1-PD01). To regulate the intensity of light used in each measurement, the forward current of the illumination unit was adjusted. The intensity was measured directly at the output of the light fibers using a bolometer (Coherent OP-2 VIS, Santa Clara, California, U.S.). The intensity of light was specified for each type of measurement.

Supplementary Note 6: Noise analysis

The data collection for the noise analyses of both types started with measurement of photocurrent dependence on the membrane voltage (IV curve). The range of voltages was from -120 mV to 60 mV with equidistant 20 mV steps. Each sweep was separated into three consecutive steps, with 2 s in the dark, 2 s under the illumination of a saturating intensity for the stationary photocurrents of the measured ChRs (4 mW/mm² for ChReef and ChRmine; 6 mW/mm² for CatCh) and 1 s in the dark. This data was used to calculate the reversal potentials, which were used to determine the electrochemical potentials on the membranes. This step was followed by different protocols and data treatment procedures for stationary and non-stationary analyses. The data treatment encompassed a thorough selection of recordings that met our strict quality control criteria, followed by the processing of the selected raw traces using our proprietary Python library and custom scripts developed in-house.

For stationary analyses, all cells were held at a voltage of -100 mV or -60 mV. 40 consecutive pairs of sweeps, 6.5 s long each, were recorded at a sampling rate of 20 kHz. Each pair of sweeps was followed by 25 s of non-recorded waiting time in the dark. The first sweep of each pair had a 6-second illumination pulse at an intensity of 0.4 mW/mm² (0.6 mW/mm² for CatCh), and the second sweep was recorded under dark conditions.

Sweeps suitable for stationary noise analysis were selected based on the following criteria. Basic parameters of the seals were assessed for each sweep, and only sweeps with a seal resistance over $1\text{ G}\Omega$, a membrane capacitance lower than 50 pF , and a series resistance below $20\text{ M}\Omega$ were used for further analysis. The parameters of the dark noise were then assessed using parts recorded under the dark conditions for the sweeps with data recorded under illumination conditions. Sweeps with a root mean square deviation (IRMS) of dark currents over 5.5 pA were disregarded. The stability of the noise was assessed by dividing the dark part of the current into 100 pieces, calculating IRMS in all of them, and disregarding sweeps with a standard deviation of IRMS over 0.3 pA . The recorded sweeps were grouped back into pairs of consecutive traces that were recorded under light and dark conditions. Only those pairs with stationary photocurrents over 200 pA during the interval from 2 to 6 s after turning on the illumination were considered. Cells that had four or more pairs of traces remaining after applying all of the aforementioned quality control criteria were selected for stationary noise analysis. For each pair, the interval from 2 to 6 s was taken. The sweep recorded under the light conditions was fitted to a double exponential function, and the resulting fit was subtracted from the sweep. A mean current was subtracted from the sweep recorded in the dark. After these corrections, the power spectral density (PSD) was calculated for both sweeps. The differences between the PSD under the light and dark conditions were determined and then averaged for each cell. The averaged difference PSDs were then fitted to the single Lorentzian function in a range from 2.5 to 25 Hz. This allowed for the determination of the corner frequency and the difference PSD at 0 Hz (f_c and S_0 correspondingly as in eq. 2). Open probabilities of the channels (P_o) were then determined for each cell, taking into consideration their relation (eq. 3) to corner frequency and off kinetics (where τ_{off} was determined from the single exponential fit of the photocurrent decrease after

turning off the light). Only cells whose difference PSD met the criteria of $1 \text{ Hz} < f_c < 15 \text{ Hz}$ and $0 < P_o < 1$ were considered in the determination of the single channel conductance values.

$$S(f) = \frac{S_0}{1 + \left(\frac{f}{f_c}\right)^2} \quad [\text{Equation 2}]$$

$$1 - P_o = \frac{1}{2 \pi f_c \tau_{off}} \quad [\text{Equation 3}]$$

The variances σ^2 of the noise associated with the opening and closing of the ChRs were determined by using the obtained values of f_c and S_0 (eq. 4). The unitary photocurrents were subsequently calculated by applying the relation between the mean and variance in the binomial distribution (eq. 5) to the mean net stationary current I and σ^2 . Afterwards, the unitary photocurrents were converted to single channel conductances by dividing them by the electrochemical potential gradient.

$$\sigma^2 = \frac{\pi f_c S_0}{2} \quad [\text{Equation 4}]$$

$$i = \frac{\sigma^2}{I (1 - P_o)} \quad [\text{Equation 5}]$$

In the non-stationary analysis, 300 sweeps were recorded for each cell at the holding voltage of -100 mV or -60 mV. At -100 mV each sweep had a 5 ms illumination step at an intensity of 14 mW/mm^2 forward current so that recordings are done close to single turnover conditions, preventing protein from going to the putative second open state upon absorption of a second photon. At -60 mV each sweep had an illumination step of 150 ms at an intensity of 0.4 mW/mm^2 . After each illumination step the dark currents were recorded for 5 s.

The non-stationary noise analysis involved several steps to select the suitable sweeps for analysis. Firstly, basic parameters of the seals were assessed, and only those sweeps that met the following criteria were used: seal resistance over 1 GΩ, membrane capacitance lower than 50 pF, and series resistance below 20 MΩ. Sweeps with root mean square deviation (IRMS) of dark currents over 4.5 pA were disregarded. Only cells with a peak photocurrent over 500 pA (over 100 pA for -60 mV traces) were considered. To minimize possible unwanted effects of the photocurrent rundown, only the sets of at least 50 consecutive recordings (25 recordings for -60 mV traces) with negligible rundown of the peak photocurrent (lower than 1 pA/sweep) were considered and the variance of the photocurrent was determined as a half of the average of the squared differences between pairs of consecutive recordings. The dependence of the variance on the photocurrent value was then fitted linearly to determine the unitary photocurrent as a proportionality factor (eq. 6) and the background current variance as the free term (σ_b^2 , squared IRMS at photocurrent of 0 pA). Finally, any cells that had linear fits indicating σ_b smaller than 4 pA were excluded from the analysis, since none of the recordings showed such a low IRMS value based on its direct calculation in the dark current. The remaining cells were used to compute the single channel conductance.

$$\sigma^2 = P_o(1 - P_o)Ni^2 + \sigma_b^2 \approx P_oNi^2 + \sigma_b^2 = I \cdot i + \sigma_b^2 \quad [\text{Equation 6}]$$

Supplementary Note 7: Comparison of basic biophysical properties of ChRs measured with automated patch clamp: photocurrent densities, stationary to peak ratios and off kinetics

The photocurrents of the ChR variants at a membrane voltage of -60 mV were measured in response to green LED pulses ($\lambda=530$ nm) for ChRmine variants and GtCCR4, or blue LED pulses ($\lambda=470$ nm) for CatCh, CoChR, CoChR-3M, and GtCCR2. Light pulses of 2 s duration with a

saturating intensity (green LED at 5.6 mW/mm² and blue LED at 8.3 mW/mm²) were used to determine photocurrent densities and desensitization kinetics. The stationary photocurrent densities of the ChR variants were calculated as the quotient of the mean stationary photocurrent upon stimulation with a 2 s light pulse and the capacitance of the cell. Due to the lack of a fluorescence control, we selected only cells with peak photocurrents greater than 20 pA. To avoid bias that could inflate the apparent mean value of photocurrent density for small photocurrent variants, cells with photocurrent densities in the lowest 15% were excluded for each variant. Desensitization kinetics were determined by fitting the decays of the photocurrents from their peak to stationary levels to a biexponential function. Normalized values for fast and slow components' amplitudes were calculated as quotients of the corresponding amplitudes and the sum of the two amplitudes.

Light pulses of 5 ms duration with an intensity of 13.0 mW/mm² for the green LED (ChRmine variants, GtCCR4) and 19.3 mW/mm² for the blue LED (CatCh, CoChR, CoChR-3M, and GtCCR2) were used to determine off-kinetics. The τ_{off} values of all ChR variants were determined by fitting the decaying photocurrent elicited in response to a 5 ms light pulse to a monoexponential function. To determine τ_{off} for CoChR, only cells with stationary photocurrent densities lower than 50 pA/pF were selected to avoid effects of intracellular proton accumulation affecting pH-dependent off-kinetics. To investigate the dependence of the off-kinetics on the membrane potential, τ_{off} values were determined at membrane potentials ranging from -120 mV to +60 mV.

Supplementary Note 8: Intensity dependence of photocurrents measured with automated patch clamp

For intensity dependence experiments, light pulses of 2 s duration were used for green light ($\lambda=530$ nm) and orange light ($\lambda=590$ nm), while light pulses of 4 s duration were used for red light ($\lambda=632$ nm). The intensity of light was regulated by adjusting the forward current of the respective illumination unit. Alternating between fixed and variable light intensities was employed to control for photocurrent rundown effects. The stationary photocurrents recorded at varying intensities were normalized against preceding and subsequent measurements at fixed intensities. The resulting dependencies for each recorded cell were fitted to hyperbolic functions and normalized by their respective amplitudes from the fits. The normalized dependencies were then averaged between the cells.

Supplementary Note 9: Relative ion permeability determination

For the determination of relative ion permeability, photocurrents of ChRmine and ChReef in response to green LED pulses ($\lambda=530$ nm) of 2 s duration were measured at different voltages, and reversal potentials were determined. Permeability ratios were calculated according to the Goldman–Hodgkin–Katz equation. To assess the relative permeability of potassium ions relative to sodium (PK/PNa), we measured photocurrent at voltages ranging from -120 mV to +60 mV in 10 mV steps and assessed reversal potential shifts after exchanging the standard intracellular solution (KF-based) with a NaF-based intracellular solution containing 10 mM NaCl, 10 mM KCl, 110 mM NaF, 10 mM HEPES, and 10 mM EGTA, with pH adjusted to 7.2 using NaOH. A reverse exchange of the intracellular solution was performed to account for reversal potential drift. The shift in reversal potential due to the solution exchange was calculated as the difference between the reversal potential in the NaF-based intracellular solution and the average of the two reversal potentials measured in the KF-based intracellular solution (before

exchange and after reverse exchange). Cells with a reversal potential drift greater than 5 mV were excluded from the analysis.

To assess the relative permeability of calcium ions relative to sodium (P_{Ca}/P_{Na}), we measured photocurrent at voltages ranging from -120 mV to +60 mV in 10 mV steps and assessed reversal potential shifts after extracellular solution dilution, which changed the NaCl concentration from $[NaCl]_{ini} = 140$ mM to $[NaCl]_{fin} = 11$ mM and the $CaCl_2$ concentration from $[CaCl_2]_{ini} = 2.5$ mM to $[CaCl_2]_{fin} = 83$ mM. An additional series of extracellular solution dilutions was performed to return sodium and calcium concentrations to their initial values to account for reversal potential drift. The shift in reversal potential due to the solution exchange was calculated as the difference between the reversal potential in the Ca-based extracellular solution and the average of the two reversal potentials measured in the Na-based extracellular solution (before dilution and after reverse dilution series). Cells with a reversal potential drift greater than 10 mV were excluded from the analysis.

To assess the relative permeability of protons relative to sodium (P_H/P_{Na}), we measured photocurrent at voltages ranging from -121 mV to 59 mV in 3 mV steps. The permeability of protons relative to sodium was calculated from the photocurrent reversal potential using a standard intracellular solution and an NMG-based extracellular solution containing 90 mM NMDG, 3.2 mM NaCl, and 10 mM MES, with pH adjusted to 6.4 using HCl.

Supplementary Note 10: Staining and data acquisition for automated spinning disc confocal microscopy

To assess the subcellular localization of ChRs in NG108-15 cells, the transfected cells were stained with Hoechst 33342 (1:2000, Invitrogen, H3570) and CellTracker Deep Red (1:1000, Invitrogen, 2521042). The culture medium was aspirated, and the cells were washed with 50

μl of DPBS. Afterward, 50 μl of Opti-MEM containing the dyes was added to the cells, followed by incubation at 37 °C for 30 minutes. Post incubation, the cells were washed again with DPBS and 200 μl of DMEM⁺ was added. The stained cells were then imaged using the CellVoyager CQ1 microscope (Yokogawa). Identical imaging parameters were employed across all experiments. A 40x/0.95 dry objective (UPLXAPO40X) was used for acquisitions. Hoechst 33342 fluorescence was excited with a 405 nm laser at 20% power and a 500 ms exposure time, using a BP447/60 emission filter. EYFP fluorescence was excited with a 488 nm laser at 20% power and a 500 ms exposure time, using a BP525/50 emission filter. CellTracker Deep Red was excited with a 640 nm laser at 20% power and a 500 ms exposure time, using a BP685/40 emission filter. Thereby an autofocus routine in the Hoechst channel ensured imaging close to the central planes of the cells.

Supplementary Note 11: Analysis of spinning disc microscopy data

We wrote a Python script for fluorescence line profile analysis. First, the program identified the centroids of the nuclei in the Hoechst channel using the mean-shift clustering algorithm with a bandwidth of 8.125 μm. These centroids were then used to generate 2D square crops of the images, each containing one complete NG cell. Cell membrane masks were automatically generated based on the cytoplasmic fluorescence from the CellTracker channel, using a threshold derived from a previously measured calibration curve. This curve represented the relationship between CellTracker fluorescence intensity at the cell border and the average foreground fluorescence. For calibration, ChRmine-TS-EYFP-ES expressing cells which showed predominant plasma membrane-localization were manually selected. The foreground fluorescence in the CellTracker channel was averaged in regions where the CellTracker fluorescence exceeded that of the nucleus, ensuring it remained above

background noise. The optimal CellTracker fluorescence threshold was determined by maximizing the average EYFP fluorescence along the cell borders, calculated using various CellTracker thresholds. Importantly, the dataset that was used for calibration curve generation was not included into the line profile analysis presented in the paper. The line profiles were automatically positioned perpendicular to these masks, ensuring not to intersect with neighboring cells. Line profiles that intersected with the Hoechst fluorescence in the nuclei were automatically excluded from analysis. Manual verification of the NG cell masks and line profile positions was performed using a custom graphical interface developed with Napari. Only cells and line profiles that passed the manual verification were included into the subsequent analysis. Cells with fewer than three confirmed line profiles were automatically excluded. Fluorescence data from the EYFP channel were recorded along each line profile and averaged across all profiles for each cell, resulting in an expression line profile for each cell. These expression line profiles from all verified cells were then averaged, and standard deviations were calculated.

In order to avoid averaging of the fluorescence from multiple cells only sectors of each cell (centered on the cell's centroid) that were not oriented towards adjacent cells were selected for analysis. The average fluorescence in the EYFP channel within these sectors was subsequently used to calculate the corrected partial cell fluorescence per area (CPCF per area). Only sectors with an angle greater than 120 degrees were included in the analysis. The CPCF per area value is a measure for the average cell fluorescence and represents an approximation of the overall ChR expression.

Supplementary Note 12: rAAV purification and cloning of constructs

A triple transfection of HEK-293T cells was performed using the pHHelper plasmid (TaKaRa, USA), trans-plasmid with either the AAV2/9, PHP.eB or PHP.S capsid⁵⁶ and cis-plasmid with either ChRmine or ChReef under the control of human synapsin or CAG promotor. Cells were regularly tested for mycoplasma contamination. Viral particles were harvested from cells and medium; precipitated from medium with 40% polyethylene glycol 8000 (Acros Organics, Germany) in 500mM NaCl and combined with cell pellets for processing. Pellets were suspended in 500mM NaCl, 40mM Tris, 2.5mM MgCl₂, pH 8, and 100 U/ml of salt-activated nuclease (Arcticzymes, USA) at 37 °C for 30 min. Cleared lysates were purified over iodixanol (Optiprep, Axis Shield, Norway) step gradients (15%, 25%, 40%, and 60%) at 350,000 × g for 2.25 h. rAAV containing fractions were concentrated using Amicon filters (EMD, UFC910024) and formulated in sterile phosphate-buffered saline (PBS) supplemented with 0.001% Pluronic F-68 (Gibco, Germany). Viral vector titers were determined by the number of DNase I resistant vg using AAV titration kit (TaKaRa/Clontech) by qPCR (StepOne, Applied Biosystems) according to the manufacturer's instructions or with adaptations to usage in crystal digital PCR (dPCR) system. Here, dilutions of purified vector DNA were subjected to crystal dPCR using 5x Naica PCR reaction mix (Stilla, R10056) supplemented with primers provided in the AAV titration kit, 0.8mg/μl Alexa 647 (Invitrogen, 11570266) and 1.5x Eva Green (Biotum, #31000-T). Formation of droplet crystals and PCR was performed in a Naica Geode (Stilla) using Naica Ruby or Sapphire Chips (Stilla) and finally analyzed in the Naica Prism3 reader (Stilla) equipped with Crystal Reader and Crystal Miner softwares (Stilla). rAAVs titers and quantification method used is indicated for each rAAV in the respective methods chapter. Purity of produced viral vectors was routinely checked by silver staining (Pierce, Germany) after gel electrophoresis (Novex™ 4–12% Tris–Glycine, Thermo Fisher Scientific) according to the manufacturer's instruction. Viral vector stocks were kept at –80 °C until injection.

Supplementary Note 13: Preparing neonatal mouse cardiomyocytes

Hearts were explanted from p0-p3 mice killed by decapitation and directly placed on ice cold PBS. Remaining tissue and atria were carefully removed, and ventricular CMs isolated with the neonatal heart dissociation kit for mouse and rat (Miltenyi, Germany). 1.5 – 2 million cells were plated on a 6-well-plate coated with 10 µg/ml fibronectin (Sigma; F1141-5MG) and maintained in IMDM (GlutaMAX, no phenol red; Gibco 21056-023) supplemented with 10% FBS superior (Sigma; S0615) and 1% Penicillin/Streptomycin (Life Technologies; 15140122) in standard cultivation conditions (37°C, 5% CO₂). One day later, medium was exchanged to reduce FBS to 0.5% and AAV transduction was performed with AAV2/9-CAG-ChRmine-TS-EYFP-ES with 1.1x10¹⁰ GC/ml (qPCR) and AAV2/9-CAG-ChReef-TS-EYFP-ES with 6x10¹⁰ GC/ml (qPCR) corresponding to ~226 and ~69 vp/cell, respectively. On day 3, the cells were dissociated and plated on Ø 10 mm round coverslips in CM clusters comprising 50,000 cells within 15 µl locally on an 8 µl 0.1% gelatine drop. Cells were incubated in this small drop for 20 min to build cardiac clusters and afterwards medium filled up in the well. After 1-2 days CM cluster started to beat spontaneously and 0.5% FBS IMDM medium was exchanged every 2-3 days.

Supplementary Note 14: Preparing hiPSC-derived cardiomyocytes

Human CMs were differentiated from the induced pluripotent stem cell line UMGi014-A clone 2, which was created from peripheral mononuclear blood cells from a healthy male donor using integration-free Sendai virus and was described previously. CMs differentiation and purification involved WNT signaling modulation and lactate-based metabolic selection as described previously^{57,58}. Differentiated CMs were cryopreserved for further use. For measurements, 1.5 – 2 million cells were thawed and plated on a 6-well-plate coated with 16 mg/mL Geltrex (Thermo Fisher Scientific; A1413302) and maintained in CM culture medium

(RPMI 1640 medium (GlutaMAX; Thermo Fisher Scientific; 72400054), B27 (Thermo Fisher Scientific; 1750404) supplemented with 2 mM thiazovivin (Sigma-Aldrich; 420220-10MG), at 37°C and 5% CO₂. Medium was replaced after two days to remove residues of thiazovivin and changed every 2-3 days afterwards. AAV transduction was performed with MyoAAV-CAG-ChRmine-TS-EYFP-ES with $\sim 1 \times 10^{11}$ GC or MyoAAV-CAG-ChReef-TS-EYFP-ES with $\sim 1.8 \times 10^{10}$ GC (CdPCR). Four days after transduction, cells were dissociated and plated on Ø10 mm round coverslips in cardiac cell clusters comprising 50,000 cells within 8 µl drop on a Geltrex/DMEM/Ham's F-12 coated area. Cells were incubated in this drop for 40 min to build CM clusters and afterwards medium was filled up with CM culture medium. After two days CM clusters started to beat spontaneously. Medium was replaced every 2-3 days.

Supplementary Note 15: Histology for cardiomyocytes

Neonatal heart cells as well as hiPSC-derived CMs were fixed in 4% formaldehyde for 20 min, permeabilised with 0.2% Triton X100 for 20 min and stained in DPBS (Sigma; D8537) supplemented with 5% donkey serum for 2 h with primary antibodies against cardiac troponin I (ab47003, Abcam: 1:800) and for 1 h with secondary antibodies conjugated with Cy5 (711-175-152, JacksonLab, U.S., 1:400) diluted in DPBS with 1:1000 DAPI (0018860.01, Th.Geyer) at room temperature. Images of single CMs for analysis of expression rate were taken through a 10x (10X/NA 0,4 Olympus UPLSAPO) or 20x objective (20x/NA 0,7 Olympus UCPLFLN PH) with an IX83 inverted fluorescence microscope equipped with an ORCA-flash 4.0 digital camera (C11440, Hamamatsu Photonics) and the MT20 illumination system as light source controlled via the CellSens® software. Acquisition of images was performed with following filter settings: 387/11 excitation, 410 beamsplitter and 440/40 emission for DAPI, 485/20, 504 and 525/30 for eYFP, 560/25, 582, and 684/24 for Cy5. Transduction rate was calculated by the percentage of eYFP positive cells among all CMs identified by cardiac troponin I antibody-staining.

CM clusters were imaged with a LSM 800 confocal microscope (Zeiss) equipped with spectral multi-alkali photomultiplier detectors. Z-stack acquisition was performed using a Plan-Apochromat 20x/0.8 M27 via the ZEN 2.6 (blue edition) software (Zeiss) with a pinhole of 55 μm for Dapi, 24 μm for eYFP, 27 μm for the red channel and 31 μm to image Cy5. Pictures were post-processed using stack correction (Background+Decay+Flickr), extended depth of focus (Wavelets, highest Z-Stack Alignment) and Image calculator (subtraction of autofluorescence) of the Zen 3.4 (blue edition) software.

Supplementary Note 16: Intravitreal injection

All *in vivo* electrophysiological experiments were carried out in compliance with the relevant national and international guidelines (European Guideline for animal experiments 2010/63/EU) as well as in accordance with German laws governing animal use. The procedures have been approved by the responsible regional government office. Rodents were kept in a 12h light/dark cycle with ad libitum access to food and water.

3-months old female and male Rd1 (C3HeB/FeJ, JAX 000658) mice were anesthetized with a subcutaneous injection of a fentanyl (0.05 mg/kg), midazolam (5 mg/kg), and medetomidine (0.5 mg/kg) (FMM) cocktail. Mice were then secured using a bite bar and placed on top of a temperature controller (Supertech) to maintain a body temperature of 37°C. For local anesthesia of the eyes, eye drops containing 0.5% Proxymetacain were applied and hydration gel (Bayer, Bepanthen) was placed on the eyes to prevent dryness whenever possible. Before injection, a hole posterior to the ora serrata was created using a 27-gauge needle. Then, a Hamilton syringe was guided through this hole into the intravitreal space and 2 μl of virus solution of PHP.eB-hsyn-ChRmine-TS-EYFP-ES (1.89×10^{13} GC/ml, dPCR) or PHP.eB-hsyn-ChReef-TS-EYFP-ES (8.59×10^{13} GC/ml, dPCR) was injected at 4 $\mu\text{l}/\text{min}$ using a motorized injector (Stoelting). After 5 min the syringe was withdrawn and the anesthesia was reversed with a subcutaneous

injection of a naloxone (1.2 mg/kg), flumazenil (0.5 mg/kg), and atipamezole (2.5 mg/kg) cocktail.

Supplementary Note 17: Analysis of neural responses to optogenetic stimulation of the visual system

Only units with stable responses across the duration of the session and high kilosort quality scores were included in subsequent analysis. To obtain continuous firing rate estimates, single unit responses were binned with a bin size of 1 ms and convolved with a gaussian kernel with a standard deviation of 10 ms. Trial-averaged responses were normalized to the mean and standard deviation of the baseline (400ms before stimulus onset) across all intensities. Units that did not respond to the highest light intensity were excluded (mean normalized firing rate during the stimulus smaller than 2.58). The Gramm toolbox⁶² was used to visualize raster plots. For significance testing across time points a permutation based method⁶³ was used as described⁶⁴. Briefly, using unpaired t-tests differences between the two conditions for each time point are determined and subsequently time clusters are identified using the `bwconncomp.m` function in Matlab (4 connected components). Time cluster significance is determined by comparison the t-statistics of the actual data against the t-statistics of shuffled data (10000 permutations with randomized labels).

Supplementary Note 18: Histology and imaging after optogenetic stimulation of the visual system

After washing in PBS, retinas were prepared and fixed again for 10 min in 4% PFA at RT. Fixed and washed retinas were put in 30% Sucrose and subjected two three rounds of freezing and thawing on dry ice. Then retinas were incubated for 1h in 10% normal donkey serum (NDS) and subsequently in primary antibody solution (rabbit-GFP (Proteintech, 50430-2-AP), 1:666 in PBS with 3% NDS and 0.5% Triton-X) for 4 days at 4°C. After incubation, retinas were

washed in PBS and incubated in secondary antibody overnight at 4°C (AlexaFluor 488 (Invitrogen, A32970), 1:500 in PBS with 3% NDS and 0.5% Triton-X). Finally, washed retinas were mounted in DAPI-containing Vectashield (Vector Laboratories, H-1200).

For post-hoc analysis of recording sites, brains were collected and incubated in 4% PFA at 4°C overnight. Then brains were washed and embedded in 4% agarose. 100µm coronal slices were cut using a vibratome (Leica microsystems, VT1000S) and stained for 2h at RT (DAPI, Thermo Fisher Scientific, D1306, 2.5 µg/ml). Washed brain slices were mounted on microscope slides in Vectashield (Vector Laboratories, H-1200).

Images were captured using a Leica TCS SP8 laser scanning confocal microscope with 63×/20x oil immersion or a 10× air objectives (Leica Microsystems). Images were merged and processed using LAS X (Leica Microsystems) and Adobe Photoshop software.

Supplementary Note 19: Behaviour experiments for vision restoration in mice

Mice of both sexes were used and experiments were performed during the daytime (corresponding to the mouse's subjective nighttime). All procedures related to the behaviour experiments were performed in accordance with the Canadian Council on Animal Care and approved by the Montreal Neurological Institute's Animal Care Committee.

Supplementary Note 20: Postnatal AAV injection into the cochlea in mice and Mongolian gerbils

The same injection approach was performed for all animals which later would be subject to either: auditory brainstem recordings, juxtacellular recordings from single putative SGNs, *ex vivo* acute slice electrophysiology in mice, or recordings from the inferior colliculus in Mongolian gerbils. AAV injections into the left ear were performed at postnatal day 6 in C57BL/6J wild-type or B6;129P2-Otof^{tm1.1Erei} (MGI: 4950055 ⁶⁶) mice or at postnatal day 7.3 ± 1.3 days in Mongolian gerbils^{18,55}. The right ear served as a non-injected control. In brief,

mouse and gerbil pups were randomly selected for virus injections. Under general isoflurane anesthesia (5% for anesthesia induction, 1–3% for maintenance with frequent monitoring of the hind-limb withdrawal reflex and anesthesia adjustments, accordingly) and local xylocaine as well as buprenorphine (0.1 mg/kg) and carprofen (5 mg/kg) administration for analgesia, the cochlea of the left ear was accessed via a retroauricular incision. Body temperature was maintained at physiological temperature. The cochlea was gently punctured using a quartz capillary pipette, which was kept in place to inject the virus of following titers:

Mice: AAV2/9-hsyn-ChRmine-TS-EYFP-ES 5.1×10^{13} GC/ml (qPCR),
 AAV2/9-hsyn-ChReef-TS-EYFP-ES 3.1×10^{13} (qPCR) and 2.45×10^{13} GC/ml
 (dPCR)

Gerbil: PHP.S-hsyn-ChReef-TS-EYFP-ES 5.25×10^{13} GC/ml (qPCR)

After virus injection the tissue in the injection area was repositioned and the wound was sutured. Carprofen (5 mg/kg) was administered for analgesia the day after surgery.

Supplementary Note 21: Description of anesthesia and analgesia for adult rodents undergoing *in vivo* optical stimulation

Surgeries and measurements were performed under anesthesia using isoflurane (5% for anesthesia induction, 1–3% for maintenance with frequent monitoring of the hind-limb withdrawal reflex and anesthesia adjustments, accordingly) and analgesia by sub-cutaneous injections of buprenorphine (0.1 mg/kg body weight) and meloxicam (5 mg/kg body weight). Body temperature was maintained at 37°C using a custom-designed heat plate through all the procedures.

Supplementary Note 22: Optical stimulation of the auditory pathway in rodents *in vivo*

The left cochlea was exposed by performing a retroauricular incision behind the pinna followed by a bullostomy, where the round window was visualized and punctured. For mice a 50 μ m

optical fiber coupled to a 594 nm (OBIS LS OPSL, 100 mW, Coherent Inc., Santa Clara, United States) or a 522 nm (Oxxius combined with a motorized Power Attenuator, Lannion, France) diode laser was used. For gerbils a 200 μ m optical fiber was only coupled to the prior mentioned 522 nm laser. Laser power was calibrated prior to each experiment using a laser power meter (Thorlabs PM100USB).

Supplementary Note 23: Kanamycin deafness model in mice and Mongolian gerbil

For the kanamycin deafness model, the cochlea was deafened by delivering 200 mg/ml of kanamycin through the round window via a microfile needle, acutely. It was left for approximately 7 minutes (for mice) or 15 to 30 minutes (for gerbils) before additional measurements were performed to confirm deafness by absence of acoustically evoked auditory brainstem responses. The post and pre-deafened auditory brainstem responses were compared to evaluate the effectiveness of the deafening procedure.

Supplementary Note 24: Experimental set-up for optical *in vivo* recordings in rodents

Stimulus generation and delivery, as well as data acquisition was performed using a custom-written software (MATLAB, MathWorks, Natick, MA, United States) employing National Instrument data acquisition cards and a custom-build laser-controller. Recordings were conducted in a soundproof chamber (IAC Acoustics, IL, United States).

Supplementary Note 25: Data analysis of acoustic and optically evoked auditory brainstem responses in mice

The mouse ABR data was analyzed using custom-made Matlab software (The MathWorks, Inc., Natick, MA, USA). Averages were expressed as mean \pm standard deviation. For statistical comparison between two groups, data sets were tested for equality of variances (F-test) followed by two-tailed unpaired Student's t-test.

Supplementary Note 26: Procedures for immunostaining cochleae of mice and Mongolian gerbils

At the end of all *in vivo* recordings of rodents, the animals were sacrificed under deep anesthesia via cervical dislocation. The cochleae were collected and fixed in 4% formaldehyde solution for 45 minutes. They were then decalcified for 3-4 days in 0.12 M ethylenediaminetetraacetic acid (EDTA), dehydrated in 25% sucrose solution for 24 hours and cryosectioned (mid-modiolar cryosections, 25 μ m thick). Immunofluorescence staining was done in 16% goat serum dilution buffer (16% normal goat serum, 450 mM NaCl, 0.6% Triton X-100, 20 mM phosphate buffer, pH 7.4). The following primary antibodies were used at 4 °C overnight: chicken anti-GFP (1:500, ab13970 Abcam, USA) and guinea pig anti-parvalbumin (1:300, 195004 Synaptic Systems, Germany); and secondary antibodies for one hour in room temperature: goat anti-chicken 488 IgG (1:200, A-11039 Thermo Fisher Scientific, USA) and goat anti-guinea pig 568 IgG (1:200, A-1107 Thermo Fisher Scientific, USA). Finally, slices were mounted in Mowiol 4-88 (Carl Roth, Germany). Samples were imaged with a confocal microscope SP8 (Leica, Germany) mounted with a 40x oil objective. For each cochlear turn (apex, middle and base) an image was taken focusing on the modiolus.

Supplementary Note 27: Preparation of brain stem slices

The brain was immediately immersed in ice cold cutting solution (Supplementary Table 8) and pinned, dorsal side down, on a wax stage. With the ventral side of the brainstem exposed, the meninges were removed with curved forceps and a mid-sagittal cut was performed using a straight razor, splitting the brain in two hemispheres. Scissors were used to cut between the cerebellum and the occipital lobe of each hemisphere in order to separate the hind-brain from the fore-brain. The two blocks of hind-brain, containing brain-stem and cerebellum, were

glued with cyanoacrylate glue, (Loctite 401, Henkel) medial side down, on the stage of a Leica (Wetzlar, Germany) VT 1200 vibratome. The lateral side of both brain blocks was facing upwards and was facing towards the advancing blade. A vibration amplitude of 1.5mm was used and the blade was placed at the height of the cerebellar flocculus. Cerebellar tissue was sectioned at an advancing speed of 0.05 – 0.1 mm/s and discarded. Thereafter, a speed of 0.02mm/s was used to obtain 150µm thick parasagittal slices of the cochlear nucleus. The slices were incubated in artificial cerebro-spinal fluid (aCSF, Table S8) for a total of 30 minutes in a 35°C water bath (Julabo, Seelbach, Germany), after which they were maintained in aCSF at room temperature (23 – 25 °C) until recording. The pH of both the cutting solution and the aCSF was adjusted to 7.4. The osmolarity was, in mOsm, 310 for the aCSF and 320 for the cutting solution. Both solutions were continuously aerated with carbogen (95% O₂, 5% CO₂).

Supplementary Note 28: Auditory brainstem slice electrophysiology

The sampling interval was set to 25µs and the filter at 7.3 kHz. For better visualization of the slice's cell layers and auditory nerve fibers (ANFs), differential interference contrast (DIC) microscopy was used on upright Olympus BX51WI microscope with a water immersion LUMPLFLN40XW objective (Olympus, Hamburg, Germany). All recordings were performed at near physiological temperature (33 – 35°C). The bath solution flowed through an inline solution heater (SC-20 with CL-200A controller; Warner Instruments, Hamden, CT, USA). The temperature of the solution was monitored by a thermistor placed between the opening of the inflow tube and the slice in the recording chamber.

Borosilicate filamentous glass capillaries (GB150F, inner diameter: 0.86 mm, outer diameter: 1.50 mm, length: 80 mm, Science Products GmbH, Hofheim, Germany) were used to pull patch pipettes on a P-1000 micropipette puller (Sutter Instruments Co., Novato, CA, USA). The resistance at the tip of the pipette was strictly 2 – 3 MΩ to avoid increases of the series

resistance (R_s) over long recordings. The pipettes were filled with intracellular solution (details on Table S8), which additionally contained 1 mM of Alexa-568 (Invitrogen / Fisher Scientific, Schwerte, Germany). The pH of the solution was adjusted to 7.4 and its osmolarity to 325 mOsm, to prevent osmotic collapse of the patched neuron, preserve the cell's vigour and prevent fluctuations of the R_s over long recordings. Voltage clamp experiments were performed with a $V_{\text{hold}} = -70$ mV, corrected for a liquid junction potential of 12 mV. Only cells with R_s values less than 8 M Ω were included in the analysis. Afferent fiber optogenetic stimulation was performed using a green laser included in the Oxxius multi-wavelength bundle (LBX-488-40-CSB, maximum Power: 40 mW; LCX-532-50CSB, maximum power: 50 mW; OBIS-594-100, maximum power: 100 mW; LBX-638-100-CSB, maximum power: 100mW; Laser 2000 GmbH, Wessling, Germany). Synapses were driven with trains of stimuli yielding varying success rates of optically eliciting excitatory postsynaptic currents, hereafter termed oEPSC probability (P_{oEPSC}). P_{oEPSC} was defined as $\frac{\text{Number of oEPSCS}}{50}$, 50 signifying the number of 1ms light pulses that were delivered to the ANF. Minimal stimulation irradiance was defined as the lowest value that could yield a $P_{\text{oEPSC}} = 1$ at 10 Hz. This irradiance value was used later in the experiment to assess the P_{oEPSC} at higher frequencies. For ANF stimulation, 5, 10, 20, 33, 40, 50 and 100 Hz were the tested frequencies. In direct transduction experiments, where the photocurrent properties of ChReef were measured, 10, 20, 30, 50, 100, 200, 300 and 350 Hz were used instead. Electrophysiology data were analysed using Igor Pro (Wavemetrics, Lake Oswego, OR, USA). Evoked release was analysed using custom Igor scripts. Confocal z-stacks were processed with the NIH ImageJ software⁶⁸. Figures were assembled for display using open-source vector graphic software Inkscape (<https://inkscape.org>).

Supplementary Note 29: Immunohistochemistry and immunofluorescence imaging for acute slice electrophysiology

Afterwards they were washed in PBS for 10 minutes to halt fixation and blocked with GSDB for 1 hour at room temperature. After fixation the slides were kept for 10 minutes in ice cold PBS to halt fixation and then washed for 1 hour at room temperature in goat serum dilution buffer, which contained in 16% normal goat serum, 450 mM NaCl, 0.3% Triton X-100, and 20 mM phosphate buffer (PB, pH 7.4). The slides were then incubated in primary antibodies diluted in GSDB, for 3 hours, in a wet chamber at room temperature. Four washing steps followed, that lasted 10 minutes each, two of them with Wash Buffer (450 mM NaCl, 0.3% Triton X-100 and 20mM PB) and two more with PBS. The slides were then incubated with secondary antibodies overnight at 4°C and, afterwards, washed twice with Wash Buffer and twice more with PBS as before. Before mounting, the slides were maintained in 5mM PB for 10 minutes and were then mounted with a drop of Mowiol (Carl Roth GmbH, Karlsruhe, Germany) and covered with a thin glass coverslip. Double sided tape spacers of 120µm thickness were used for mounting to flank the slice before the application of Mowiol. This way, the coverslip's weight would not be applied fully on the slice, avoiding extra vertical pressure, which resulted in better preservation of structural integrity of the tissue. Immunofluorescence imaging was performed on a Zeiss LSM 780 Microscope with a 40x NA1.4 *Oil Plan-Apochromat* objective. *Primary antibodies:* chicken-anti-GFP (1:500, Abcam, Berlin, Germany), guinea-pig-anti-vGLUT1 (1:1000, Synaptic Systems GmbH, Göttingen, Germany). *Secondary antibodies:* goat-anti-chicken 488 (1:200, Thermo Fisher Scientific, Waltham, USA) goat-anti-guinea-pig 568 (1:200, Thermo Fisher Scientific, Waltham, USA).

Supplementary Note 30: Cumulative discrimination index (d') calculation

Post-stimulus time histograms (PSTH) were computed by binning spike counts in 0.2 ms bins. The first three consecutive bins crossing threshold of 3x MAD indicate t_{on} and, respectively, the last three consecutive bins over threshold indicate t_{off} . Based on the time window extracted, the signal was further analyzed and sorted in a two-dimensional matrix according

to stimulus intensity and corresponding recording site. From this matrix, we calculated the cumulative distribution index (d') based on spike rates calculated across increasing intensities starting with 0 intensity condition.

Supplementary Note 31: Temporal analysis of neural clusters

To calculate the number of spikes per stimulus, we divided the spike counts recorded by the number of repeats per recording and by the number of pulses from stimulation rate used. See supp,ecalculate the vector strength, a measure of spike timing relative to stimulation cycle the following formula was previously⁴⁰:

$$VS = \frac{\sqrt{[\sum_{i=1}^n \cos \theta_i]^2 + [\sum_{i=1}^n \sin \theta_i]^2}}{n} \quad \text{[Equation 7]}$$

With θ describing the spike timing computed from stimulus onset to following stimulus onset for a given stimulus cycle (phase). The Rayleigh test (eq. 8) was then performed in order to test the significance of vector strength for each unit and each repeat.

$$L = 2 * length(\theta_i) * (VS^2) \quad \text{[Equation 8]}$$

If $L < 13.8$, $p > 0.001$ and vector strength significance is rejected and set to 0. Firing rates were computed across all recordings by dividing the spike counts recorded in the determined spike window by the duration of that spike window. These values were normalized to the highest firing rate recorded for plotting.

Supplementary Note 32: Subcellular expression profiles for SGNs in cochlear cryosections

To assess the subcellular expression profiles of ChRmine and ChReef in SGNs, we used a custom-written Python program to plot fluorescence line profiles, incorporating a manual verification process. The process began by using the manually detected centroids (using custom MATLAB script as explained in methods section) of all cells to generate 2D square crops of the images, each containing one complete SGN. For each 2D crop, the Z-plane was selected by maximizing fluorescence in the cytoplasmic parvalbumin channel.

Cell membrane masks were automatically generated based on the cytoplasmic parvalbumin channel fluorescence using a fixed threshold. Line profiles were then automatically positioned perpendicular to these masks and avoiding intersection with surrounding cells. Manual verification of SGN masks and line profile positions was conducted using a custom graphical interface developed with Napari. The Z-plane was manually checked for a noticeable fluorescence drop indicating the position of the nucleus; cells lacking a discernible nucleus were excluded to prevent bias from including line profiles in the nuclear region or parallel to the cell surface. Any line profiles that intersected visually identifiable nuclei were excluded from further analysis.

Only cells and line profiles that passed manual verification were used for further analysis. Cells with fewer than three confirmed line profiles were automatically excluded. Fluorescence data from the YFP channel was recorded along each line profile and averaged across all lines for each cell, creating an expression line profile for each cell. These expression line profiles from all verified cells were then averaged, and the standard deviation was calculated.

Supplementary Note 33: Brain histology

Brains were left in 8% FA over a week and transferred to 30% sucrose for 24 hours. Brains were then carefully mounted using cryomatrix gel (Shandon Cryomatrix, Thermo Fisher Scientific, Waltham MA, USA) and sectioned coronally. Slices were 50 µm thick, transferred onto microscope slides (Thermo Superfrost/ColorFrost Plus, Charged 90° - CS/1440CS/1440, Erie Scientific, Ramsey MI, USA) and prepared for antibody staining. The staining follows the cochleae staining protocol, after PBS washing, sections were blocked with goat serum dilution buffer (GSDB) for 1h at room temperature before primary antibodies for parvalbumin (1:300, guinea pig, Synaptic Systems, Goettingen, Germany) and GFP (to label ChReef, 1:500, chicken, Abcam, Cambridge, UK). Goat anti-guinea-pig-568 and goat anti-chicken-488 were used for secondary antibodies and incubated at room temperature for 1h – slides were ultimately mounted with Mowiol and imaged the following day. Images were taken in oil at 40x using LSM510 (Zeiss, 467 Jena, Germany) microscope and analyzed with ImageJ (U. S. National Institutes of Health, Bethesda, Maryland, USA).

Supplementary Note 34: Animal housing

Data were obtained from nine 2.5 to 3.75 year old common marmosets of either sex (5 male, 4 female). Animals were pair housed in a colony of about 50 animals consisting of several rooms with acoustic but no visual contact to neighboring pairs. The colony maintained a 12h:12h light-dark cycle at a temperature of 26 ± 1.5 °C and a relative humidity of 60 - 80 %. Animals were fed *ad libitum* a diet of fresh fruits, vegetables, nuts, arabic gum, rice, pasta, potatoes, meal worms, crickets, yoghurt, various minerals as well as pellets. Water was always available and was occasionally mixed up with unsweetened tea.

Supplementary Note 35: Acoustic auditory brainstem recordings

Animals were anesthetized with a mixture of Alfaxan (10mg/kg BW, i.m.) and Midazolam (0.125 mg per animal, i.m.). Further, Metacam (0.2 mg/kg BW) was administered either orally – or if not possible – via s.c. injection. After anesthesia initiation, animals were placed on a heat pad, wrapped in a forced air warming blanket and body temperature was maintained at 37 to 38 °C. Otoscopic evaluation of ear canals was performed next to rule out signs of infection and was found to be normal in all cases. Afterwards, animals were transferred onto a warmed saline bag on a heat pad within a stereotaxic frame. Animals were not fixed inside the frame but made use of custom-made ear bars containing earphone (Etymotic ER-4PT) and microphone (Sennheiser MKE 2 P-C) inserts. Ear bars were gently inserted into the outer ear canals. Monitoring of the microphone signal upon acoustic stimulation ensured correct placement. Auditory stimuli were calibrated separately with 3D printed ear molds of common marmosets where a 1/8th inch microphone (G.R.A.S. 46 BE) was placed at the position of the tympanic membrane. Stimulus generation and delivery, as well as data acquisition was performed using a custom-written software (MATLAB, MathWorks, Natick, MA, United States) employing National Instrument data acquisition cards and a custom-build laser-controller. Recordings were conducted in a dedicated operating theater for non-human primate surgery. If necessary, anesthesia was maintained by re-injecting Alfaxan (5 mg/kg BW). Acoustically evoked ABRs (aABRs) were recorded by placing needle electrodes behind the pinna, on the vertex, and on the neck of the anesthetized animals. The difference in potential between the vertex and mastoid subdermal needles was amplified using a custom-designed amplifier, sampled at a rate of 50 kHz for 10 ms, filtered (300–3000 Hz) and averaged across at least 750 stimulus presentations. In case of pure tone stimulation a bandpass filter centered on the pure tone frequency removed stimulus artifacts observed occasionally. The ABRs threshold was

defined and determined as the lowest light or sound intensity for which one of the 5 waves (aABR) or 2 waves (oABR) was reliably visible.

Supplementary Note 36: Injection method

First, animals received Metacam (0.2 mg/kg BW) either orally – or if not possible – via s.c. injection and were anesthetized with injections of Alfaxan (10mg/kg BW, i.m.) and Midazolam (0.125 mg per animal, i.m.). Additionally, dexamethasone (5 mg/kg BW, i.m.) and Cerenia (1 mg/kg BW, s.c.) were also applied. The fur around the surgical site was removed. Then, an intravenous catheter was placed in the vena saphena and the animal was intubated using a 00 Miller blade and a custom-made unblocked endotracheal tube for artificial ventilation. Next, anesthesia was transferred to a combined volatile-intravenous anesthesia with Sevoflurane (ca. 2 – 3 %) and Propofol-Remifentanyl (0.3 – 0.4 mg/kg/min; 10 – 25 µg/kg/h, respectively) to effect. During surgery, body temperature was maintained between 37 and 38°C with a heating pad and a forced air warming blanket wrapped around the animals' body. Additionally, physiological parameters were monitored throughout the surgery via ECG and pulse oximetry. Surgery itself was performed under standard aseptic technique. Local analgesia was achieved with Carbostesin injections around the surgical site. The cochlea was accessed via a retroauricular incision, blunt dissection of post-auricular as well as temporal muscles to expose the linea temporalis and mastoidectomy ventral to the linea temporalis. Utmost care was used to avoid damaging the horizontal semicircular canal and facial nerve which served as guiding landmarks. Animals were initially deafened with flushes of 10 % Neomycin as described previously ⁶⁰. In later experiments, Neomycin was added to the viral suspension to a final concentration of 10 %. In addition, the ossicle chain was disrupted by removal of the malleus. The viral suspension was administered either via a pipette pulled from

borosilicate and pressure injection or a silicone catheter was used to slowly (15 μ l/30 min; UMP3, World Precision Instruments) inject. In both cases, the round window membrane was identified and gently ruptured. To prevent pressure build-up inside the cochlea during slow injection, a ventilation hole was opened either with a rose burr next to the oval window or by removing the stapes when surgical access was favorable. Excess viral suspension was carefully suctioned to avoid unwanted transfection of surrounding tissue. In later experiments, Dexamethasone was added to the viral suspension (2 %). Three different titers of viral suspension (15 μ l) were used 5×10^{10} , 10^{11} , and 5×10^{11} GC) and injected in three animals each. Animals were randomly assigned to each group and experimenters were blinded to the condition. After virus injection, the round window and vent holes were closed with autologous tissue, the mastoidectomy closed by replacing the temporal and post-auricular muscles. The skin and muscles were then sutured with 5/0 absorbable suture. For direct post-operative pain management, Buprenorphine (0.005 mg/kg BW, s.c.) was administered. To prevent hypoglycemia Glucose (5%, 2 ml) was administered s.c. Post-operative care included repeated antibiotic administration (Amoxicillin 37.5 mg/kg BW) every 48 h for 8 days as well as analgesia via Metacam administration (0.2 mkg/kg BW, p.o.).

Supplementary Note 37: Immunostaining and confocal imaging of cochlear cryosections

The facial nerves exiting the foramen stylomastoideus were dissected and the soft tissue overlying the temporal bones were removed to allow trimming bone around the cochlea under visual guidance. Next, the cochlea and vestibular organs were transferred into 5 M EDTA for decalcification. During a period of at least 2 weeks, EDTA was regularly exchanged and softened bone removed from the cochlea. Additionally, the facial nerve was removed from its bony capsule overlying the cochlea. Once completed, the cochlea was prepared for whole

mounts of the organ of Corti and mid-modiolar cochlear cryosections. Here, the spiral ligament and bone lamella of the apex were carefully removed to access the organ of Corti and dissecting it by cutting the spiral lamina. Next, the stria vascularis and tectorial membrane were removed. This procedure was repeated until the whole organ of Corti was dissected into consecutive whole mounts and the cochlear modioli. Finally, the whole mounts and modioli were stored in phosphate buffered saline. The modioli were then processed similarly to rodent samples: after a 24 h dehydration step in 25 % sucrose solution, samples were cryosectioned (mid-modiolar cryosections, 16 μ m tick). Immunofluorescence staining was performed in 16% goat serum dilution buffer (16% normal goat serum, 450 mM NaCl, 0.6% Triton X-100, 20 mM phosphate buffer, pH 7.4). The following primary antibodies were used at 4 °C overnight: chicken anti-GFP (1:500, ab13970 Abcam, USA) and guinea pig anti-parvalbumin (1:300, 195004 Synaptic Systems, Germany) as well as mouse anti-NF200 (1:400, Sigma, St. Louis, USA); and secondary antibodies for one hour in room temperature: goat anti-chicken 488 IgG (1:200, Invitrogen Scientific, USA), goat anti-guinea pig 568 IgG (1:200, Invitrogen, USA) and anti-mouse 633 (1:200, Invitrogen). Finally, slices were mounted in Mowiol 4-88 (Carl Roth, Germany). Whole mounts were first permeabilized with TritonX 0,5% in PBS. Staining was then performed in 10 % goat serum dilution buffer and guinea pig anti-parvalbumin (1:200; Synaptic systems, Germany), rabbit anti-Otoferlin (1:500; SySy) and chicken anti-GFP (1:500; Abcam) were used as primary antibodies. As secondary antibodies anti-chicken 488 (1:1000; Invitrogen), anti-guinea pig 568 (1:1000; Invitrogen) and anti-rabbit 633 (1:1000; Thermo Fisher) were used. Samples were imaged with a confocal microscope SP8 (Leica, Germany) mounted with a 40x oil objective. For each cochlear turn (apex, middle and base) an image was taken focusing on the modioli. Image analysis was performed by a custom-written MATLAB script modified from⁶¹. Briefly, SGN somas and modioli area were manually

detected using a touch screen from the parvalbumin images. Next, individual somas were automatically segmented using Otsu's threshold method from every Z-stack and a mask corresponding to the given SGN was defined for the Z-stack for which the mask was fulfilling the criteria of size (area and diameter) and circularity. In case the segmentation was not deemed to be sufficient, the segmentation of the given SGN soma was performed manually. Next, the median GFP brightness of each SGN was measured and its distribution was fitted with a Gaussian mixture model with up to 3 components. A threshold, above which SGNs somas were considered as transduced, was defined as average + 3 x standard deviation of the Gaussian distribution with the lowest mean. The density of inner hair cells (IHCs) along the whole mounts was calculated by placing a curve along the (presumed) IHC, measuring its length and assessing the number of identified IHC.